AM-BASEBAND TELEMETRY SYSTEMS

Volume 5: Summary

by

RICHARD S. SIMPSON
Professor of Electrical Engineering

and

WILLIAM H. TRANTER
Research Associate

August, 1969

TECHNICAL REPORT NUMBER 108-102

COMMUNICATION SYSTEMS GROUP

BUREAU OF ENGINEERING RESEARCH
UNIVERSITY OF ALABAMA UNIVERSITY, ALABAMA

07

AM-BASEBAND TELEMETRY SYSTEMS

Volume 5: Summary

by

RICHARD S. SIMPSON
WILLIAM H. TRANTER

AUGUST, 1969

TECHNICAL REPORT NUMBER 108-102

Prepared for
National Aeronautics and Space Administration
Marshall Space Flight Center
Huntsville, Alabama

Under

Contract Number NAS8-20172

Communication Systems Group
Bureau of Engineering Research
University of Alabama

ABSTRACT

The process of coherently demodulating a suppressed carrier AM-baseband is analyzed. Carrier synthesis from a pilot and from AM modulated carriers is considered in the presence of additive noise and baseband recorder flutter. The results illustrate the magnitude of phase error in the demodulation carrier arising from each source, and the design parameters which minimize this error.

The manner in which automatic-gain-control affects an AM-baseband system is studied for first- and second-order loops. Tracking error is investigated using an analytical approach for the first-order loop and computer simulation for both first- and second-order loops. Results presented include curves which illustrate the relationship between tracking error and various system parameters. Steady-state errors and the dependence of the time constants upon the loop input are also investigated.

ACKNOWLEDGEMENT

The authors would like to express their appreciation to the Telemetry Systems Branch, Marshall Space Flight Center, for the support of this work. In particular, Mr. Walter O. Frost and Mr. Frank H. Emens have contributed significantly to this work through the many discussions which were held at MSFC.

TABLE OF CONTENTS

Page

Page

LIST OF ILLUSTRATIONS

LIST OF SYMBOLS

B_m	modulation bandwidth
B_n	noise bandwidth
C	constant
D	rms transmitter deviation
D_m	maximum rms transmitter deviation
E_p	nominal pilot amplitude
$e_{DSB}(t)$	DSB signal
$e_{SSB}(t)$	SSB signal
$e_Q(t)$	quadrature DSB (QDSB) signal
$e_n(t)$	Channel n carrier
$e_d(t)$	demodulated output
$e_{sc}(t)$	synthesized demodulation carrier
$e_{in}(t)$	input waveform
$e_{out}(t)$	output waveform
$e_{VCO}(t)$	VCO output
$e_2(t)$	VCO output phase shifted 90 degrees
$e_{ns}(t)$	Channel n signal
$e_{np}(t)$	pilot signal
$e_v(t)$	VCO input
$e_\phi(t)$	phase detector output
$e_i(t)$	envelope of pilot at ground loop input
$e_o(t)$	envelope of pilot at ground loop output
$E_i(s)$	Laplace transform of $e_i(t)$
$E_o(s)$	Laplace transform of $e_o(t)$

$e_{cf}(t)$	channel filter output
$e^{r}_{DSB}(t)$	DSB signal at recorder output
$e^{r}_{SSB}(t)$	SSB signal at recorder output
$e_{pf}(t)$	pilot filter output
$e_{r}(t)$	tape recorder input
$e_{p}(t)$	tape recorder output
f_{PDO}	frequency above which pulse dropout (PDO) occurs
f	frequency in hertz
f_{n}	Channel n carrier frequency
g(t)	flutter
g_{peak}	peak value of g(t)
$H(\omega)$	network transfer function
$\lvert H(\omega) \rvert$	network amplitude response
h(t)	time-base error
K_{d}	phase-detector constant
K_{p}	phase-step magnitude
K_{VCO}	VCO constant
L	load factor
m(t)	modulation signal
n(t)	noise signal
N	total number of Channels in the system
P(SP)	probability of a shifted pulse
P(PDO)	probability of pulse dropout
p(x)	probability density of x
R(t)	envelope of signal plus noise
S_{n}	slope of the phase characteristic of the Channel n filter

S_p	slope of the phase characteristic of the pilot channel filter
S_t	rms value of the baseband signal
S_j	rms value of the Channel j signal
S_m	maximum rms value of the baseband signal
s	Laplace operator
s_k	poles of transfer function
t	time
T_c	carrier period
T_o	value of $T_c/2$ below which PDO occurs
T_c	time of load factor change
T_t	transmitter AGC loop time constant
T_r	receiver AGC loop time constant
v(t)	instantaneous tape velocity
$\bar{V}$	mean tape velocity
w	distance along tape
x, τ, y	dummy variables
z_m	average number of zero crossings per second of the modulating signal
ζ	damping constant
ρ	signal-to-noise ratio
δ	monostable multivibrator
σ_x^2	variance of x
σ_x	standard deviation of x
n	channel number
ω	frequency in radians per second
ω_m	modulating frequency

ω_n	Channel n carrier frequency
ω_i	instantaneous frequency
ω_p	pilot frequency
ω_o	master oscillator frequency
δ_k	k'th MSMV trigger
$\mu(t)$	instantaneous phase deviation
$\dot{\mu}(t)$	instantaneous frequency deviation
$\phi(\omega)$	network phase response
Δ	total change in pilot amplitude
$\theta(t)$	phase deviation due to flutter
$\phi(t)$	phase deviation due to noise
$\dot{\phi}(t)$	frequency deviation of the channel carrier due to noise
$\dot{\theta}(t)$	frequency deviation of the channel carrier due to flutter
$\dot{\theta}_{peak}$	peak value of $\dot{\theta}(t)$
$\theta_e(t)$	phase error
$\theta_i(t)$	phase-lock loop input
$\theta_o(t)$	phase-lock loop output
θ_{peak}	peak phase error
α	reciprocal of first-order transmitter-loop time constant
ε_T	tracking error
β	reciprocal of receiver-loop lowpass filter time constant
ε_{ss}	steady-state error

CHAPTER I

INTRODUCTION

In the past, most of the analog aerospace telemetry systems have been FM/FM. Today, the need for a large number of wideband channels on the same telemetry link has increased interest in AM/FM systems, such as those which have been used in telephone transmission. It has been shown that a multiplex of 10 or more wideband DSB channels requires about one-fifth of the baseband bandwidth that would be required for FM channels, if equivalent noise performance is required.[1] If the baseband contains SSB or quadrature DSB channels, the bandwidth saving is even greater.

Power is usually limited in a typical aerospace telemetry link because of size and weight restrictions placed on the airborne package; therefore, suppressed carrier modulation is used to form the baseband. This leads to problems at the baseband demodulator since the carriers necessary for demodulation must first be synthesized.

There are two basic techniques for synthesizing the demodulation carriers in an AM/FM system. The first technique is to transmit a pilot, which has a fixed phase relationship with the channel carriers, along with the baseband. At the demodulator this pilot can be divided or multiplied in frequency to yield the required demodulation carrier. The basic block diagram for this type of system is illustrated in Figure 1-1. For clarity only a single channel is shown. Other channels can be included by the addition of an amplitude modulator,

---

[1] Superscripts refer to numbered references.

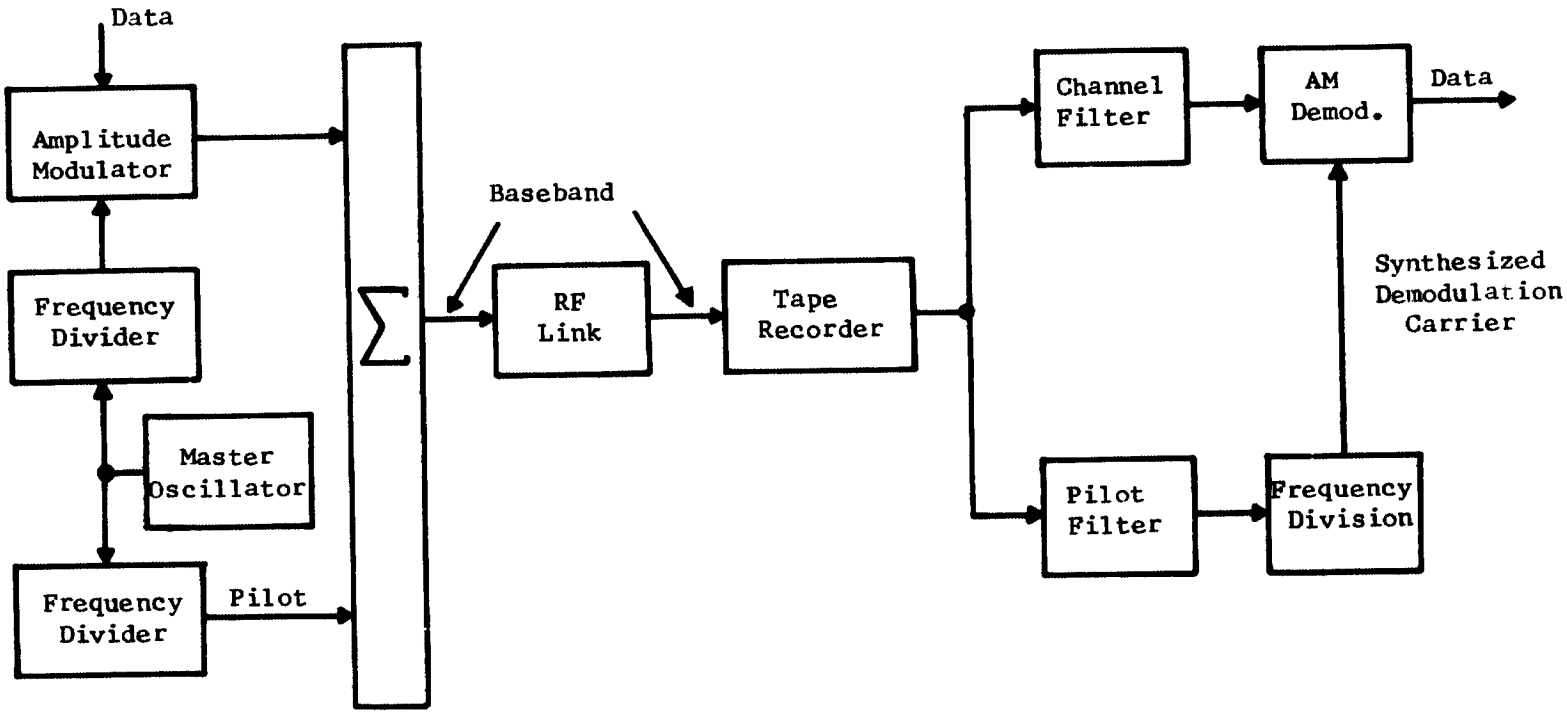

Figure 1-1 AM-Baseband System Using Common Pilot Synthesis

AM demodulator, and data filter for each channel. All channel carriers and the pilot are derived from a master oscillator to insure that they have the required phase relationship.

The other technique of carrier synthesis is to perform a nonlinear operation on the modulated channel carrier to produce a frequency component at either the channel carrier or some harmonic of the channel carrier, which can then be divided in frequency to give the required demodulation carrier. A general system using this technique is illustrated in Figure 1-2.

In this work, several problems associated with carrier-synthesis in the presence of noise and tape recorder flutter are investigated. Both techniques of carrier-synthesis are studied. Analysis is performed to determine the effect of various system parameters on demodulation phase error due to both noise and tape recorder flutter. Techniques for reducing this error are also investigated.

Automatic-gain-control (AGC) can be useful in AM-baseband systems when the demodulated channel output signal-to-noise ratio is to be maximized. However, the use of AGC results in both static and dynamic errors being introduced into the demodulated data. These errors are investigated for both first- and second-order AGC loops, and curves are given which show the dependency of these errors on the system parameters. Additionally, the relationship between the AGC-loop time constant and the loop input is studied.

Several appendices are included to provide additional information and to help the reader in following certain developments.

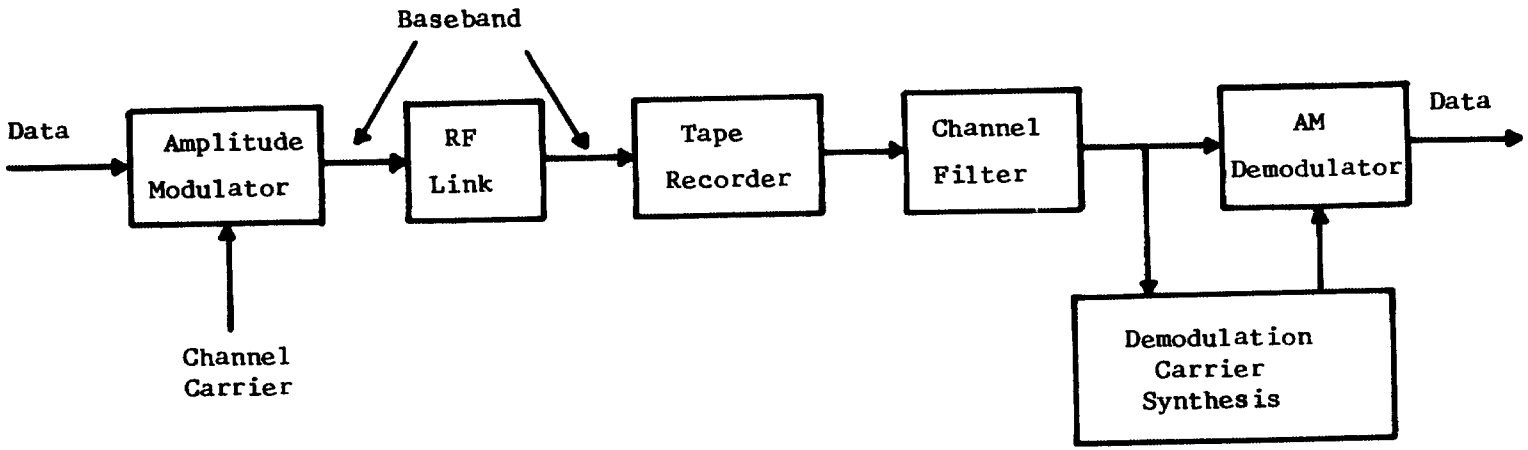

Figure 1-2 AM-Baseband System Using Modulated Channel Carrier Synthesis

CHAPTER II

CARRIER SYNTHESIS FROM A COMMON PILOT

In a suppressed carrier system, the synthesized demodulation carrier must be phase coherent with the carrier position in the channel to be demodulated if the error in the demodulated output is to be minimized. The reduction of demodulation phase errors requires careful attention if the baseband is perturbed in some manner. In this chapter the effect of baseband recorder flutter is investigated for the case where the demodulation carriers are derived from a common pilot. The effect of pilot noise is also investigated, since high pilot phase stability is a requirement for good system performance. The analysis will yield the design requirements necessary to minimize the effect of tape recorder flutter, the mean-square value of waveform distortion resulting from flutter, and the pilot signal-to-noise ratio necessary for a given degree of pilot phase stability.

Before the analysis can be performed, a mathematical model of the system must be developed. This is easily done after showing that the tape recorder can be represented as a phase modulator. Also, when a pilot is used for synthesis of all demodulation carriers, the phase characteristic of the RF link and the baseband crest factor are of interest. These parameters will also be investigated in this chapter.

A. REPRESENTATION OF TAPE RECORDER FLUTTER

Flutter arises from variations in the instantaneous speed of the tape across the record and playback heads in an instrumentation

recorder. The major effect of these speed variations is to introduce a time-base error (TBE) in the signals which the recorder processes.[2] In mathematical terms, if a signal is recorded, the recorder output, upon playback, can be approximated as

$$e_p(t) = e_r\left[t + h(t)\right] \quad , \tag{2.1}$$

where h(t) represents the composite TBE due to both record and playback flutter. It is shown in Appendix A that if the peak value of flutter is small, (2.1) can be used to describe both pre-detection and post-detection recording. If the recorded signal is

$$e_r(t) = \sum_{j=1}^{m} \sin \omega_j t \tag{2.2}$$

(2.1) yields

$$e_p(t) = \sum_{j=1}^{m} \sin \omega_j\left[t + h(t)\right] \quad , \tag{2.3}$$

which becomes

$$e_p(t) = \sum_{j=1}^{m} \sin\left[\omega_j t + \theta_j(t)\right] \tag{2.4}$$

by defining

$$\theta_j(t) = \omega_j h(t) \quad . \tag{2.5}$$

The effect of the recorder is to impart a phase perturbation, $\theta_j(t)$, to each of the components in the recorded spectrum. Each of these perturbations has the same waveshape and a magnitude directly proportional to the recorded frequency. Thus, the tape recorder can be modeled by a phase modulator having the appropriate inputs.

B. DEVELOPMENT OF THE SYSTEM MODEL

The Channel-n carrier, $e_n(t)$, is obtained by dividing the frequency of a master oscillator, ω_o, by ω_o/ω_n, to yield

$$e_n(t) = \cos \omega_n t \ . \tag{2.6}$$

If the modulation signal $e_m(t)$ is assumed to be

$$e_m(t) = 2 \cos \omega_m t \ , \tag{2.7}$$

the modulator output is

$$e_{DSB}(t) = \cos (\omega_n + \omega_m)t + \cos (\omega_n - \omega_m)t \tag{2.8}$$

for DSB modulation and

$$e_{SSB}(t) = \cos (\omega_n + \omega_m)t \tag{2.9}$$

for SSB modulation. The decision to work with the upper sideband is arbitrary.

After the individual carriers have been modulated by the information-carrying signals, they are added to the pilot, which is formed by dividing the master oscillator frequency by ω_o/ω_p, to form the baseband. The resulting signal is transmitted to the ground station through an RF link which is assumed distortionless.

A single-channel model is illustrated in Figure 2-1 for the AM-portion of the system without the tape recorder. Comparison with Figure 1-1 makes the meaning of each block evident. Demodulation-carrier synthesis is accomplished by dividing the pilot frequency, ω_p, by ω_p/ω_r. The AM demodulator is represented by a product device and a lowpass filter.

The tape recorder model is derived by first considering a recorded SSB signal. Since the phase perturbations due to flutter are

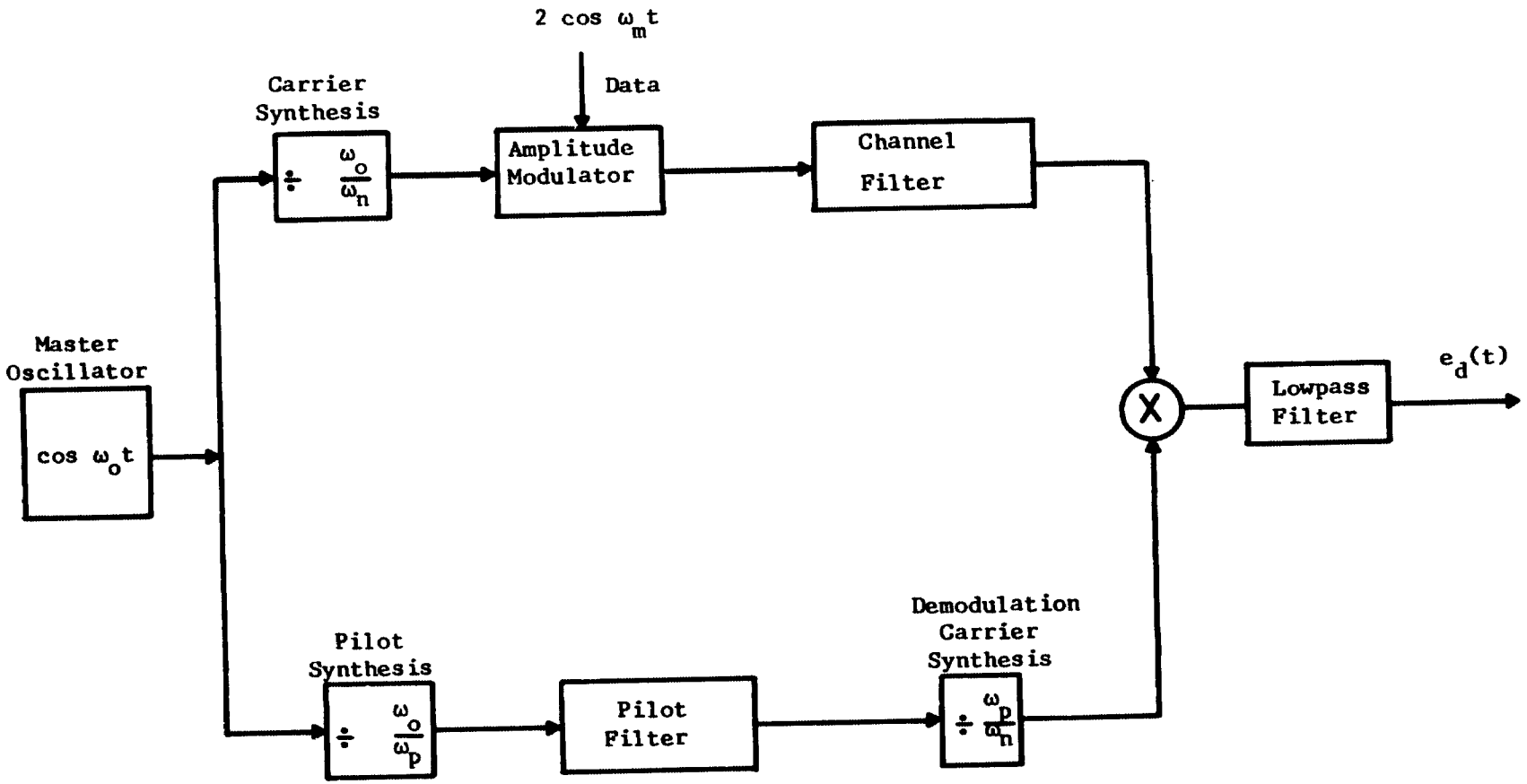

Figure 2-1 System Model without Tape Recorder

proportional to the recorded frequency, the perturbation of the upper-sideband SSB signal is

$$\frac{\omega_n + \omega_m}{\omega_p}\,\theta(t) \ ,$$

where $\theta(t)$ is the phase perturbation of the pilot due to flutter. Therefore, after the SSB signal given in (2.9) is recorded and played back, the expression describing it can be expressed as

$$e^r_{SSB}(t) = \cos\left[(\omega_n + \omega_m)t + \frac{\omega_n + \omega_m}{\omega_p}\,\theta(t)\right] \ . \qquad (2.10)$$

Thus, the tape recorder can be represented by a phase modulator with modulation input $\left[(\omega_n + \omega_m)/\omega_p\right]\theta(t)$. This representation yields the model illustrated in Figure 2-2. The symbols used in this Figure will be described in the following paragraphs.

C. ANALYSIS OF THE MODEL FOR SSB AND DSB

A first-order analysis of the model for SSB can be made neglecting the effect of the data filter and the pilot filter. For this case the inputs to the demodulator are

$$e^r_{SSB}(t) = \cos\left[(\omega_n + \omega_m)t + \frac{\omega_n + \omega_m}{\omega_p}\,\theta(t)\right] \qquad (2.11)$$

and

$$e_{sc}(t) = \cos\frac{\omega_n}{\omega_p}\left[\omega_p t + \theta(t)\right] \ . \qquad (2.12)$$

Therefore, the output of the demodulator is

$$e_d = \frac{1}{2}\cos\left[\omega_m t + \frac{\omega_m}{\omega_p}\,\theta(t)\right] \ . \qquad (2.13)$$

From the above expression it is observed that the effect of the recorder is to impart a phase error proportional to the modulating frequency. There is no interaction between the modulation process and

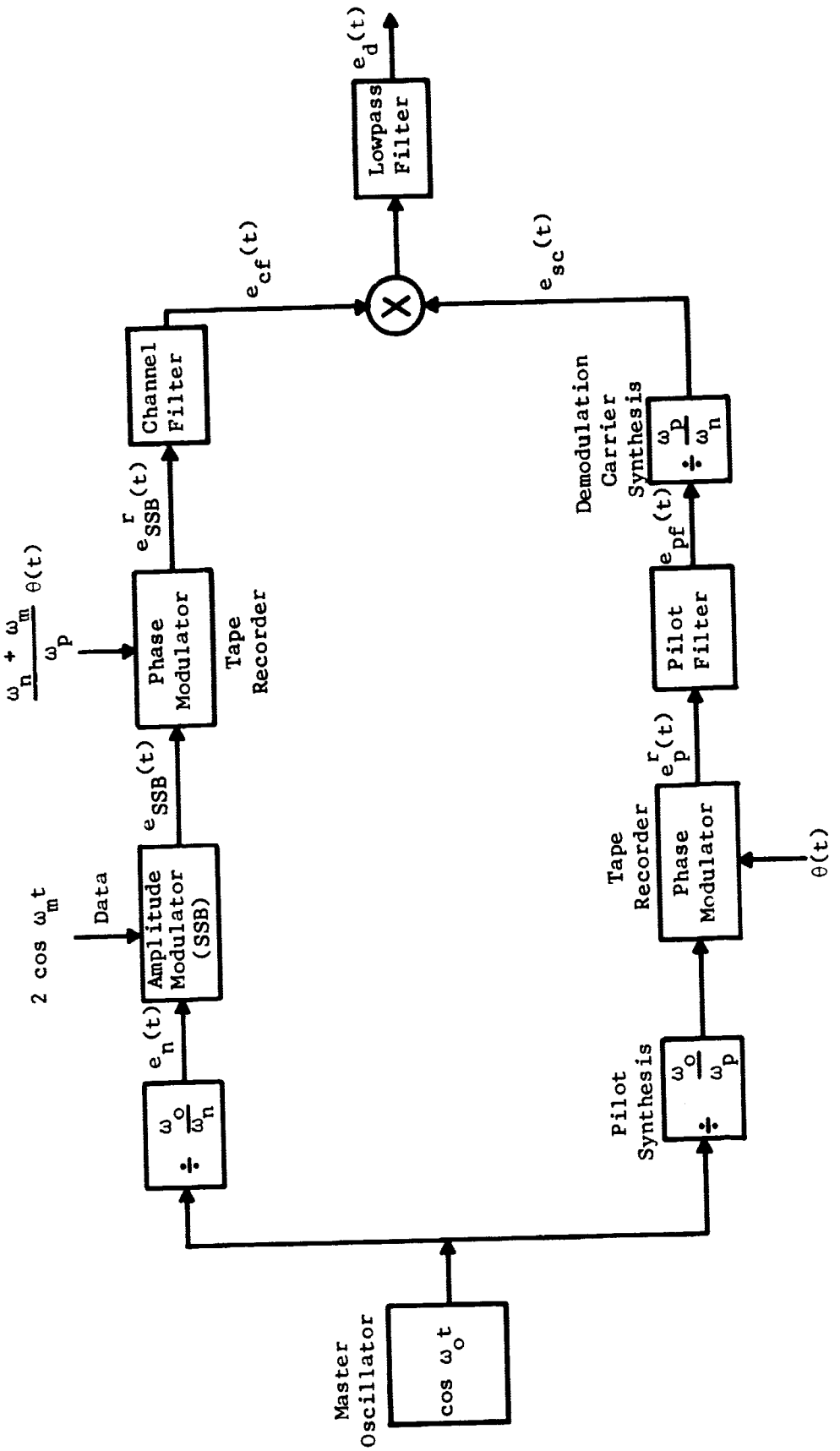

Figure 2-2 System Model with Tape Recorder

the recorder, since (2.13) would be unchanged if the modulating signal were directly recorded and played back.

A more complete analysis requires that the effect of the bandpass channel and pilot filters be considered, which involves determining the response of a linear network to a phase-modulated signal. The output of the filters will be determined using the quasi-steady-state approximation.[3] As shown in Appendix B, the quasi-steady-state approximation of the output for a sinusoidal input is

$$e_{out}(t) = e_{in}(t)H\left[\omega_n + \dot{\mu}(t)\right] \tag{2.14}$$

where

$$e_{in}(t) = \text{Re}\ \exp\left[j\left[\omega_n t + \mu(t)\right]\right],$$

$H[\ ]$ = network transfer function,

ω_n = carrier frequency,

$\mu(t)$ = instantaneous phase deviation, and

$\dot{\mu}(t)$ = instantaneous frequency deviation.

Using (2.14) the channel filter output, $e_{cf}(t)$, can be written as

$$e_{cf}(t) = \text{Re}\left[\exp\ j\left[(\omega_n + \omega_m)t + \frac{\omega_n + \omega_m}{\omega_p}\,\theta(t)\right]\right] \times H_n\left[(\omega_n + \omega_m) + \frac{\omega_n + \omega_m}{\omega_p}\,\dot{\theta}(t)\right]\Bigg], \tag{2.15}$$

where $H_n[\ ]$ is the channel filter transfer function. Assuming that this filter has linear phase with slope S_n, unit amplitude in the passband, and phase θ_n at ω_n, as shown in Figure 2-3, the transfer function can be written as

$$H_n(\omega) = \exp\ j\left[S_n(\omega - \omega_n) + \theta_n\right]. \tag{2.16}$$

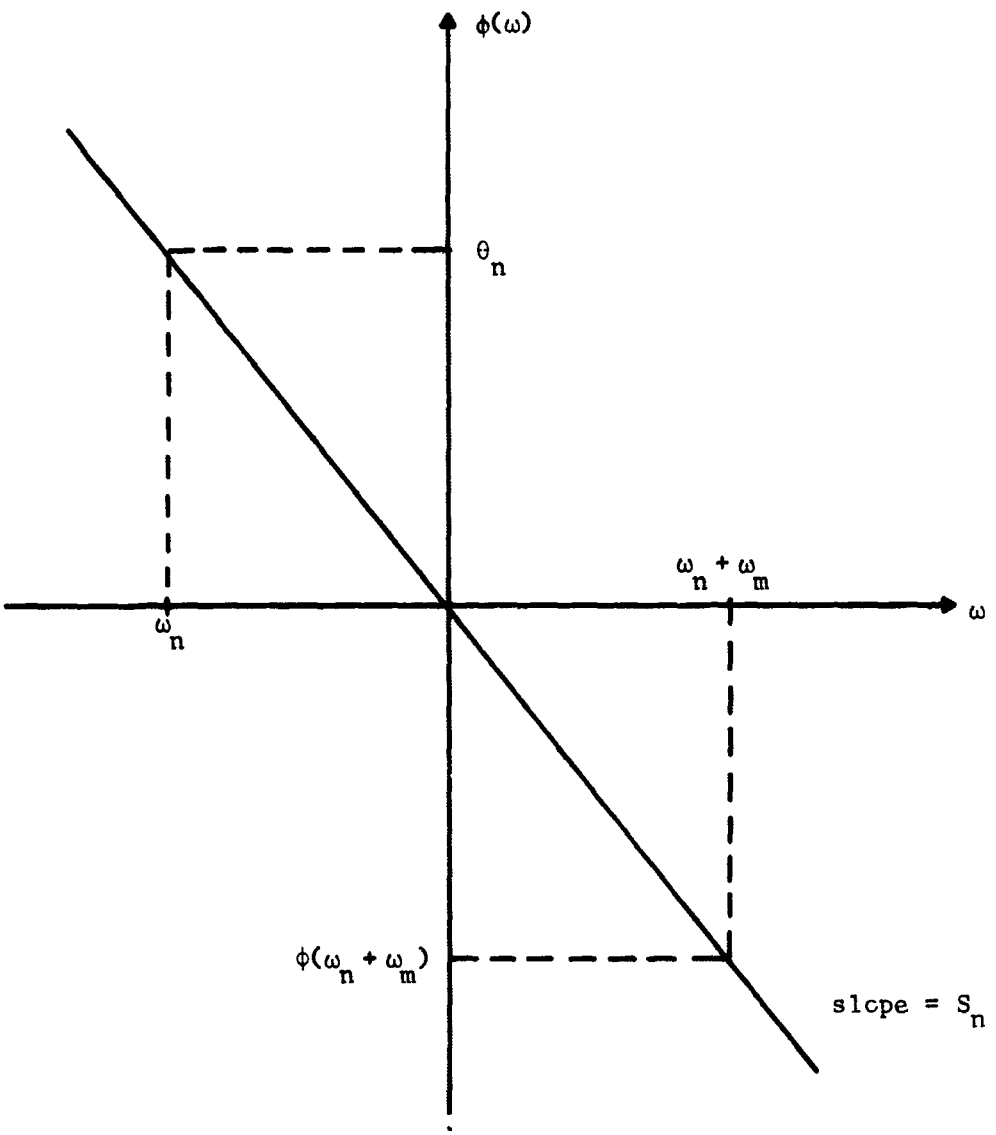

Figure 2-3 Channel Filter Phase Characteristic

Therefore, from (2.15) and (2.16)

$$e_{cf}(t) = \mathrm{Re}\left[\exp\, j\left[(\omega_n + \omega_m)t + \frac{\omega_n + \omega_m}{\omega_p}\,\theta(t)\right]\right.$$
$$\left. \times \exp\, j\left[\theta_n + S_n\omega_m + \frac{\omega_n + \omega_m}{\omega_p}\, S_n\dot{\theta}(t)\right]\right] . \qquad (2.17)$$

Combining the exponential terms and taking the real part yields

$$e_{cf}(t) = \cos\left[(\omega_n + \omega_m)t + \theta_n + S_n\omega_m + \frac{\omega_n + \omega_m}{\omega_p}\,\theta(t) + \frac{\omega_n + \omega_m}{\omega_p}\, S_n\dot{\theta}(t)\right] . \qquad (2.18)$$

The output of the pilot filter, $e_{pf}(t)$, can be computed in exactly the same manner yielding

$$e_{pf}(t) = \cos\left[\omega_p t + \theta(t) + S_p\dot{\theta}(t)\right] , \qquad (2.19)$$

where S_p is the slope of the phase characteristic of the pilot filter. A term analogous to θ_n does not appear because the pilot signal is assumed to be centered in the pilot filter passband; therefore there is no phase shift at the carrier frequency. The synthesized demodulation carrier, $e_{sc}(t)$, is obtained by dividing the instantaneous frequency of $e_{pf}(t)$ by $\frac{\omega_p}{\omega_n}$, a process which is discussed in detail in Appendix F. The result is

$$e_{sc}(t) = \cos\left[\omega_n t + \frac{\omega_n}{\omega_p}\,\theta(t) + \frac{\omega_n}{\omega_p}\, S_p\dot{\theta}(t)\right] . \qquad (2.20)$$

Multiplying (2.18) by (2.20) yields, after lowpass filtering,

$$e_d(t) = \frac{1}{2}\cos\left[\omega_m t + \frac{\omega_m}{\omega_p}\,\theta(t) + S_n\omega_m\right.$$
$$\left. + (S_n - S_p)\,\frac{\omega_n}{\omega_p}\,\dot{\theta}(t) + S_n\,\frac{\omega_m}{\omega_p}\,\dot{\theta}(t) + \theta_n\right] , \qquad (2.21)$$

which becomes

$$\overset{A}{\underset{|}{}}\quad \overset{B}{\underset{|}{}}\quad \overset{C}{\underset{|}{}}\quad \overset{D}{\underset{|}{}}\qquad \overset{E}{\underset{|}{}}$$
$$e_d(t) = \frac{1}{2}\cos\left[\omega_m t + \theta_n + S_n\omega_m + \frac{\omega_m}{\omega_p}\,\theta(t) + \frac{\omega_m}{\omega_p}\, S_n\dot{\theta}(t)\right] \qquad (2.22)$$

if the phase slopes of the linear-phase filters are equal. This condition essentially requires that the time delay through the data channel and the pilot channel be equal. Term A is the desired term, since the modulating signal is $\cos \omega_m t$. Terms B and C do not cause distortion, since B can be eliminated by passing the pilot through a constant phase-shift network, and C is a phase shift proportional to frequency, i.e., a constant time delay. Term D represents distortion caused by flutter without consideration of the filters, i.e., the distortion term in (2.13), and finally, Term E represents distortion caused by the interaction of the flutter perturbation with the data filter. Therefore, the effect of flutter on an SSB system can be reduced to the two distortion terms D and E if the proper linear-phase filters are used and if a phase-shift network is used to compensate for the carrier frequency not being centered in the data filter passband.

A DSB system can be analyzed by using the model for upper and lower sideband SSB and applying superposition. Thus, for a DSB system, the output of the channel filter can be written by adding a cosine term to (2.18) to account for the lower sideband. Additionally, the θ_n term can be eliminated by assuming the DSB signal to be centered in the channel filter passband. The result of these operations is

$$e_{cf}(t) = \cos\left[(\omega_n + \omega_m)t + \frac{\omega_n + \omega_m}{\omega_p}\theta(t) + S_n\omega_m + S_n\frac{\omega_n + \omega_m}{\omega_p}\dot{\theta}(t)\right] + \cos\left[(\omega_n - \omega_m)t + \frac{\omega_n - \omega_m}{\omega_p}\theta(t) - S_n\omega_m + S_n\frac{\omega_n - \omega_m}{\omega_p}\dot{\theta}(t)\right] . \tag{2.23}$$

The synthesized demodulation carrier is the same for DSB as for SSB. Thus, the demodulated output is determined by multiplying (2.20) by

(2.23) and filtering to eliminate the $2\omega_n$ components. The result is

$$e_d(t) = \frac{1}{2}\cos\left[\omega_m t + \frac{\omega_m}{\omega_p}\theta(t) + S_n\omega_m + (S_n - S_p)\frac{\omega_n}{\omega_p}\dot{\theta}(t) + S_n\frac{\omega_m}{\omega_p}\dot{\theta}(t)\right]$$
$$+\frac{1}{2}\cos\left[-\omega_m t - \frac{\omega_m}{\omega_p}\theta(t) - S_n\omega_m + (S_n - S_p)\frac{\omega_n}{\omega_p}\dot{\theta}(t) - S_n\frac{\omega_m}{\omega_p}\dot{\theta}(t)\right] \quad (2.24)$$

for the demodulated output. If $S_n = S_p$, the sidebands add coherently in the demodulation process, and (2.24) becomes

$$e_d(t) = \cos\left[\omega_m t + S_n\omega_m + \frac{\omega_m}{\omega_p}\theta(t) + S_n\frac{\omega_m}{\omega_p}\dot{\theta}(t)\right] \quad , \quad (2.25)$$

which is identical with the result obtained for SSB except for the θ_n term. Thus, assuming that the synthesized demodulation carrier perfectly tracks the channel carrier position, the distortion in $e_d(t)$ is the same for both SSB and DSB modulation. It is important to note that if S_n does not equal S_p, coherent addition of the sidebands does not occur, and additional distortion results.

D. DEGREE OF WAVEFORM DISTORTION

The degree of waveform distortion resulting from flutter, which remains after matching S_n and S_p, can be determined by comparing (2.25) and

$$\cos(\omega_m t + S_n\omega_m) \quad ,$$

the ideal demodulated output. This residual distortion is

$$E(t) = \cos(\omega_m t + S_n\omega_m)$$
$$-\cos\left[\omega_m t + S_n\omega_m + \frac{\omega_m}{\omega_p}\theta(t) + S_n\frac{\omega_m}{\omega_p}\dot{\theta}(t)\right] \quad . \quad (2.26)$$

Since

$$\cos\left[\omega_m t + S_n\omega_m + \frac{\omega_m}{\omega_p}\theta(t) + S_n\frac{\omega_m}{\omega_p}\dot{\theta}(t)\right] =$$

$$\cos(\omega_m t + S_n\omega_m)\cos\left[\frac{\omega_m}{\omega_p}\theta(t) + S_n\frac{\omega_m}{\omega_p}\dot{\theta}(t)\right] \qquad (2.27)$$

$$-\sin(\omega_m t + S_n\omega_m)\sin\left[\frac{\omega_m}{\omega_p}\theta(t) + S_n\frac{\omega_m}{\omega_p}\dot{\theta}(t)\right] ,$$

(2.26) becomes

$$E(t) = \left[1 - \cos\left[\frac{\omega_m}{\omega_p}\theta(t) + S_n\frac{\omega_m}{\omega_p}\dot{\theta}(t)\right]\right]\cos(\omega_m t + S_n\omega_m) \qquad (2.28)$$

$$+ \sin\frac{\omega_m}{\omega_p}\theta(t) + S_n\frac{\omega_m}{\omega_p}\dot{\theta}(t)\,\sin(\omega_m t + S_n\omega_m) .$$

In a practical system the maximum value of

$$\left[\frac{\omega_m}{\omega_p}\theta(t) + S_n\frac{\omega_m}{\omega_p}\dot{\theta}(t)\right]$$

is sufficiently small to permit the approximations

$$\cos\left[\frac{\omega_m}{\omega_p}\theta(t) + S_n\frac{\omega_m}{\omega_p}\dot{\theta}(t)\right] \approx 1$$

and

$$\sin\left[\frac{\omega_m}{\omega_p}\theta(t) + S_n\frac{\omega_m}{\omega_p}\dot{\theta}(t)\right] \approx \left[\frac{\omega_m}{\omega_p}\theta(t) + S_n\frac{\omega_m}{\omega_p}\dot{\theta}(t)\right] .$$

Thus, (2.28) becomes

$$E(t) = \left[\frac{\omega_m}{\omega_p}\theta(t) + S_n\frac{\omega_m}{\omega_p}\dot{\theta}(t)\right]\sin(\omega_m t + S_n\omega_m) . \qquad (2.29)$$

The mean-square error, $\overline{E^2(t)}$, is

$$\overline{E^2(t)} = \frac{1}{2}\overline{\left[\frac{\omega_m}{\omega_p}\theta(t) + S_n\frac{\omega_m}{\omega_p}\dot{\theta}(t)\right]^2} \qquad (2.30)$$

since the mean-square value of a unit amplitude sinusoid is 1/2. It has been shown that samples of flutter and TBE approximate sample functions of a zero-mean, Gaussian, process.[4] Therefore, $\theta(t)$ and $\dot{\theta}(t)$ are uncorrelated; hence, they are statistically independent.[5] This allows (2.30) to be written

$$\overline{E^2(t)} = \frac{1}{2}\left[\frac{\omega_m}{\omega_p}\right]^2\left[\overline{\theta^2(t)} + S_n^2\ \overline{\dot{\theta}(t)}\right] , \qquad (2.31)$$

which, from (2.5) and (A.4) is

$$\overline{E^2(t)} = \frac{1}{2}\,\omega_m^2\left[\overline{h^2(t)} + S_n^2\ \overline{g^2(t)}\right] . \qquad (2.32)$$

In many wideband systems S_n can be sufficiently small to allow (2.32) to be approximated by

$$\overline{E^2(t)} = \frac{1}{2}\,\omega_m^2\ \sigma_h^2 , \qquad (2.33)$$

where σ_h^2 is the variance of TBE.

As an example of the above expression, if the modulation frequency is 1 kHz and the mean-square error is to be kept below 0.01, then the rms TBE, σ_h, will be less than 22.3 μs. This is easily accomplished with present-day recorders using servo speed control and high tape speeds. It should be noted that if S_n is such that (2.32) must be used, then mean-square error will be larger because of the additional term.

E. EFFECT OF PILOT NOISE

Since the pilot is used for synthesis of all demodulation carriers, it must have high phase stability if errors in the demodulated output are to be avoided. In Appendix D the effect of phase

errors in the demodulation carrier are studied for DSB, SSB, and quadrature DSB systems.

The analysis to determine the effect of noise on the pilot phase stability will assume that the pilot is perturbed by additive Gaussian noise, which, by virture of the pilot filter, is narrowband. Thus, the problem is the familiar one of a sinewave plus Gaussian noise, first solved by S. O. Rice.[6] The general expression for the pilot, after having been perturbed by noise is

$$e_p(t) + n(t) = R(t)\cos\left[\omega_p t + \phi(t)\right] \tag{2.34}$$

where $\phi(t)$ is a slowly-varying phase deviation.[7]

From the properties of narrowband noise, the statistics of $R(t)$ and $\phi(t)$ can be determined. The behavior of $R(t)$ is of no interest since variations in the envelope of the pilot can be removed by a limiter in the carrier synthesis loop, i.e., the carrier synthesis process is not amplitude sensitive. However, the density function for $\phi(t)$, $q(\phi)$, must be examined since it gives the degree of phase perturbation of the pilot due to noise.

The density function $q(\phi)$ is obtained by determining the joint density $q(R,\phi)$ and integrating over all R. The result is[8]

$$q(\phi) = \frac{e^{-\rho}}{2\pi}\left[1 + \sqrt{4\pi\rho}\,(\cos\,\phi)\Psi(\sqrt{2\rho}\cos\,\phi)e^{\rho\cos^2\phi}\right], \tag{2.35}$$

where $\Psi(x)$ is the normalized probability integral defined by

$$\Psi(x) = \frac{1}{\sqrt{2\pi}}\int_{-\infty}^{x} e^{-t^2/2}\,dt, \tag{2.36}$$

and ρ is the pilot signal-to-noise ratio.

Equation (2.35) is plotted in Figure 2-4 for three values of ρ. For convenience, the abscissa is plotted in degrees. For ρ equal to zero the density function, $q(\phi)$, is uniform, and as ρ increases, the probability of large phase perturbations decreases. As ρ continues to increase, the phase perturbations decrease and the density function, $q(\phi)$, begins to approximate a Gaussian distribution. This can be seen by noting that, for $x > 2.5$, the approximation

$$\Psi(x) = 1 - \frac{e^{-x^{2/2}}}{\sqrt{2\pi}\, x} \tag{2.37}$$

can be made with an error of less than 0.001. Thus, for $\sqrt{2\rho}\cos\phi > 2.5$

$$\Psi(\sqrt{2\rho}\cos\phi) \approx 1 - \frac{e^{-\rho\cos^2\phi}}{2\sqrt{\pi\rho}\cos\phi}, \tag{2.38}$$

and

$$q(\phi) \approx \frac{e^{-\rho}}{2\pi}\left[1 + 2\sqrt{\pi\rho}\cos\phi\, e^{\rho\cos^2\phi}\left[1 - \frac{e^{-\rho\cos^2\phi}}{2\sqrt{\pi\rho}\cos\phi}\right]\right], \tag{2.39}$$

which becomes

$$q(\phi) \approx \sqrt{\frac{\rho}{\pi}}\cos\phi\, e^{-\rho\sin^2\phi}. \tag{2.40}$$

For large ρ most of the density function will lie in the region of ϕ equal to zero. Thus, for sufficiently large ρ, (2.40) can be written as

$$q(\phi) \approx \sqrt{\frac{\rho}{\pi}}\, e^{-\rho\phi^2}, \tag{2.41}$$

which is a normal distribution with zero mean and variance

$$\sigma_\phi^2 = \frac{1}{2\rho}. \tag{2.42}$$

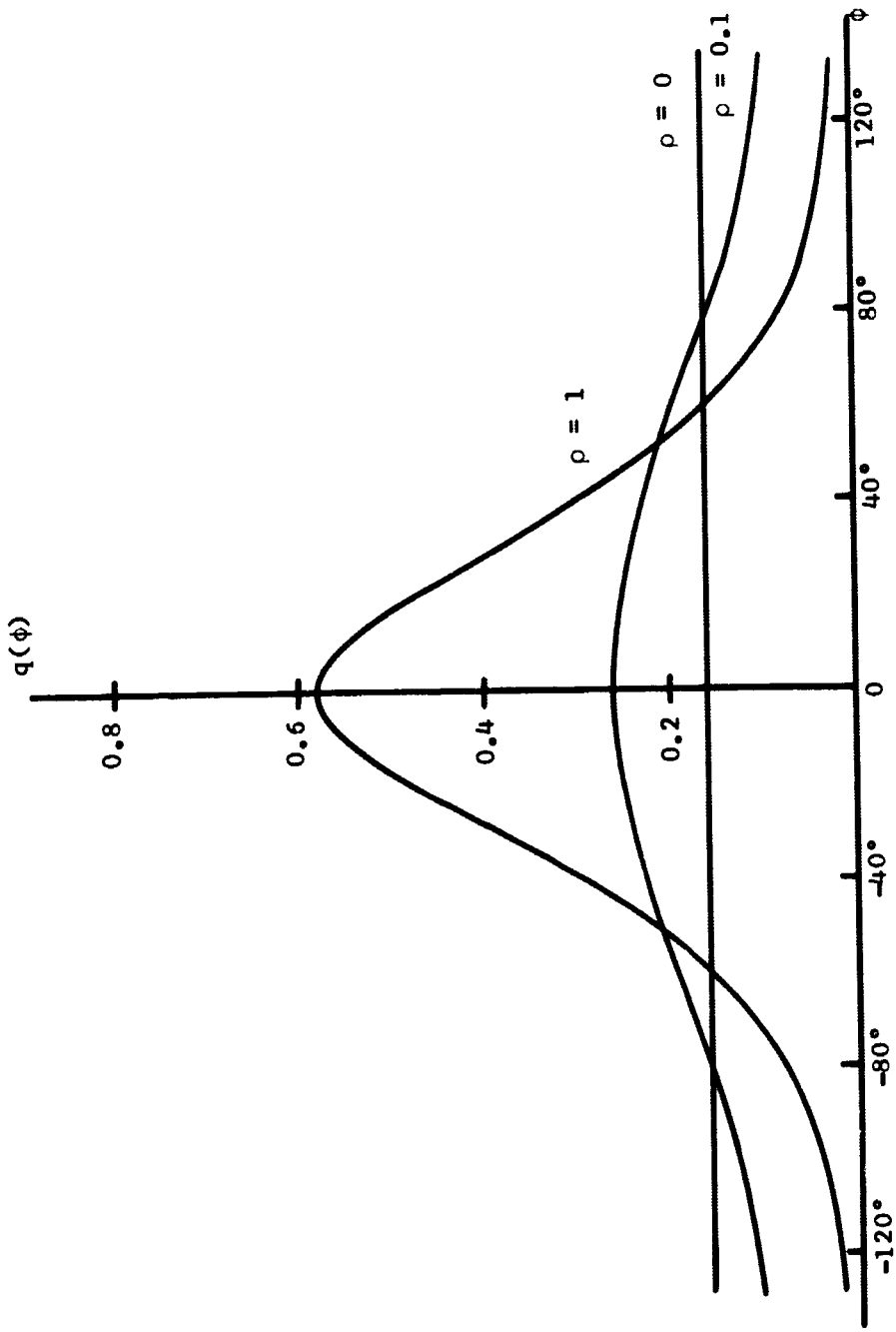

Figure 2-4 Density Function $q(\psi)$ for Small ρ

This expression is useful because the standard deviation,

$$\sigma_\phi = \frac{1}{\sqrt{2\rho}} , \tag{2.43}$$

is the rms phase error. The above equation is plotted in Figure 2-5, where ϕ is expressed in degrees. This phase error is divided in phase for channel carrier frequencies less than the pilot frequency and multiplied for higher carrier frequencies. In other words, if a pilot on Channel 16 has a phase error of 6 degrees, the Channel 8 demodulation carrier would have a phase error of 3 degrees. The mechanism by which this occurs is illustrated in Appendix F. As stated previously, the effect of these phase errors is given in Appendix D for several modulation schemes.

F. OTHER CONSIDERATIONS

RF phase linearity and the baseband crest factor are of interest when the demodulation carriers are to be synthesized from a common pilot. Both of these problems arise because in order to derive the demodulation carrier from the pilot, all carriers must be harmonically related and have a known phase relationship. This relationship is established prior to transmission and must be maintained through the RF link. Also, because of this fixed phase relationship, the crest factor of the baseband can be adversely affected.

RF Phase Linearity. Since the exact phase characteristic of a typical RF link is unknown, the assumption of linear phase was verified experimentally using standard telemetry hardware.[9] Typical results are illustrated in Figures 2-6 and 2-7. As the IF and output filters in the receiver were changed, the slope of the phase characteristic also changed, but all filters exhibited excellent linearity to approximately 150 kHz.

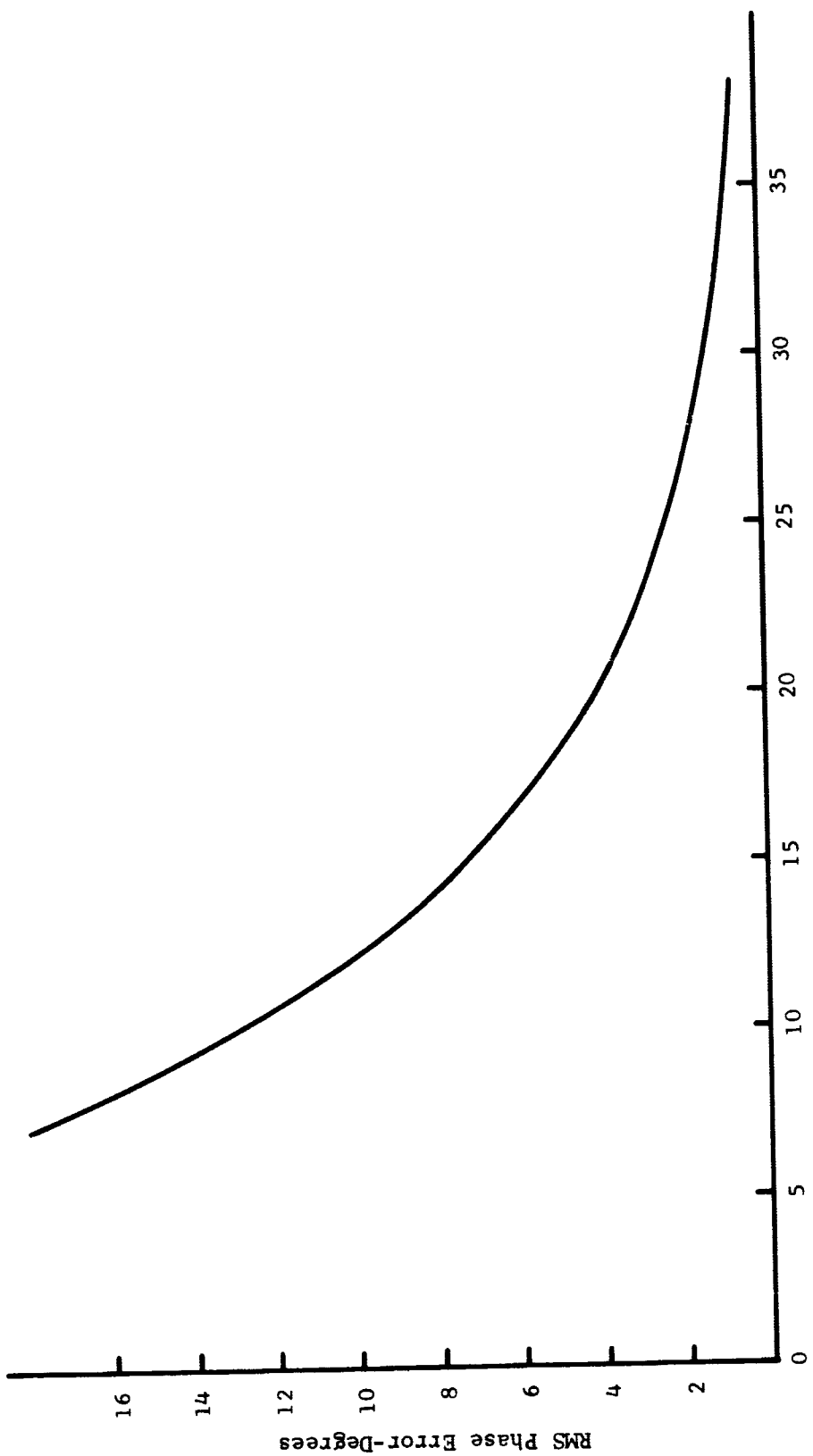

Figure 2-5 RMS Phase Error vs. Signal-to-Noise Ratio

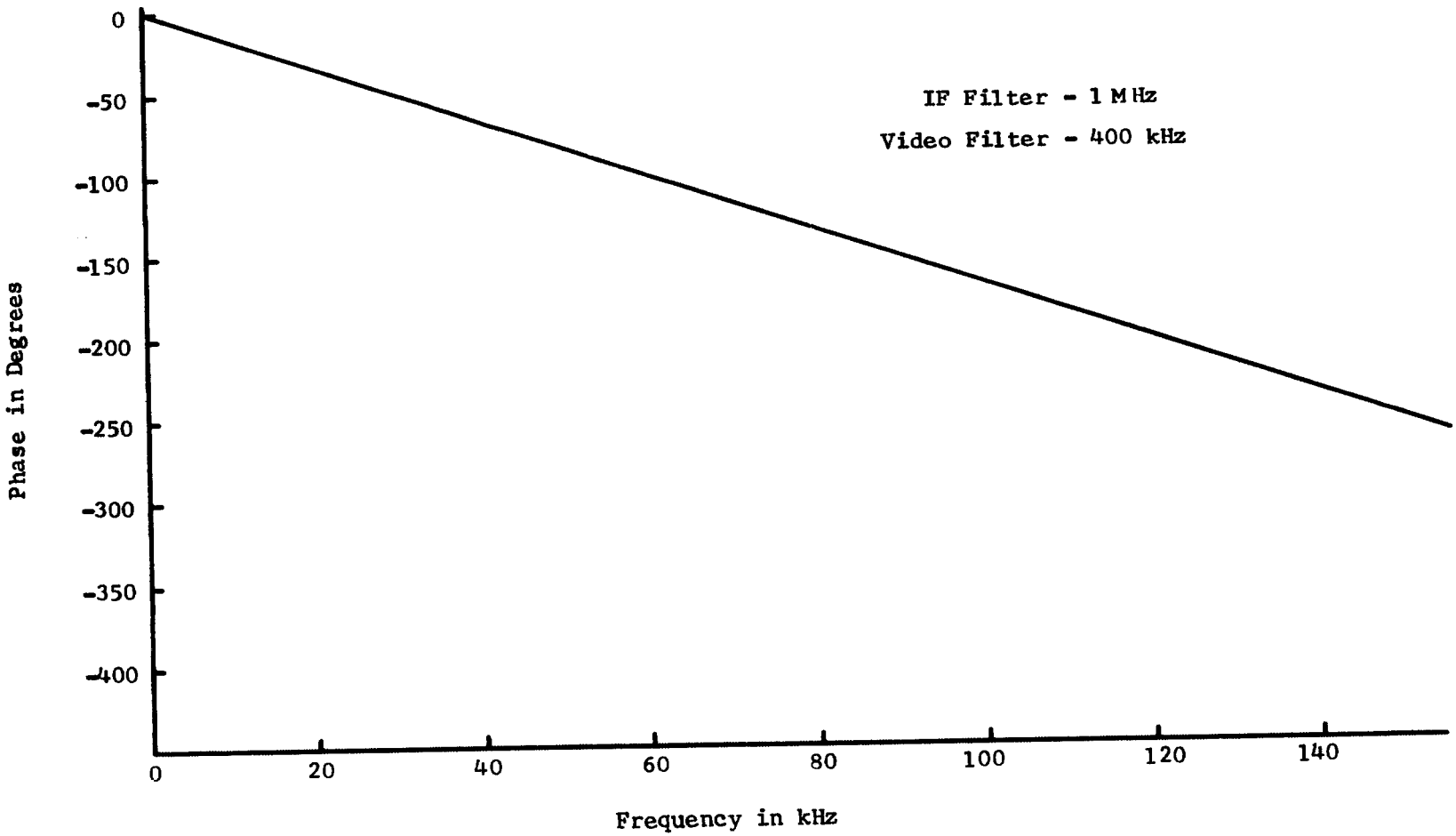

Figure 2-6 Phase Characteristic of 248.6 MHz RF Link

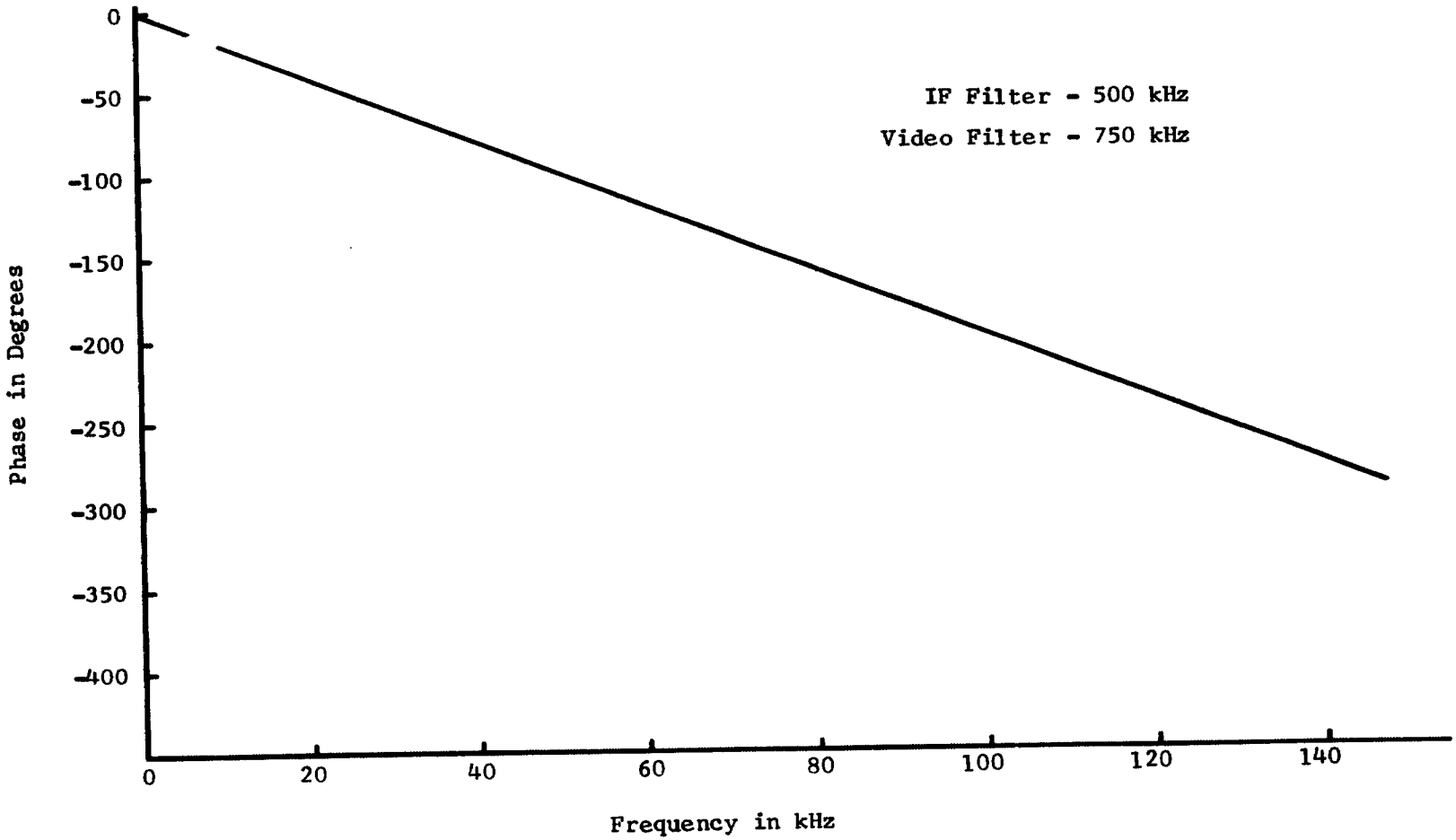

Figure 2-7 Phase Characteristic of 2277.5 MHz RF Link

Baseband Crest Factor. Since the baseband signal is used to deviate the FM transmitter, the crest factor of the baseband signal determines the peak deviation; thus, it is an important parameter. If the crest factor is high the transmitter sensitivity must be sufficiently low so that the signal peaks do not deviate the transmitter beyond its linear region. This yields a low rms deviation resulting in a lower signal-to-noise ratio.

The baseband crest factor was determined by programming a digital computer to represent a 15 channel baseband with statistically independent random modulation on each channel. The channel carriers were harmonically related and had a fixed phase relationship. The modulation signal for a given channel was represented by 10 sinusoids having random initial phase. The peak value of the total baseband signal, S(t), was defined as that value which $|S(t)|$ exceeded one percent of the time.

Since pre-emphasis is usually used in FM links to compensate for the triangular noise spectrum at the output of the FM receiver, this was also considered. The pre-emphasis characteristic was assumed to have a breakpoint midway in the baseband with a slope of 6 dB per octave.

The results of the investigation are illustrated in the table, where ψ_n is the initial phase of the Channel-n carrier. The values given in the table represent an average obtained from six computer runs. This was done to compensate round-off errors and the initial phase effects of the modulation. For random modulation it is concluded that the carrier phase is unimportant. This is expected, since in a suppressed carrier system the carrier phase is masked

Channel Modulation	Case	Ratio of Peak to RMS	
		With Pre-Emphasis	Without Pre-Emphasis
Random Modulation on all Channels	$\psi_n = 0$ all n	2.62	2.58
	$\psi_n = \begin{cases} 0 & n \text{ odd} \\ \pi & n \text{ even} \end{cases}$	2.65	2.63
	ψ_n Random	2.65	2.58
Dc Modulation on all Channels	$\psi_n = 0$ all n	4.72	5.10
	$\psi_n = \begin{cases} 0 & n \text{ odd} \\ \pi & n \text{ even} \end{cases}$	4.35	4.72
	ψ_n Random	2.40	2.55

Baseband Crest Factor as a Function of Carrier Phase

by the modulation, i.e., there is no component in the baseband spectrum having identically the channel carrier phase. It is also clear from the results that pre-emphasis has little effect on the crest factor.

For random modulation without pre-emphasis, the theoretical value of the crest factor is approximately 2.58. This follows from the fact that S(t) will be nearly Gaussian since S(t) will be the sum of a large number of statistically independent sinusoids. With the definition of peak value, assuming a Gaussian distribution yields

$$\frac{1}{\sqrt{2\pi}} \int_{-z}^{z} \exp\left[\frac{-t^2}{2}\right] dt = 0.99$$

or

$$\frac{1}{\sqrt{2\pi}} \int_{0}^{z} \exp\left[\frac{-t^2}{2}\right] dt = 0.495 \ ,$$

where z is the crest factor. The value of z is found from a normal probability table to be 2.58, a value agreeing well with the experimental results.

For the case of dc modulation, the modulation was assumed to be 1 unit in amplitude and, as expected, the crest factor is a strong function of carrier phase.

G. SUMMARY

The results of the analysis show that even if the synthesized demodulation carrier perfectly tracks the carrier position in the channel, an error due to flutter occurs in both SSB and DSB systems. The error is identical in both systems and can only be reduced by

using recorders having lower flutter or by employing a scheme for TBE compensation.

In order to minimize distortion of the demodulated output, the time delay of the pilot and data channels must be matched. It should be noted that this does not require that the channel and pilot filters be identical, but only that their phase characteristics be matched.

In the SSB system a phase correction is needed to compensate for the phase imparted to the channel carrier. For the DSB case the channel carrier is assumed centered in the data channel filter resulting in no phase shift of the carrier. Therefore, the only difference in the implementation of the demodulation portion of the two systems is a phase compensation network.

Pilot noise yields a demodulation phase error which, for a given pilot signal-to-noise ratio, is a function of the channel carrier frequency relative to the pilot frequency. The pilot phase error can be determined for a given signal-to-noise ratio using Figure 2-5. In Appendix D it is shown that these errors are much more severe for SSB and QDSB than for DSB.

If all demodulation carriers in a frequency multiplexed system are to be derived from a common pilot, the phase characteristic of the RF link must be linear. The results of measurements performed on typical modern telemetry hardware indicates that basebands in excess of 150 kHz are possible before this effect becomes significant.

Finally, it appears that the phase coherence necessary between the channel carriers will not result in a high crest factor, hence no large transmitter deviations, as long as the majority of channels

are modulated with statistically independent random data. If dc modulation is expected on a large number of channels, the channel carrier phases should be chosen to minimize the baseband crest factor.

CHAPTER III

CARRIER SYNTHESIS FROM AM MODULATED CARRIERS

The carriers necessary for demodulation of a suppressed carrier AM baseband can be constructed from the modulated channel carriers instead of using a pilot. However, it will be shown that this technique is only applicable to DSB channels. In this chapter several different methods of deriving demodulation carriers will be investigated, and it will be shown that these methods have common problem areas.

A. SQUARING

One of the simplest methods of generating the carrier component from a DSB signal is to use a nonlinear network to generate a component at a harmonic of the carrier frequency, which can be divided in frequency to give the required carrier. As an example of this process consider the network defined by

$$y(t) = \beta_1 x(t) + \beta_2 x^2(t) + \beta_3 x^3(t) + \cdots , \tag{3.1}$$

to have as an input

$$x(t) = m(t) \cos \omega_n t . \tag{3.2}$$

Substitution of (3.2) into (3.1) yields the output

$$y(t) = \beta_1 m(t) \cos \omega_n t + \frac{\beta_2}{2} m^2(t)\left[1 + \cos 2\omega_n t\right]$$

$$+ \frac{\beta_3}{4} m^3(t)\left[3 \cos \omega_n t + \cos 3\omega_n t + \cdots\right]. \tag{3.3}$$

For k even, $m^k(t)$ has a positive dc value; consequently, even harmonics of the Channel-n carrier are always present at the nonlinear network output. One of these components can be extracted from y(t) by a narrow bandwidth filter or a zero detection scheme, which will be discussed in a following section. After extraction, the frequency of the selected harmonic is divided by the appropriate integer to yield the required demodulation carrier.

There are two general problems resulting from this method of carrier synthesis, which can be illustrated by assuming the nonlinear network to be a square-law device, i.e.,

$$\beta_n = \begin{cases} 0 & n \neq 2 \\ 1 & n = 2 \end{cases}$$

For this special case

$$y(t) = e^2_{DSB}(t) = \frac{1}{2} m^2(t) + \frac{1}{2} m^2(t)\cos 2\omega_n t \ . \qquad (3.4)$$

The second term in (3.4) is equivalent to a carrier, $\cos 2\omega_n t$, amplitude modulated by a signal $\frac{1}{2} m^2(t)$. Since $m^2(t)$ has a positive dc value, the modulation is not suppressed carrier, i.e., a carrier component is present at $2\omega_n$.

The first problem is that if m(t) is zero, the DSB signal vanishes, and the carrier synthesis system ceases to operate resulting in a loss of the demodulation carrier. When the modulation, m(t), again becomes nonzero, the carrier synthesis system takes a finite time to restore the demodulation carrier, and during this acquisition time, which can be several ms., data can be lost. One method of correcting this problem is to place a pilot on each channel, having a frequency higher

than the highest modulation frequency, as shown in Figure 3-1(a). The DSB signal for this case is

$$e_{DSB}(t) = \left[\cos \omega_p t + m(t)\right] \cos \omega_n t \ , \tag{3.5}$$

a signal having components at $\omega_n + \omega_p$ and $\omega_n - \omega_p$ independent of the modulation. Thus, if m(t) becomes zero, the carrier synthesis portion of the system can still operate. The main difficulty with this approach lies in the pilot position relative to the modulation spectrum, since the pilot must be removed from the data in the demodulator. If the pilot is placed too close to the data spectrum, the filtering problem for removing the pilot becomes difficult. Placing the pilot at a higher frequency results in poor spectrum utilization because of the bandwidth requirements. Spectrum utilization becomes quite important when a large number of channels are frequency multiplexed to form a baseband, as illustrated in Figure 3-1(b).

The second problem arises because the carrier is formed from its second harmonic. This gives rise to a phase ambiguity in the synthesized carrier because the initial phase of the synthesized carrier can be in error by π radians if only second harmonic information is available. Mathematically, this can be seen in the following manner. If $\cos \omega t$ is squared the result is

$$\cos^2 \omega t = \frac{1}{2} + \frac{1}{2} \cos 2\omega t \ , \tag{3.6}$$

and squaring $\cos\left[\omega t + \pi\right]$ yields

$$\begin{aligned} \cos^2\left[\omega t + \pi\right] &= \frac{1}{2} + \frac{1}{2} \cos\left[2\omega t + 2\pi\right] \\ &= \frac{1}{2} + \frac{1}{2} \cos 2\omega t \ , \end{aligned} \tag{3.7}$$

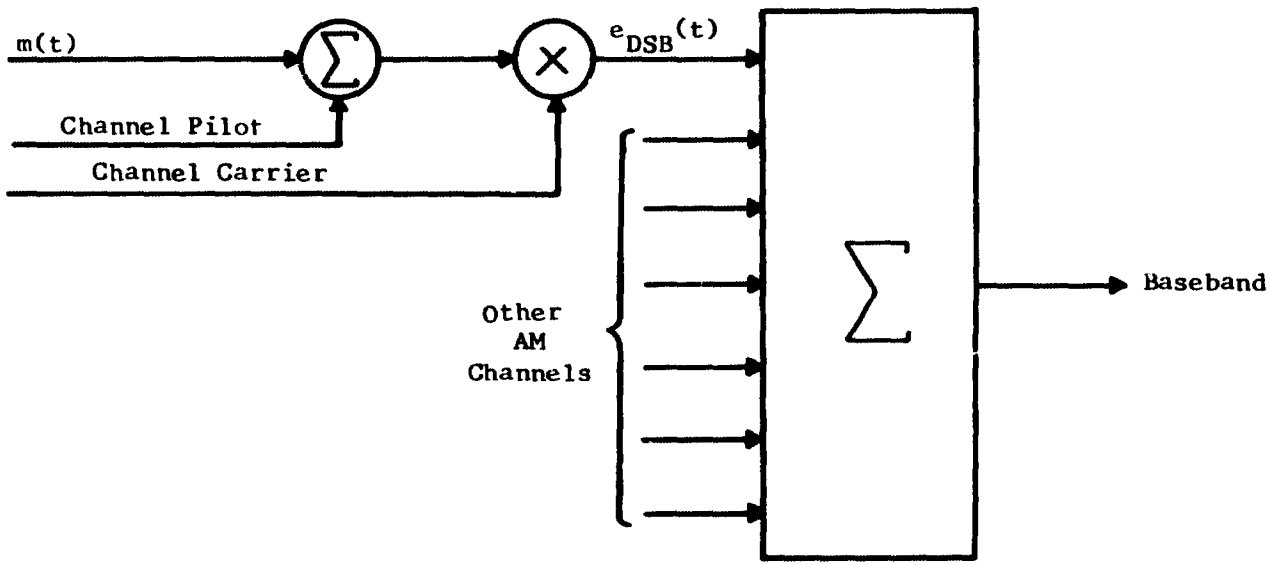

(a) Baseband Construction

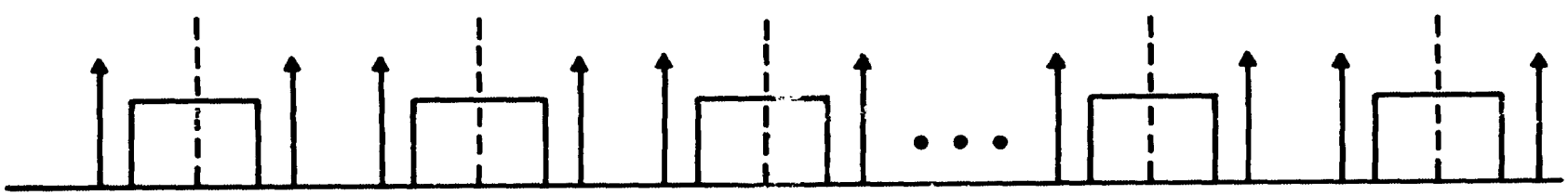

(b) Baseband Spectrum

Figure 3-1 AM-Baseband Formation

which is an identical result. Thus, given the signal

$$e^2(t) = \frac{1}{2} + \frac{1}{2}\cos 2\omega t \ , \qquad (3.8)$$

there is no way of determining the phase of e(t) without additional information. A π radian phase ambiguity in the demodulation carrier is equivalent to a polarity ambiguity in the demodulated data.

It should be noted that a phase ambiguity exists in any system in which the demodulation carrier is derived by dividing some harmonic of the carrier. The degree of ambiguity depends upon which harmonic is used to generate the demodulation carrier. As we have seen, using the second harmonic led to a situation where two initial phases of the fundamental gave the same second harmonic. Four different phases will give the same fourth harmonic, and so on. Thus, the higher the harmonic used for synthesis, the more difficult ambiguity resolution becomes. This ambiguity must be removed prior to demodulation.

In order to completely remove all phase ambiguities the fundamental carrier, usually the Channel-1 carrier, must be established. This can be accomplished by letting the Channel-1 carrier be unmodulated, modulated such that the modulation index of the Channel-1 signal is less than unity, or by using pilots on two adjacent channels such that their beat frequency is the Channel-1 carrier.

B. COSTAS DEMODULATORS

The Costas demodulator,[10] often referred to as the Costas or quadrature phase-lock loop (PLL), is a scheme by which a DSB signal is demodulated with a carrier generated from the sidebands of a DSB

signal with a voltage-controlled oscillator (VCO). The VCO output is the demodulation carrier.

In order to investigate the operation of the Costas demodulator, illustrated in Figure 3-2, assume that the input to the loop is

$$e_{in}(t) = m(t) \cos \omega_n t \ , \tag{3.9}$$

where m(t) represents the modulation. The nominal VCO frequency is equal to the carrier frequency, ω_n, and its output can be expressed as

$$e_{VCO}(t) = \cos\left[\omega_n t + \theta_e(t)\right] \ , \tag{3.10}$$

where $\theta_e(t)$ is a time-varying phase error. The action of the loop is to generate a signal proportional to $\theta_e(t)$, which is then applied to the VCO input in order to correct the VCO phase. Thus, $\theta_e(t)$ is driven to zero.

The manner in which this is accomplished is easily explained. The output of the first phase detector is $\left[e_{in}(t)\ e_{VCO}(t)\right]$, with the high frequency term filtered out. Now

$$e_{in}(t)e_{VCO}(t) = m(t) \cos \omega_n t \cos\left[\omega_n t + \theta_e(t)\right] \ , \tag{3.11}$$

which, after filtering, yields

$$e_{\phi 1}(t) = \frac{1}{2} m(t) \cos \theta_e(t) \ . \tag{3.12}$$

In the same manner, $e_{\phi 2}(t)$ is given by $e_{in}(t)\ e_2(t)$ with the high frequency term filtered out, where $e_2(t)$ is $e_{VCO}(t)$ shifted 90° in phase. The result is

$$e_{\phi 2}(t) = \frac{1}{2} m(t) \sin \theta_e(t) \ . \tag{3.13}$$

The output of the product device preceding the loop filter can be written as

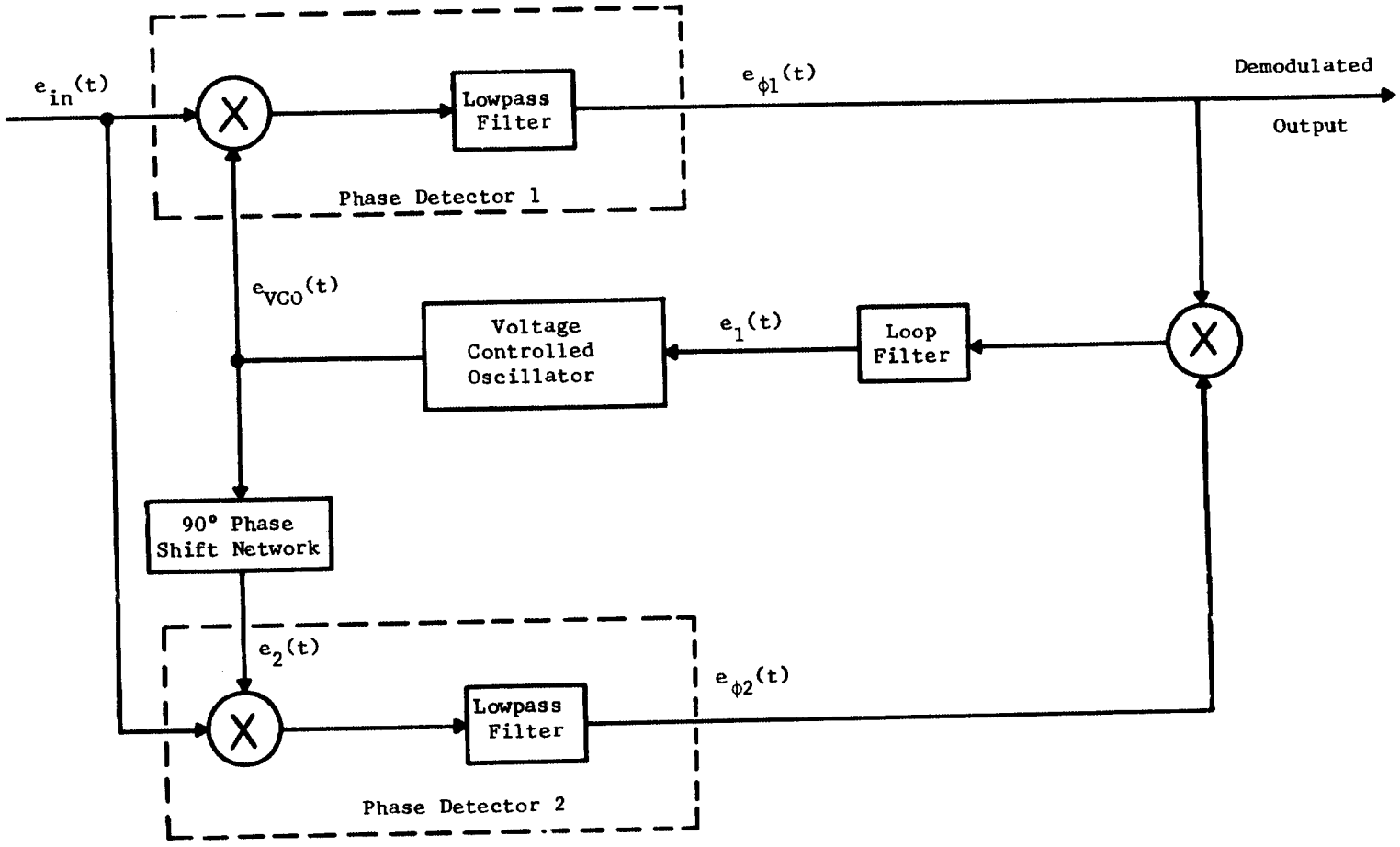

Figure 3-2 Costas Demodulator

$$e_{\phi 1}(t)e_{\phi 2}(t) = \frac{1}{8} m^2(t) \sin 2\theta_e(t) , \qquad (3.14)$$

which is

$$\frac{1}{8} m^2(t)\ 2\theta_e(t)$$

for small values of $\theta_e(t)$. The phase error, $\theta_e(t)$, is a slowly varying function of time, while $m^2(t)$ has much higher spectral content. The loop filter is a lowpass filter which ideally passes $\theta_e(t)$ but not the modulation. Thus

$$e_1(t) = K\ \theta_e(t) , \qquad (3.15)$$

which controls the VCO in such a manner as to reduce $\theta_e(t)$. Therefore, the output of the first phase detector is the demodulated output for the channel.

One disadvantage of this scheme is that modulating signals having near dc components are passed by the loop filter and adversely affect the VCO control voltage. This effect limits the low-frequency response of the channel using this type of demodulator.

There are also two other problems of interest, both of which also arise in the squaring scheme. These are phase ambiguity and the effect of zero modulation. Equation (3.17) shows that the error control voltage is proportional to $\sin 2\theta_e(t)$; thus the error voltage is the same for incremental changes in $\theta_e(t)$ about zero as for incremental changes about π radians. This is equivalent to stating that a π-radian phase ambiguity exists in the synthesizsd demodulation carrier. As with the squaring scheme, resolution of the ambiguity requires additional information such as could be obtained from a pilot.

Another problem with the Costas loop, as with the squaring scheme, is that if m(t) should go to zero and remain there for several cycles of the channel carrier, the input to the loop would fall to zero, and consequently the loop would cease operating properly. The loop would have to re-acquire lock when m(t) becomes nonzero, the result being lost data. This problem can be eliminated by using pilots for each channel as discussed previously. In the absence of modulation, the pilot signal remains as an input to the Costas loop, allowing continuous operation.

C. THE LDRM SCHEME

Since the output of a DSB modulator is given by the product of the modulation and carrier signals, the DSB signal has zero crossings at both the carrier and modulation zeros. The carrier necessary for demodulation can be synthesized from these zero crossings.[11,12,13]

The demodulation system is illustrated in Figure 3-3. The channel filter selects the proper channel from the baseband spectrum. The output of the channel filter is the DSB signal to be demodulated and to be used for synthesis of the demodulation carrier. The operation of the carrier synthesis loop can be explained using Figure 3-4, which illustrates the waveforms present at various points in the loop.

The DSB signal is first amplitude limited to form a pulse train. Differentiating this pulse train forms a series of impulse functions which mark the time of the carrier and modulation zero crossings. The full-wave rectifier gives all impulses a positive polarity and provides triggers for a monostable-multivibrator (MSMV) of duty cycle δ, which is defined as

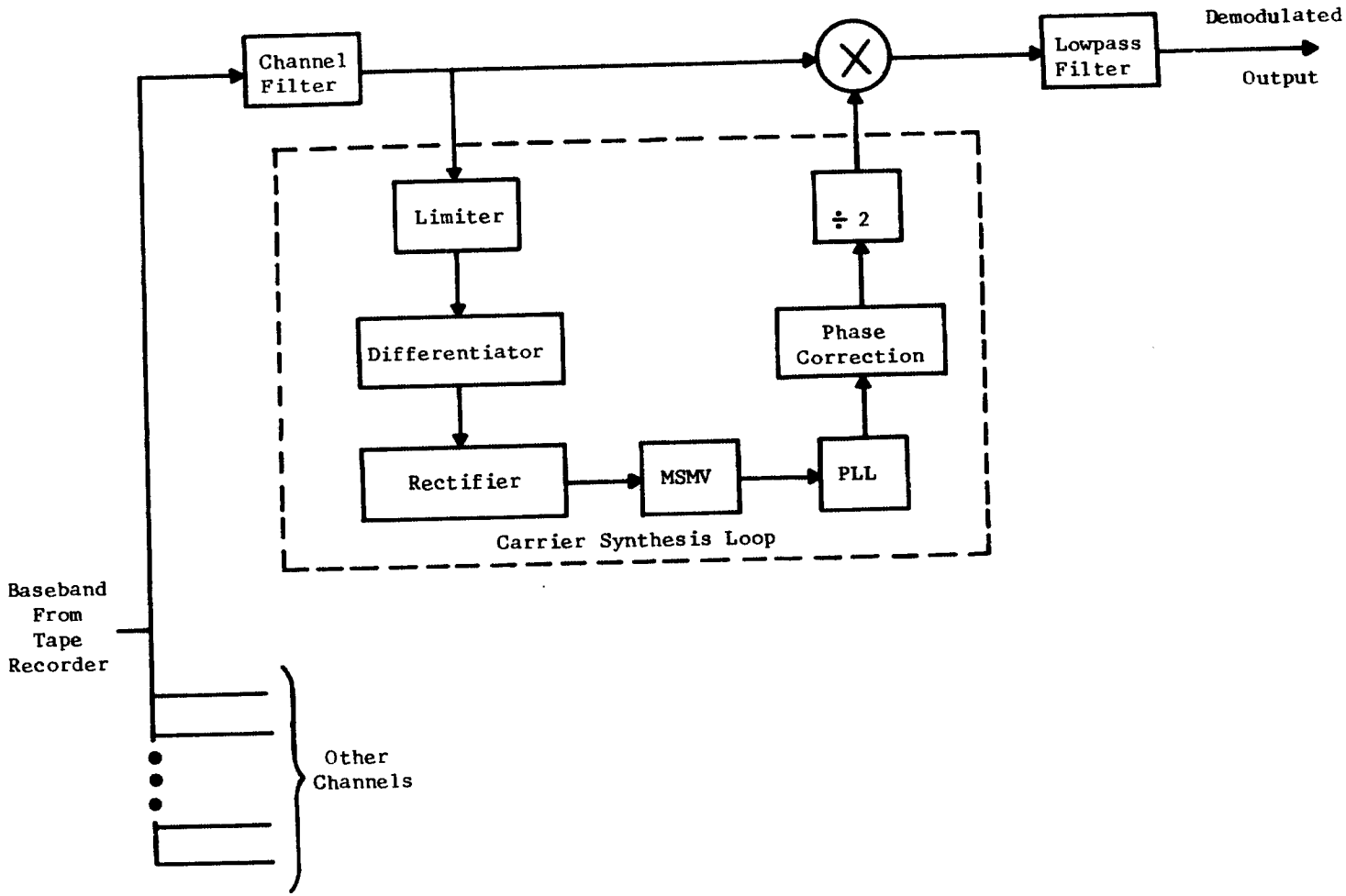

Figure 3-3 AM-Baseband Demodulator

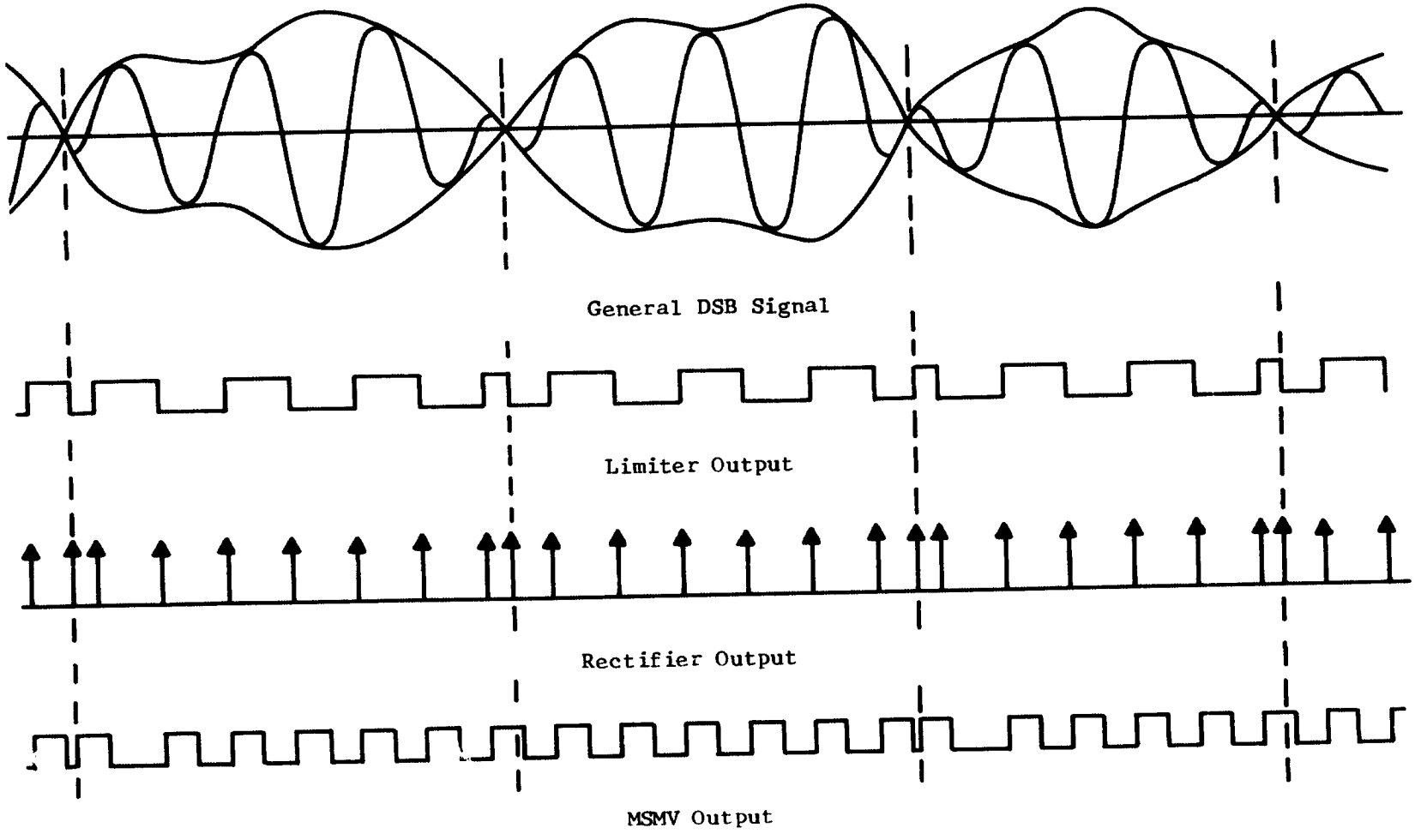

Figure 3-4 Generation of MSMV Output

$$\delta = \frac{\text{MSMV "on" time}}{\text{MSMV period}} \quad . \tag{3.16}$$

The MSMV output is a pulse train having a nominal repetition rate equal to twice the channel carrier frequency.

The leading edges of the MSMV output exactly marks the time of the carrier zero crossings, except perhaps upon the occurrence of a modulation zero crossing. The modulation zero crossings perturb the MSMV output only when they occur during the MSMV "off" times. This perturbation, when present, takes the form of a MSMV pulse shifted to the left. If δ is 0.5 or greater, no additional pulses can appear in the MSMV output.

Since perturbations result only when modulation zeros occur during the MSMV "off" time, the action of the MSMV is to eliminate the effect of a certain percentage of modulation zeros. This percentage is directly dependent upon δ. As δ approaches one, the percentage of perturbations resulting from modulation zero becomes small. The result of this action will be discussed in Chapter IV, where it will be shown that large duty cycles in the presence of noise can lead to undesirable results.

The PLL is assumed to track the fundamental of the MSMV output pulse train. The signal formed, after phase correction and division by two, yields the demodulation carrier. The frequency division is necessary because the MSMV is triggered twice every carrier period making the MSMV fundamental twice the carrier frequency. The need for phase correction results from the inherent 90° phase shift in the PLL, and the phase shift caused by the MSMV if δ is different from 0.5. The action of the divide-by-two network will be discussed

in the following chapter when a signal is carried through the carrier-synthesis system to determine the effect of recorder flutter.

Because of the cascade connection of a limiter, differentiator, rectifier and MSMV, this carrier synthesis technique will be referred to as the LDRM scheme.

D. SIGNAL RESTRICTIONS

In order for the LDRM synthesis scheme to operate properly, there must exist a one-to-one correspondence between the carrier zero crossings and the zero crossings of the signal present at the input to the carrier-synthesis loop. Since a DSB signal is given by

$$e_{DSB}(t) = m(t)c(t) , \tag{3.17}$$

it is clear that zero crossings of both m(t) and c(t) yield zero crossings of $e_{DSB}(t)$. If the carrier frequency is much larger than the highest frequency contained in m(t), most of the zero crossings will be due to the carrier and the scheme will not function properly. The effect of the zero crossings of m(t) will be investigated in Chapter IV.

The zero crossings of a single-sideband signal do not in general correspond to the carrier zero crossings. This can be seen by considering the SSB signal

$$e_{SSB}(t) = \cos(\omega_n + \omega_m)t . \tag{3.18}$$

Since $(\omega_n + \omega_m)$ is not the carrier frequency, the zeros of $e_{SSB}(t)$ are not those of the channel carrier.

Similarly, demodulation carriers cannot be derived from the QDSB signal

$$e_Q(t) = m_1(t) \cos \omega_n t + m_2(t) \sin \omega_n t \ , \qquad (3.19)$$

where $m_1(t)$ and $m_2(t)$ are the modulating signals on the direct and quadrature carriers. The above expression can be written as

$$e_Q(t) = \sqrt{m_1^2(t) + m_2^2(t)} \cos\left[\omega_n t + \phi(t)\right] \ , \qquad (3.20)$$

where

$$\phi(t) = -\tan^{-1} \frac{m_2(t)}{m_1(t)} \ . \qquad (3.21)$$

Since $\phi(t)$ is zero only if $m_2(t)$ is zero, the QDSB signal does not in general have zeros independent of the modulation; therefore, the demodulation carriers cannot be synthesized from a quadrature multiplexed signal.

There are special cases where a demodulation carrier can be synthesized from a QDSB signal. For example, when the spectra of one modulating signal has significant frequency content in a region where the spectra of the other modulating signal is zero, filtering can be utilized to yield a DSB signal. This is illustrated in Figure 3-5 for the case where $m_2(t)$ has no low frequency content. Filtering $e_Q(t)$ yields a DSB signal from which a demodulation carrier can be synthesized. When $m_1(t)$ and $m_2(t)$ have similar spectra, a pilot can be added to one of the signals. The pilot can then be filtered out to yield a DSB signal.

It has been shown that demodulation carriers can only be derived from modulated channel carriers if the modulation is DSB. In the following chapter the LDRM synthesis technique will be analyzed to determine the effect of tape recorder flutter, noise and modulation zeros.

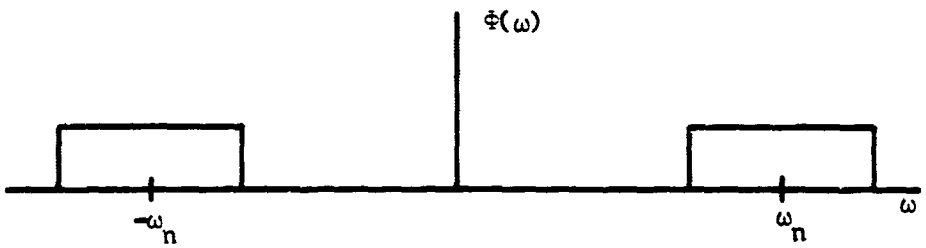

Spectra of $m_1(t) \cos \omega_n t$

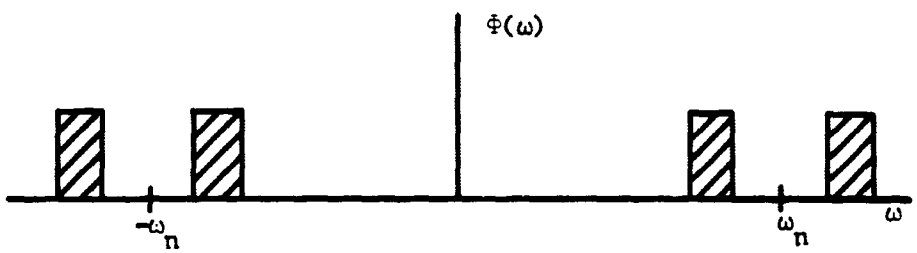

Spectra of $m_2(t) \sin \omega_n t$

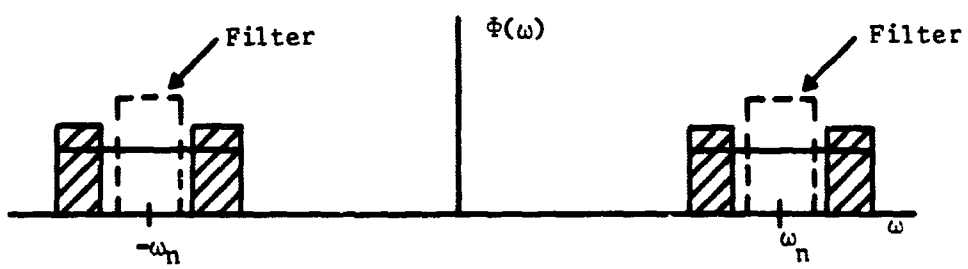

Spectra of $e_Q(t)$

(Filtering with a filter having the illustrated chatacteristic yield a DSB signal which can be used for synthesis.)

Figure 3-5 Carrier Synthesis from a Quadrature DSB Signal

CHAPTER IV

ANALYSIS OF THE LDRM CARRIER SYNTHESIS METHOD

The effect of flutter, modulation zeros and noise on the LDRM carrier synthesis system will be determined in this chapter. The analysis will yield the demodulation carrier phase error due to each of these effects, and the design techniques necessary to minimize this phase error. The rms error in the demodulated data output is related to the demodulation phase error in the DSB analysis in Appendix D. The analysis will consider only DSB signals since, as shown in Chapter III, the LDRM technique can only be used for carrier synthesis if DSB modulation is used to form the channel carrier.

A. EFFECT OF FLUTTER FOR SINUSOIDAL MODULATION

As stated in Chapter II, the major effect of tape recorder flutter is to impart a time-base error (TBE) to the signal being recorded. The TBE results in a phase modulation of each component in the recorded spectrum, the magnitude of which is proportional to the frequency of the recorded signal. The Channel-n signal is therefore

$$e_n(t) = \cos\left[(\omega_n + \omega_m)t + \frac{\omega_n + \omega_m}{\omega_n}\,\theta(t)\right] + \cos\left[(\omega_n - \omega_m)t + \frac{\omega_n - \omega_m}{\omega_n}\,\theta(t)\right] , \tag{4.1}$$

where $\theta(t)$ is the phase perturbation of the channel carrier due to flutter. Since the expression for the channel pilots will be (4.1) with the modulating frequency, ω_m, replaced by the pilot frequency, ω_p, the pilots can be neglected with no loss in generality.

If the pilots are neglected, (4.1) becomes the expression for the Channel-n portion of the channel filter input illustrated in Figure 2-4. The channel filter output is computed using the quasi-state approximation, as was done in Chapter II. Since (4.1) is the DSB signal assumed in Chapter II, the channel filter output, $e_{cf}(t)$, is (2.23) with ω_p replaced by ω_n. This yields

$$e_{cf}(t) = \cos\left[(\omega_n + \omega_m)t + \frac{\omega_n + \omega_m}{\omega_n}\theta(t) + S_n\omega_m + S_n\frac{\omega_n + \omega_m}{\omega_n}\dot{\theta}(t)\right] + \cos\left[(\omega_n - \omega_m)t + \frac{\omega_n - \omega_m}{\omega_n}\theta(t) - S_n\omega_m + S_m\frac{\omega_n - \omega_m}{\omega_n}\dot{\theta}(t)\right] , \tag{4.2}$$

where S_n is the slope of the phase characteristic of the channel filter. This is the signal which is to be demodulated, and the signal from which the demodulation carrier is to be synthesized.

The response of the carrier synthesis loop to $e_{cf}(t)$ is easily explained. The limiter removes all amplitude information from the filter output and retains only carrier and modulation zero crossings. The effect of modulation zero crossings on the carrier-synthesis loop will be determined in the next section so that here ω_m will be assumed zero. Under this assumption, the input to the limiter is

$$e_{cf}(t) = 2\cos\left[\omega_n t + \theta(t) + S_n\dot{\theta}(t)\right] . \tag{4.3}$$

As illustrated in Figure 3-4, the leading edges of the MSMV output are at the zero crossings of $e_{cf}(t)$.

Figure 4-1 illustrates three zero crossings of the carrier and consequently three MSMV output pulses. The MSMV duty cycle, δ, is 0.50 in the illustration; therefore, the positive-going zero crossings of the MSMV fundamental frequency are coincident with the channel-

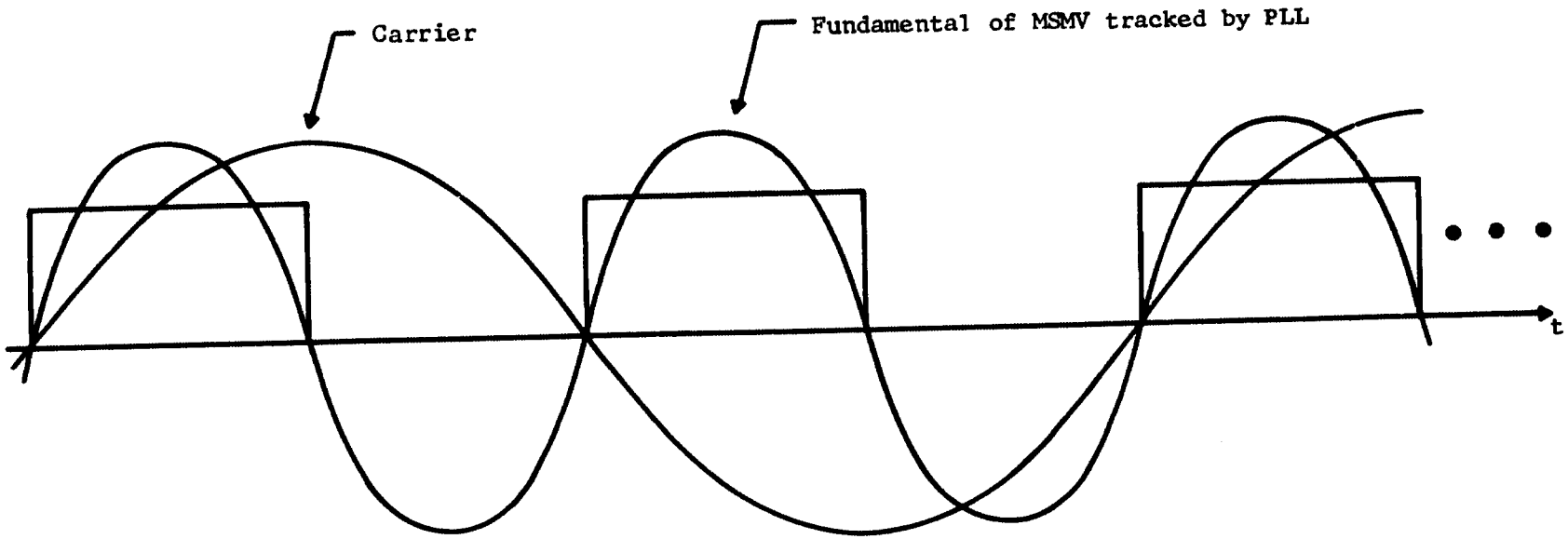

Figure 4-1 MSMV Output

carrier zero crossings. If δ is not 0.50, the zero crossings of the MSMV fundamental are offset by a fixed value, which can be compensated in the phase-correction network following the PLL. Assuming that the PLL bandwidth is sufficiently large to track the phase perturbations due to tape recorder flutter, the PLL output will be the input shifted by $\pi/2$ radians.[14] This phase shift can also be compensated by the phase-correction network. Thus, assuming perfect tracking, the output of the phase-correction network will be the MSMV fundamental. This is, after frequency division

$$e_{sc}(t) = \cos\left[\omega_n t + \theta(t) + S_n\dot{\theta}(t)\right] \quad , \tag{4.4}$$

which is the demodulation carrier.

The divide-by-two network is the source of a π radian phase ambiguity which exists in the squaring process and in the Costas demodulator. This ambiguity arises from the rectification process which doubles the fundamental frequency of the MSMV output. This is illustrated in Figure 4-2. It can be seen that there are two possible carriers which can be derived from this divider input. The result is a π radian phase ambiguity in the synthesized demodulation carrier; consequently, a polarity ambiguity in the demodulated output.

Multiplying (4.2) by (4.4) and filtering the components centered at $2\omega_n$ yields

$$e_d(t) = \cos\Big[\underset{A}{\omega_m t} + \underset{B}{S_n\omega_m} + \underset{C}{\frac{\omega_m}{\omega_n}\theta(t)} + \underset{D}{S_n\frac{\omega_m}{\omega_n}\dot{\theta}(t)}\Big] \tag{4.5}$$

for the demodulated output. As in (2.25), the last two terms are the distortion terms. Comparison of (4.5) and (2.25) illustrates

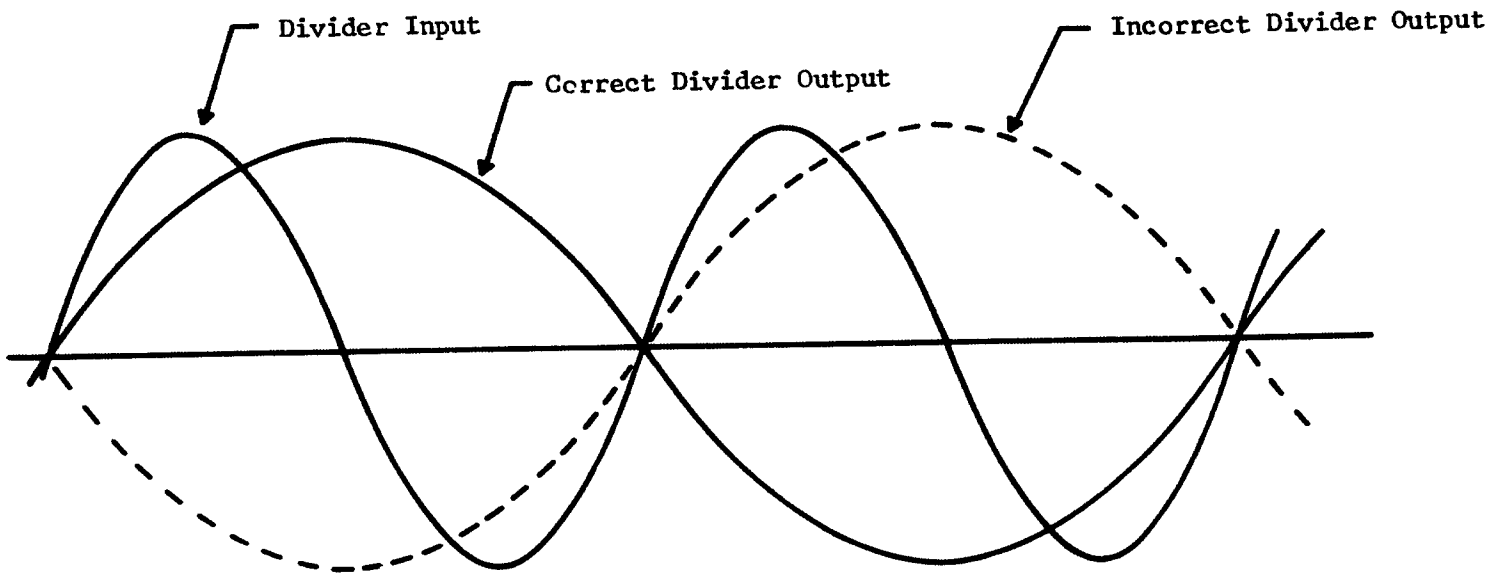

Figure 4-2 Source of Phase Ambiguity

that there is no difference in the two demodulation schemes under the conditions assumed.

Equation (4.5) was developed assuming perfect tracking of the PLL. If the bandwidth of the PLL is too small, imperfect tracking of the PLL results. If $2\psi(t)$ is the dynamic phase error due to this effect, the demodulated output becomes

$$e_d(t) = \cos\ \psi(t)\ \cos\left[\omega_n t + \frac{\omega_m}{\omega_n}\theta(t) + S_n\omega_m + S_n\frac{\omega_m}{\omega_n}\dot{\theta}(t)\right] \quad . \qquad (4.6)$$

The effect of a non-zero $\psi(t)$ on a DSB signal is studied in Appendix D and the effect of flutter on $\psi(t)$ is developed in Appendix E. The result of Appendix D illustrates that a system accuracy of one percent dictates that $\psi(t)$ must not exceed approximately eight degrees. As shown in Appendix E, $\psi(t)$ is reduced by increasing the PLL bandwidth. However, as will be shown in the following sections, when the effect of modulation zeros and noise are to be reduced, the PLL bandwidth should be as small as possible. With typical recorders, the results show that a PLL bandwidth of 200-500 Hz offers a good compromise.

B. MODULATION ZEROS

An understanding of the mechanism by which modulation zeros affect the carrier-synthesis scheme can be obtained from Figure 3-4. The limited DSB signal is a periodic pulse train except in the region of a modulation zero crossing. When the limiter output is differentiated and rectified, a series of impulses are formed, which trigger the MSMV. The MSMV output consists of a pulse train whose leading edges correspond to the carrier zero crossings except for the pulses perturbed by modulation zeros. Observation reveals that modulation

zeros result in shifted pulses when they occur during the MSMV "off" time and have no effect otherwise. The shift is always in the same direction, and the PLL responds to these pulses in a manner dependent upon the loop bandwidth. If the loop bandwidth is sufficiently large, significant phase errors in the demodulation carrier can result.

The probability that a pulse in the MSMV output will be shifted can be determined by considering the modulating waveform to have an "ideal" lowpass spectrum of bandwidth B_m Hz. For this case the average number of zero crossings per second can be written as[15]

$$z_m = 1.155\ B_m \ . \tag{4.7}$$

If the MSMV duty cycle, δ, is 50 percent or greater, no additional pulses can be inserted in the MSMV output by modulation zeros, and the number of pulses per second in the output is constant at $2f_n$. Therefore, the probability of a shifted pulse, P(SP), is the ratio of perturbed pulses to total pulses in the output or

$$P(SP) = \frac{\text{Number modulation zeros}}{\text{Number of carrier zeros}} \ \frac{\text{MSMV "off" time}}{\text{MSMV period}} \ .$$

This yields

$$P(SP) = \frac{1.155\ B_m}{2f_n}\,(1 - \delta) \ , \tag{4.8}$$

which is plotted in Figure 4-3 for three different values of MSMV duty cycle.

It is necessary to examine the behavior of the PLL to determine the effect of a shifted pulse on the demodulation carrier. A modulation zero has equal probability of falling anywhere in a carrier period since the modulation signal and the carrier are statistically independent. Therefore, the probability density function

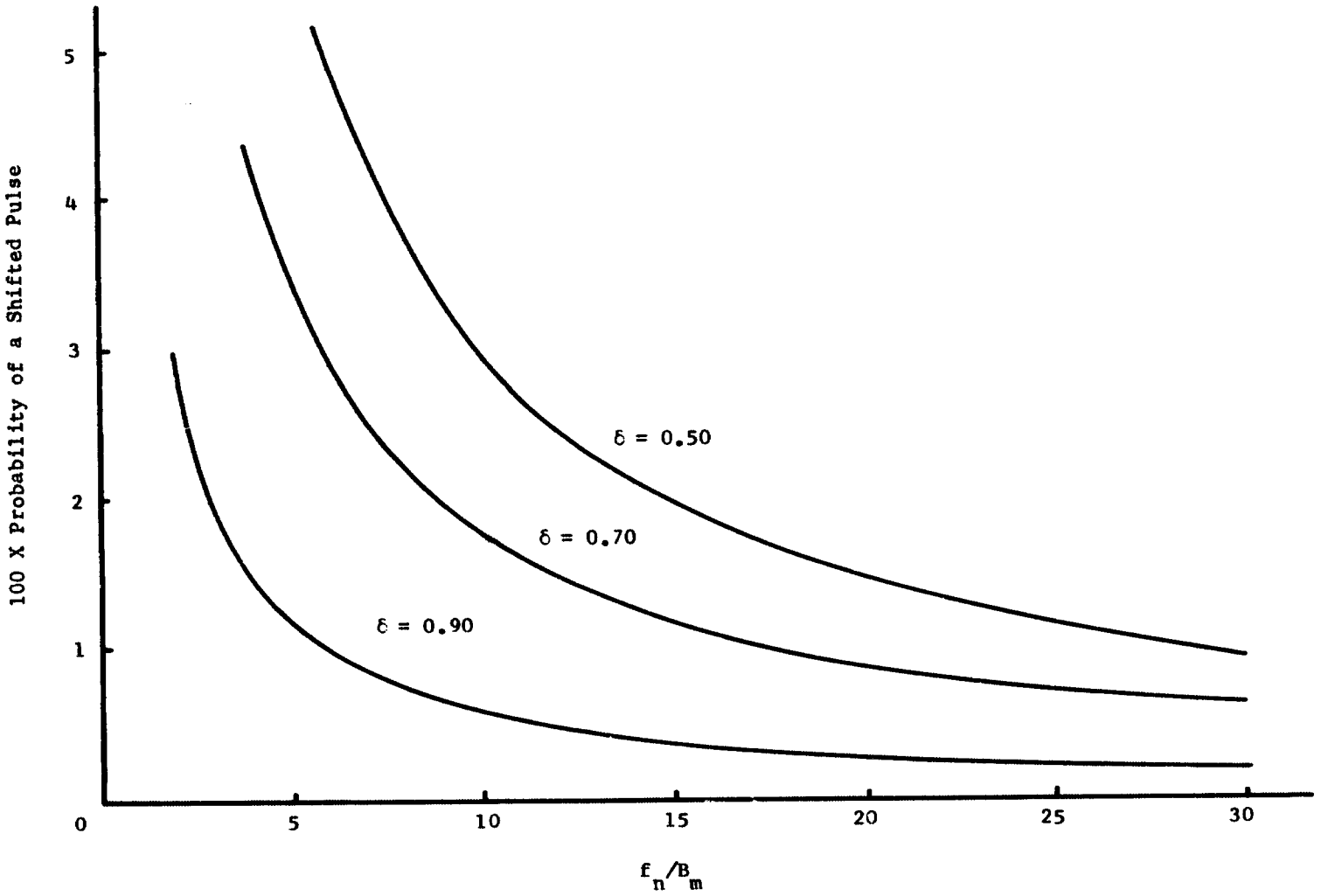

Figure 4-3 Probability of a Shifted Pulse

describing the time shift will be uniform from zero to the total MSMV "off" time, $(1 - \delta)/2f_n$. The average time shift is therefore $(1 - \delta)/4f_n$, which corresponds to a phase shift of $\pi(1 - \delta)$ radians at $2f_n$.

The peak phase shift of the PLL output corresponding to a phase shift of an input pulse can be obtained by considering the perturbed pulse to be a phase pulse, of $1/2f_n$ duration, applied directly to the input of the PLL. The response by a second-order PLL to a phase pulse is[16]

$$\theta_o(t) = K_p\left[1 - e^{-\zeta\omega_N t}\left[\cos\ \omega_N\sqrt{1-\zeta^2}\,t - \frac{\zeta}{\sqrt{1-\zeta^2}}\sin\ \omega_N\sqrt{1-\zeta^2}\,t\right]\right] \quad (4.9)$$

where K_p is the magnitude of the step input, ζ is the PLL damping factor and ω_N is the PLL natural frequency. The dynamic phase error, $\theta_e(t)$, of the PLL is

$$\theta_e(t) = \theta_i(t) - \theta_o(t) \quad (4.10)$$

and is illustrated in Figure 4-4 for two values of ζ. Also shown is the function

$$\theta_m(t) = K_p\ \exp\left[-\zeta\omega_N t\right] \quad (4.11)$$

which is used to approximate the envelope of $\theta_e(t)$.

Using the envelope approximation, the PLL output can be written as

$$\theta_o(t) = \pi(1 - \delta)\left[1 - \exp\left[-\zeta\omega_N t\right]\right] \quad , \quad (4.12)$$

for

$$0 \leq t \leq \frac{1}{2f_n}$$

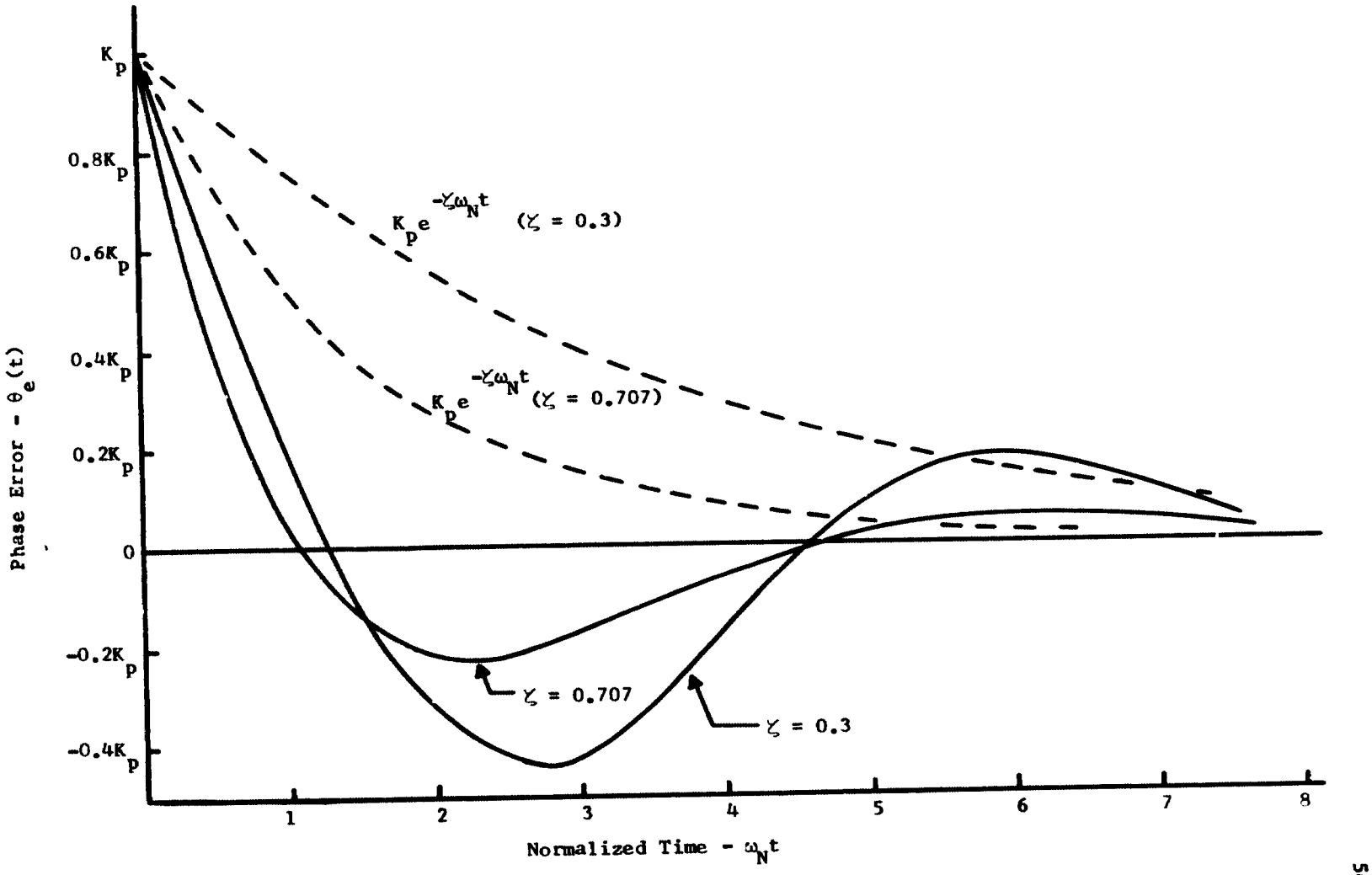

Figure 4-4 Phase-Lock Loop Response to a Phase Step

Thus, for the average phase shift the peak phase error, θ_p, in the demodulation carrier at f_n is

$$\theta_p = \frac{\pi}{2}(1 - \delta)\left[1 - \exp\left[-\frac{\zeta\omega_N}{2f_n}\right]\right] \quad , \tag{4.13}$$

which is plotted in Figure 4-5 for $\zeta = 0.707$, $\omega_N = 2\pi(500)$, and several values of δ. As the product $\zeta\omega_N$ increases, the PLL has less of a smoothing effect, and the peak phase errors become correspondingly higher. This analysis is based upon the linear model of the PLL, from which (4.9) is easily derived; therefore, lock must be maintained in order for the results to be valid.

Figure 4-3 indicates that for values of f_n/B_m greater than 10, the probability of a shifted pulse is less than 0.03. Figure 4-5 indicates that when a shifted pulse does occur, the peak phase error for the average shift is less than 3 degrees if the duty cycle is 0.50 or higher. As a rough rule it is concluded that the effect of modulation zeros will be negligible, i.e., the peak phase error will be less than approximately 3 degrees, if f_n is greater than both 15 kHz and 5 B_m, and if δ is greater than 70 percent.

C. MSMV PERTURBATIONS DUE TO NOISE

Increasing δ to minimize the effect of modulation zeros can add to other difficulties, the most important of which results from additive noise in the baseband. This difficulty can be explained by assuming the modulating signal to be a unit dc level. Under this condition, the DSB signal becomes a sinusoid at the channel carrier frequency, ω_n. The input to the limiter can be written as

$$e_{cf}(t) = \cos\left[\omega_n t + n(t)\right], \tag{4.14}$$

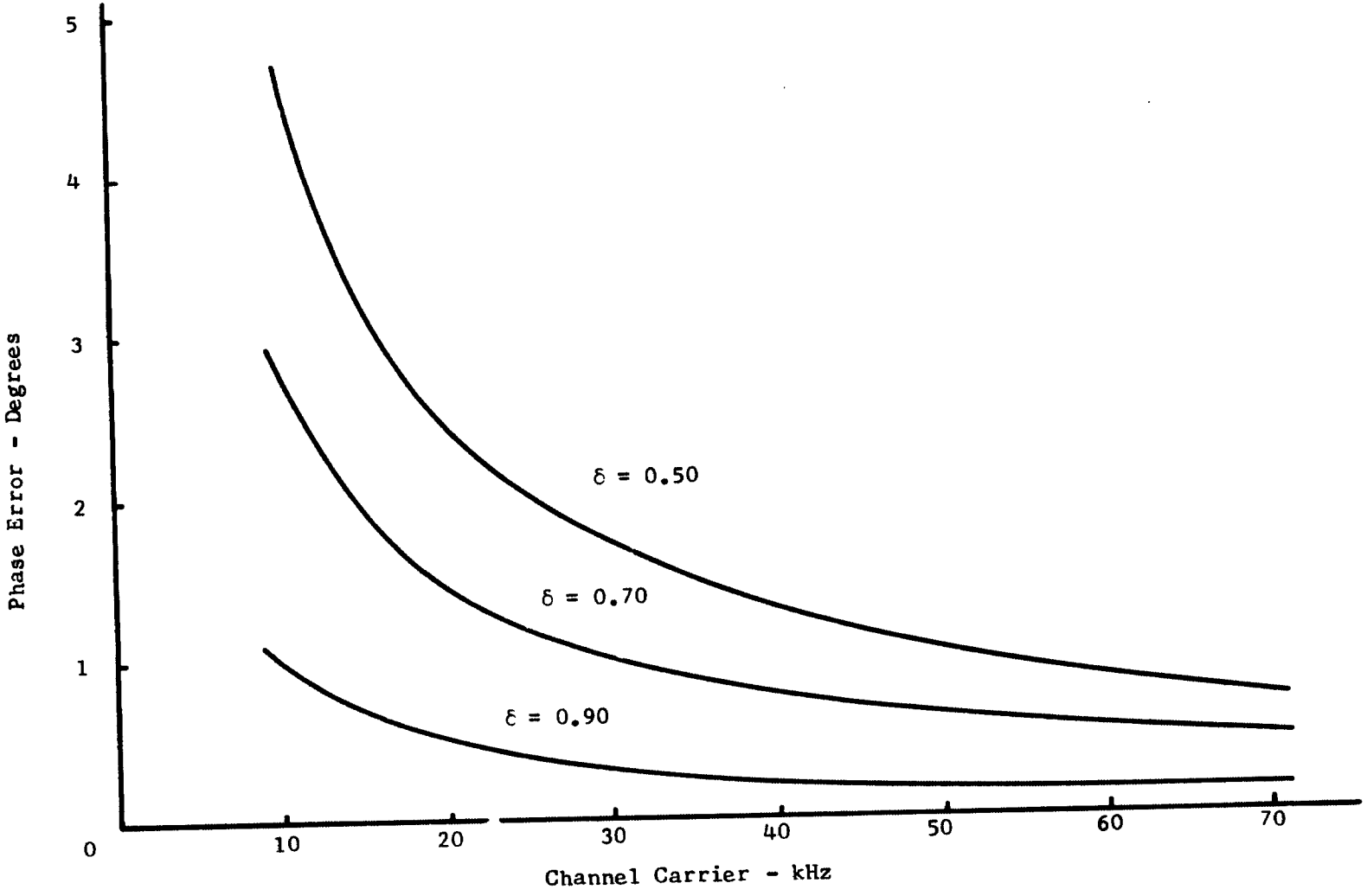

Figure 4-5 Peak Phase Error Due to Modulation Zeros

where n(t) represents additive noise which is narrowband by virture of the channel filter. Since n(t) is narrowband, (4.14) can be placed in the form[17]

$$e_{cf}(t) = R(t)\cos\left[\omega_n t + \phi(t)\right] \quad , \tag{4.15}$$

where R(t) represents the envelope and $\phi(t)$ represents phase deviation due to noise. Both R(t) and $\phi(t)$ are slowly varying functions compared to ω_n. The quantity of interest is the instantaneous frequency

$$\omega_i = \omega_n + \dot{\phi}(t) \quad . \tag{4.16}$$

The MSMV output pulse train is illustrated in Figure 4-6, where the impulse functions, δ_k, represent the MSMV triggers. As the instantaneous frequency increases, due to an increase in $\dot{\phi}(t)$ resulting from noise, the zero crossings, and hence the MSMV triggers, move closer together. This effectively increases the MSMV duty cycle since the MSMV "on" time is fixed. This is illustrated in Figure 4-7.

At a particular point, the zero crossings are separated by an amount equal to the "on" time of the MSMV, and any increase in frequency above this value results in a condition called pulse dropout (PDO). The frequency at which PDO first occurs is denoted f_{PDO}, and is illustrated in Figure 4-6. The carrier period, T_c, is

$$T_c = \frac{1}{f_n} \tag{4.17}$$

and the MSMV on-time, T_o, is

$$T = \delta \frac{T_c}{2} = \frac{\delta}{2f_n} \quad . \tag{4.18}$$

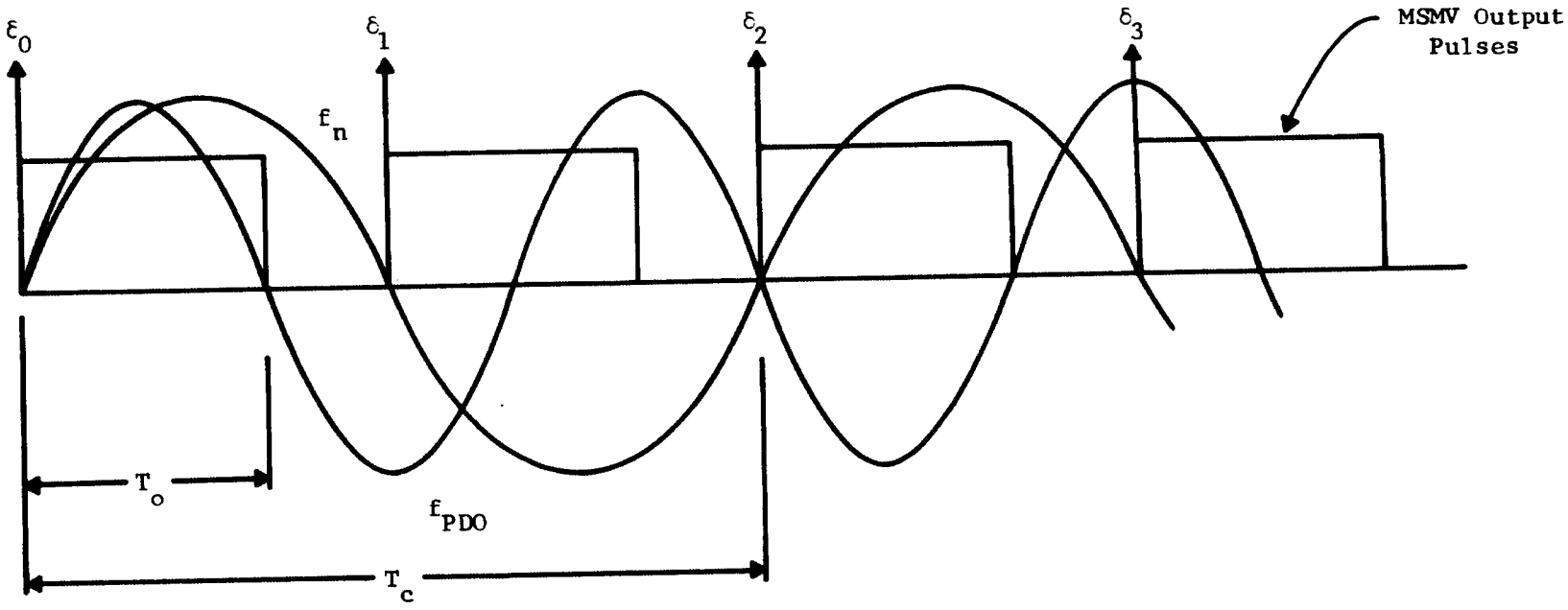

Figure 4-6 MSMV Output Illustrating the Frequency of Pulse Dropout

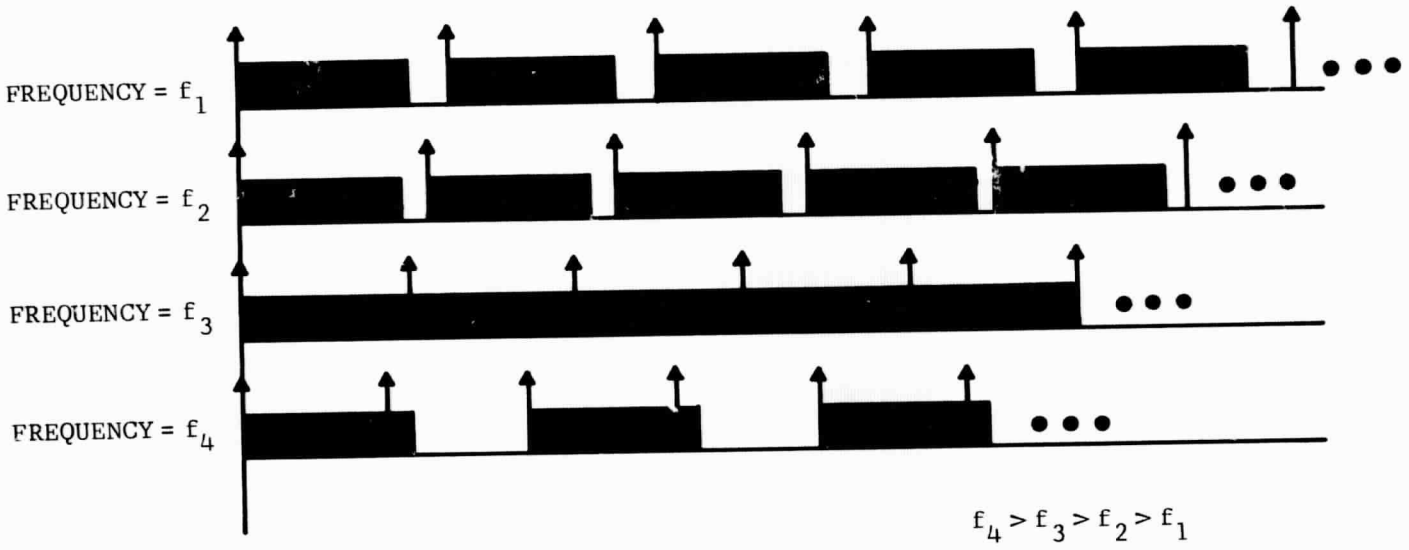

Figure 4-7 MSMV Output for Increasing Frequency Deviation

The frequency for PDO is given by

$$f_{PDO} = \frac{1}{2T_o} = \frac{f_n}{\delta} \quad . \tag{4.19}$$

The instantaneous frequency in hertz is given by

$$f_i = f_n + \frac{1}{2\pi} \dot{\phi}(t) \quad , \tag{4.20}$$

which, at the threshold of PDO, becomes

$$\frac{f_n}{\delta} = f_n + \frac{1}{2\pi} \dot{\phi}(t) \quad , \tag{4.21}$$

or

$$\dot{\phi}(t) = 2\pi f_n \left(\frac{1 - \delta}{\delta}\right) . \tag{4.22}$$

Thus, PDO occurs when

$$\dot{\phi}(t) \geq 2\pi f_n \left(\frac{1 - \delta}{\delta}\right) . \tag{4.23}$$

Since PDO can have an adverse effect on the PLL such as causing it to lose lock, it is of interest to determine the probability of PDO, P(PDO), given f_n, δ, and the noise statistics. Because of the complexity of the general analysis, this will be done only for dc modulation.

For dc modulation $e_{cf}(t)$ is a sine wave perturbed by additive, narrowband noise. S. O. Rice has developed a curve which yields the probability that $\dot{\phi}$ is less than some particular value when the signal-to-noise ratio, ρ, and the noise bandwidth, B_n, are known.[18] Equation (4.23) can be used to adapt Rice's curve to the one illustrated in Figure 4-8.

Figure 4-8 illustrates that P(PDO) is highly dependent upon the ratio of the channel carrier frequency to the noise bandwidth, as would be expected. Thus, this effect is greatest in wideband,

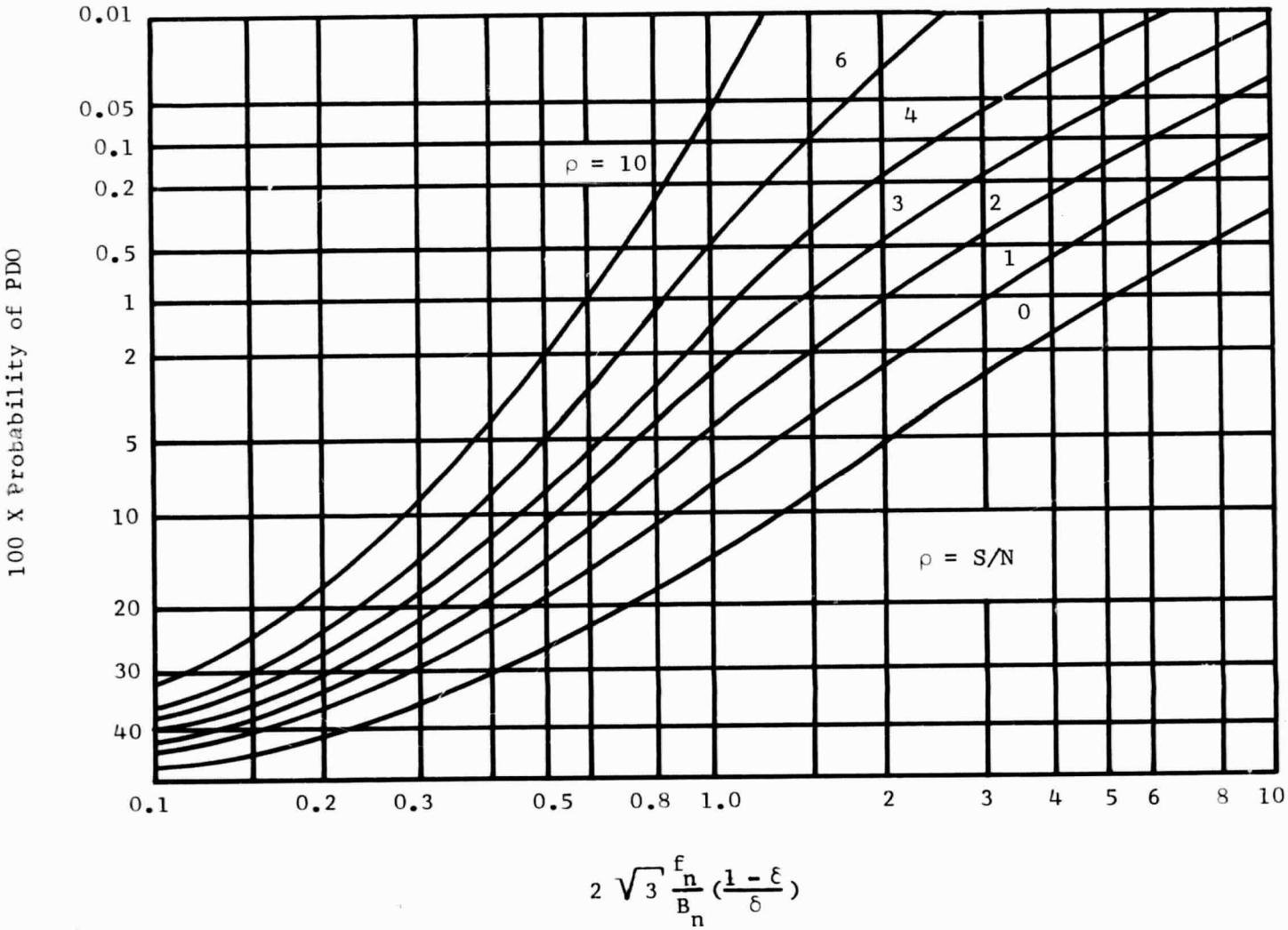

Figure 4-8 PDO Distribution Function

low-carrier-frequency channels. The effect on such channels is illustrated in Figure 4-9 for a data channel having a bandwidth of 3 kHz and a carrier of 15 kHz. As the signal-to-noise ratio and the channel carrier frequency increase, the effect becomes negligible.

D. MSMV PERTURBATIONS DUE TO FLUTTER

In the preceding section it was shown that MSMV pulse dropout occurred when additive noise deviated the carrier frequency by an amount such that the distance between adjacent carrier zero crossings is less than the MSMV "on" time. Since flutter also results in such deviations, there is a non-zero probability of pulse dropout, i.e., finite P(PDO), due to flutter. The work which follows proves that the probability of this occurrence is negligibly small.

The analysis will be performed by assuming flutter to approximate a Gaussian distribution of zero mean, an assumption supported by experimental evidence.[19] The frequency deviation of a frequency ω_n, due to flutter, can be written as

$$\dot{\theta}(t) = \omega_n \, g(t) \ , \tag{4.24}$$

where $\dot{\theta}(t)$ and $g(t)$ represent frequency deviation and flutter, respectively. If a 3σ approximation is employed to relate the peak and rms values of $\dot{\theta}(t)$, the result is

$$3\sigma = \dot{\theta}_{peak} = \omega_n \, g_{peak} \tag{4.25}$$

where σ represents the rms value of $\dot{\theta}(t)$, and $\dot{\theta}_{peak}$ and g_{peak} represent the peak values of $\dot{\theta}(t)$ and $g(t)$, respectively. As before, P(PDO) is given by

$$P(PDO) = P(\dot{\theta} \geq \omega_n \frac{1 - \delta}{\delta}) \ , \tag{4.26}$$

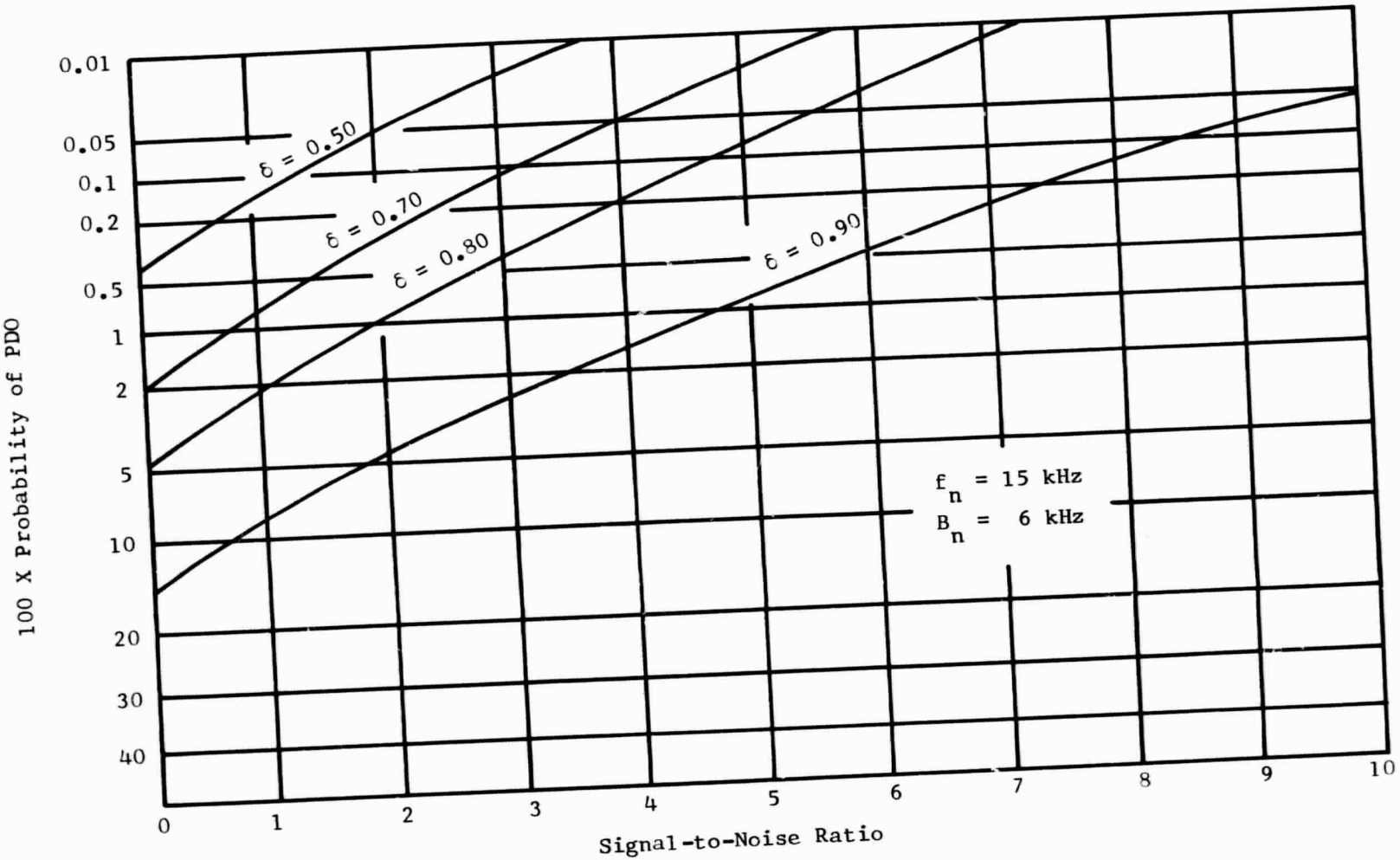

Figure 4-9 Probability of PDO for a Low Frequency Channel

or since $p(\dot{\theta})$ is assumed Gaussian with zero mean

$$P(PDO) = \frac{1}{\sqrt{2\pi}\sigma} \int_{\omega_n \frac{1-\delta}{\delta}}^{\infty} \exp\left[-x^2/2\sigma^2\right] dx \ . \tag{4.27}$$

This is equivalent to

$$P(PDO) = \frac{1}{2} - \frac{1}{\sqrt{2\pi}\sigma} \int_{o}^{\omega_n(\frac{1-\delta}{\delta})} \exp\left[-x^2/2\sigma^2\right] dx \ . \tag{4.28}$$

If the preceding is placed into the form of a normal distribution, the result is

$$P(PDO) = \frac{1}{2} - \frac{1}{\sqrt{2\pi}} \int_{o}^{\xi} \exp\left[-x^2/2\right] dx \ , \tag{4.29}$$

where

$$\xi = \frac{\omega_n}{\sigma} \left(\frac{1-\delta}{\delta}\right) \ . \tag{4.30}$$

The expression for P(PDO) can be stated in terms of flutter by substituting (4.25) into (4.30) to yield

$$\xi = \frac{3}{g_{peak}} \left(\frac{1-\delta}{\delta}\right) . \tag{4.31}$$

It is easily shown that P(PDO) is negligible by picking worst case values in (4.31). In a typical system δ would be less than 0.9 and modern tape recorders have less than one percent peak flutter. Substituting these values in (4.31) yields $\xi = 33.3$, which when substituted into (4.29) illustrates that P(PDO) is negligible. In a typical application δ and g_{peak} will be such that an even smaller P(PDO) results.

E. PHASE-LOCK LOOP PERTURBATIONS DUE TO NOISE

Noise which falls within the channel bandwidth perturbs the carrier phase and affects the stability of the demodulation carrier. Since the output of the channel filter is amplitude limited, only phase perturbations are of interest. The phase perturbations of the channel zero crossings have an approximate Gaussian density function for high signal-to-noise ratios and the rms value of these perturbations is given by

$$\sigma_{\phi} = \frac{1}{\sqrt{2\ S/N}} \quad , \tag{4.32}$$

where S/N represents the average signal-to-noise ratio in the data channel. Equation (4.32) is plotted in Figure 4-10. The rms value of phase jitter on the PLL output is less than that given by (4.32) because of the additional bandlimiting action of the PLL. The variance of the PLL output can be written as

$$\sigma_{out}^{2} = \frac{\sigma_{in}^{2}}{B} \int_{o}^{\infty} \left|H(\omega)\right|^{2} \frac{d\omega}{2\pi} \quad , \tag{4.33}$$

where σ_{out}^{2} and σ_{in}^{2} represent the phase variances of the PLL output and input, $H(\omega)$ is the PLL transfer function, and B is the input noise bandwidth. The integral is simply the noise bandwidth of the PLL.[20]

F. SUMMARY

In the LDRM carrier synthesis system, perturbations result from modulation zeros, flutter and noise. Modulation zeros cause perturbations in the form of shifted pulses in the MSMV output, which yield phase errors in the demodulation carrier. The analysis illus-

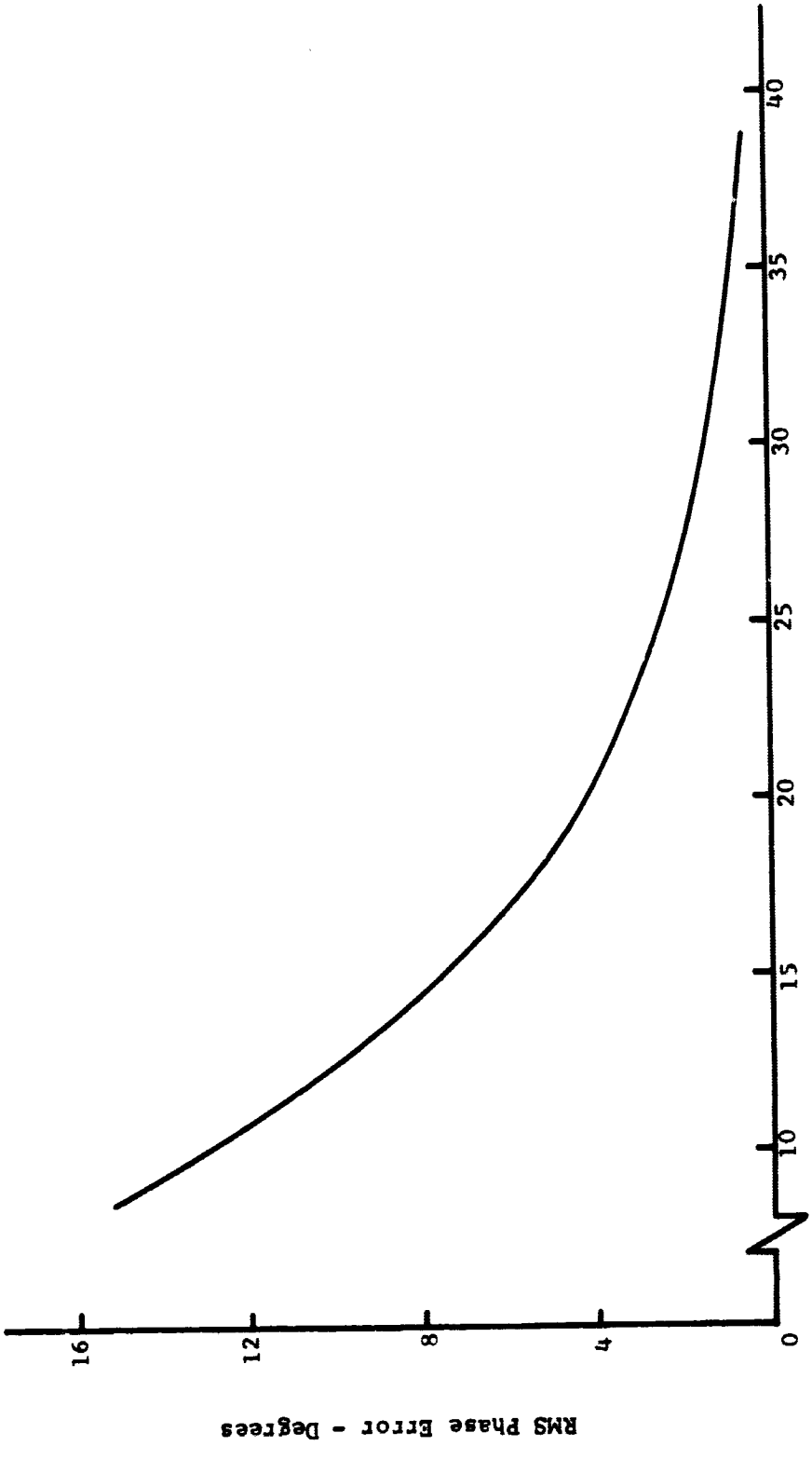

Figure 4-10 RMS Phase Perturbation Due to Noise

trates that this effect is worst on low-frequency, wideband channels. The probability of a shifted pulse is less than 0.04 if the carrier frequency is five times the bandwidth of the data signal and if the MSMV duty is 70 percent or greater. For a carrier frequency greater than 15 kHz the phase-lock loop error is negligible if the bandwidth of the phase-lock loop is made only large enough for flutter compensation. In a physical system, the effect of modulation zeros restricts the lowest channel carrier frequency so that if the LDRM technique is utilized, approximately the first 15 kHz of the baseband cannot be used if the phase error is to be kept below 3 degrees.

For low signal-to-noise ratios problems arise because of excessive phase jitter in the synthesized demodulation carrier and because of pulse dropout in the MSMV output. The probability of pulse dropout is less than 0.01 for duty cycles less than 80 percent, signal-to-noise ratios greater than 10 dB and channel carrier frequencies greater than 15 kHz.

Pulse dropout due to flutter is a negligible effect. However, dynamic error in the demodulated data due to TBE is essentially the same in the LDRM system as in the common pilot system. The need for recorders with low peak TBE is evident.

CHAPTER V

AGC IN AM-BASEBAND SYSTEMS

Automatic-gain-control (AGC) can be used in any AM/FM system and is sometimes desirable when the receiver output signal-to-noise ratio is considered. This follows from the fact that the signal-to-noise ratio at the output of an FM receiver is proportional to the mean-square value of transmitter deviation.[21] Thus, the transmitter deviation must be kept close to its maximum permissible value if the average individual channel signal-to-noise ratio at the receiver output is to be maximized. This is easily accomplished if the data being transmitted is stationary, i.e., if the data statistics do not change with time. However, a multichannel system can be required to carry non-stationary data in which it is likely that all channels in the multiplex will be at maximum activity simultaneously. If the system parameters are chosen so that maximum permissible rms transmitter deviation occurs at these periods of maximum activity, serious degradation of the individual channel output signal-to-noise ratio will result when the baseband activity is low. Using a higher, constant transmitter sensitivity can result in either nonlinear transmitter operation or in an excessively wide RF spectrum during periods of high activity.

These difficulties can be overcome by employing an AGC loop at the FM link input to hold the rms value of the baseband signal constant and a second loop at the output to restore data calibration. Hereafter, the input and output loops will be referred to as

the transmitter and receiver loops, respectively. However, using AGC results in system errors because, in general, the receiver loop does not perfectly track gain variations in the transmitter loop. This type of error is known as tracking error. Also, errors result because of additive noise perturbations of the pilot amplitude, which are tracked by the receiver AGC loop. Additionally, the tracking error can have a steady-state value. These errors are studied using theoretical analysis and simulation.

A. SIGNAL-TO-NOISE RATIO INCREASE DUE TO AGC

A block diagram of a baseband AGC system is shown in Figure 5-1. The increase in the output signal-to-noise ratio of an individual channel can be determined from a consideration of mean-square transmitter deviation. Let $S_j(t)$ represent the instantaneous value of the Channel-j signal so that the baseband signal, S(t), is given by

$$S(t) = \sum_{j=1}^{n} S_j(t) \ . \tag{5.1}$$

If all the channel signals are statistically independent, the rms value of S(t), S, is

$$S = \left[\sum_{j=1}^{n} S_j^2 \right]^{1/2} , \tag{5.2}$$

where S_j is the rms value of $S_j(t)$. The rms transmitter deviation, D, is determined by S. Therefore, maximum rms transmitter deviation, D_m, results when S assumes maximum value, S_m, so that

$$D = \frac{S}{S_m} D_m = LD_m \ , \tag{5.3}$$

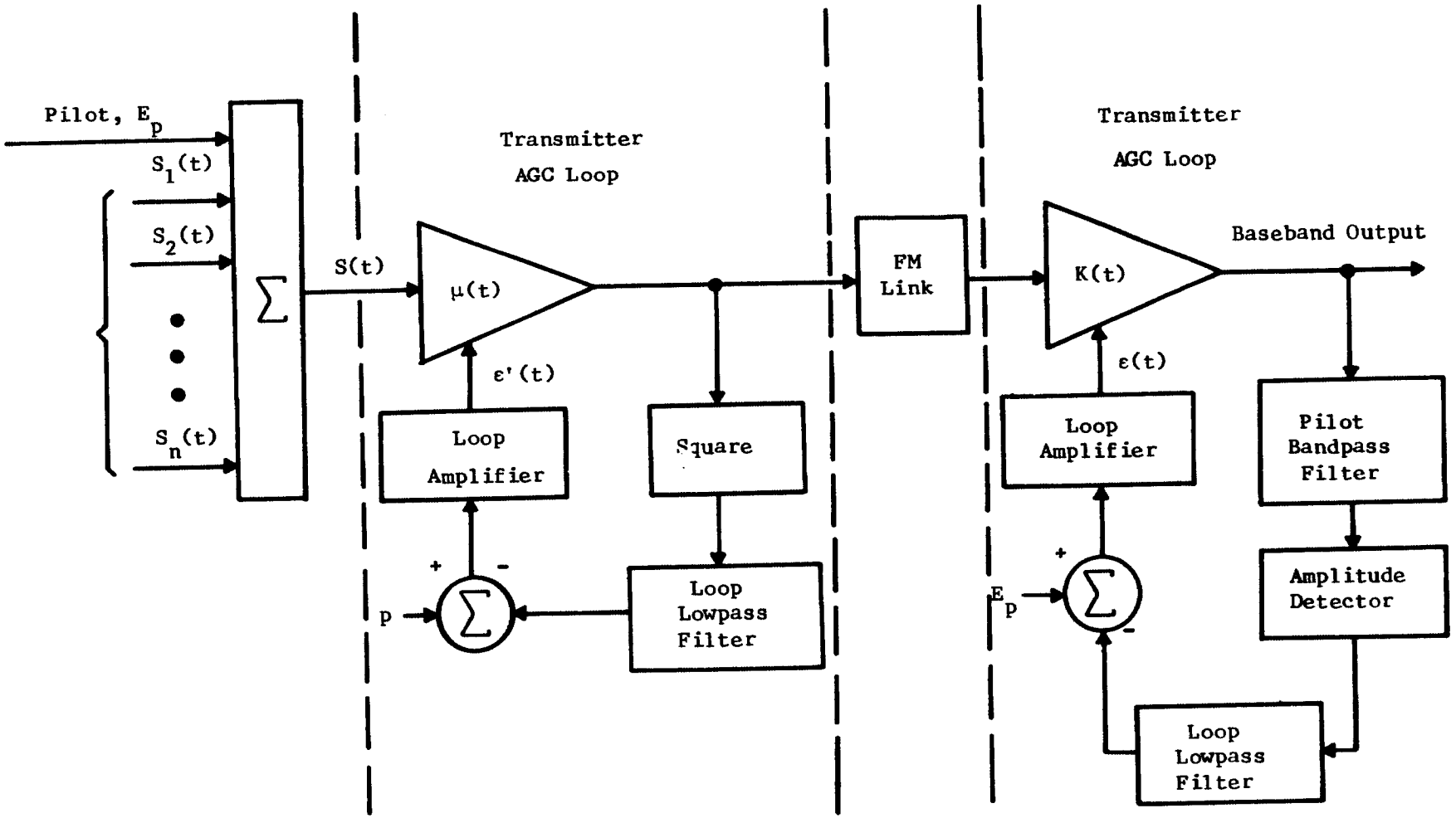

Figure 5-1 Complete AGC System

where $L = S/S_m$ is the load factor.[22] It follows that if a controlled amplifier with gain $\mu(t) = L^{-1}$ is placed ahead of the FM link, the rms transmitter deviation will be maintained constant at D_m. Since the individual channel signal-to-noise ratio is proportional to the mean-square transmitter deviation, this ratio is increased by a factor of $(L^{-1})^2$. This gain represents the actual signal-to-noise ratio increase which results from using AGC over the case where no AGC is used and the transmitter is adjusted for maximum deviation when the load factor is one.

B. TRACKING ERROR

The mechanism by which tracking error occurs can be demonstrated by considering a change in baseband load factor from 0.5 to 1.0 at time t_c. In order for the transmitter deviation to remain constant, the transmitter amplifier gain, $\mu(t)$, should change instantaneously from two to one. However, the gain actually changes as shown in Figure 5-2(a) with time constant T_t dependent upon the bandwidth of the transmitter loop. It follows that the pilot amplitude at the receiver loop output is, assuming a perfect FM link, $E_p\mu(t)$, where E_p is the nominal pilot amplitude. If the gain of the receiver loop amplifier, $K(t)$, were $\mu^{-1}(t)$, no error would exist since the pilot amplitude at the receiver loop output would be constant at E_p. However, this would require that the receiver loop respond instantaneously to changes in $E_p\mu(t)$, which would necessitate an infinite loop bandwidth. Therefore, in a practical system the pilot will be returned to its proper level, E_p, as illustrated in Figure 5-2(b), yielding a tracking error, ε_T, as shown in Figures 5-2(b) and 5-2(c).

(a)

Pilot Amplitude at Output of Transmitter AGC

(b)

Pilot Amplitude at Output of Receiver AGC

(c)

Tracking Error

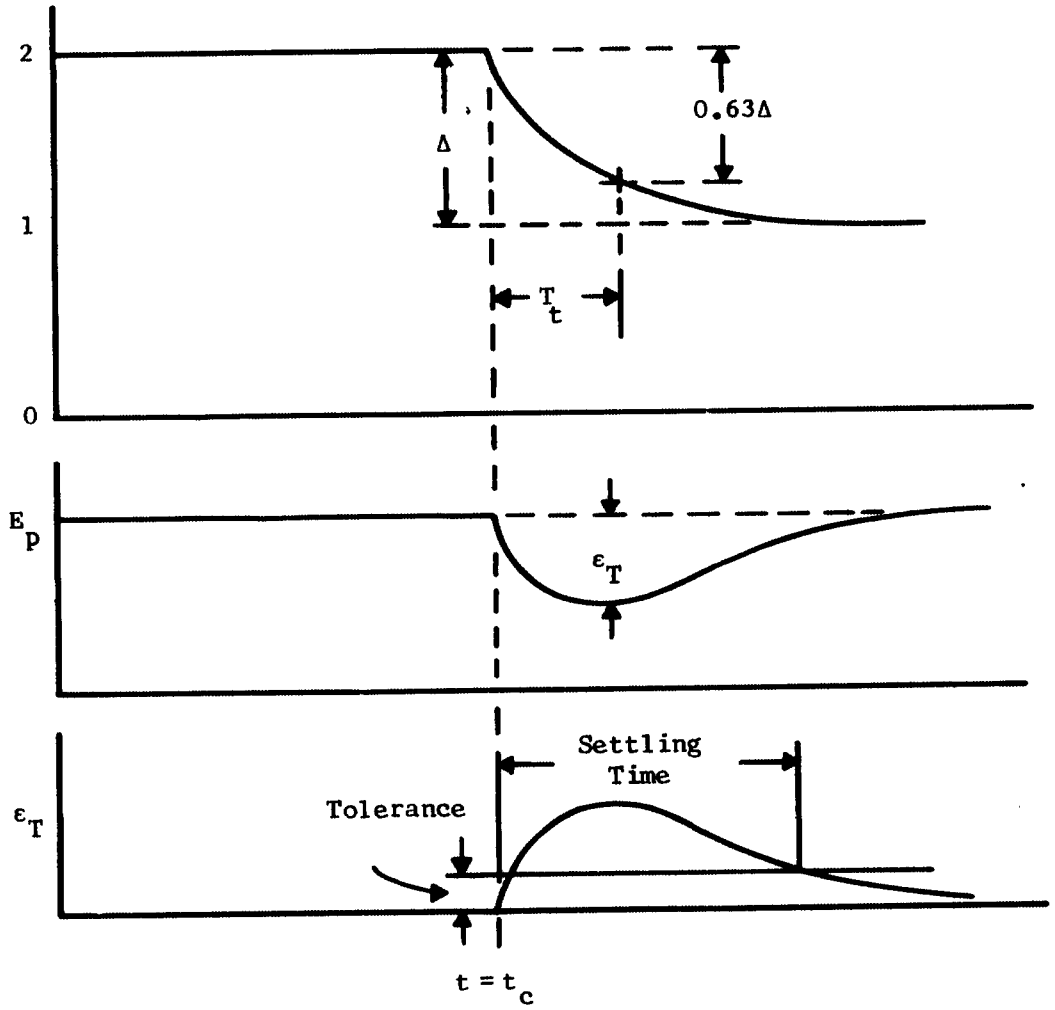

Figure 5-2 Response to a Step Change in Load Factor

This error for a step increase in baseband load factor can be used to define the AGC system settling time as illustrated in Figure 5-2(c), where the tolerance is the desired system accuracy. Since tracking error only depends upon the ability of the receiver loop to track changes in the transmitter loop gain, the error can be made arbitrarily small by increasing the bandwidth of the receiver loop or decreasing the bandwidth of the transmitter loop. Thus, the time constant ratio

$$\lambda = \frac{\text{transmitter loop time constant}}{\text{receiver loop time constant}} = \frac{T_t}{T_r} \qquad (5.4)$$

is the parameter which controls tracking error. However, λ may not be freely varied in a practical system because increasing the transmitter-loop time constant can result in errors due to transmitter overdeviation, while decreasing the receiver-loop time constant can result in errors due to interference from data channels adjacent to the pilot in the baseband.

C. THEORETICAL ANALYSIS

Because of the variable gain element, an AGC loop is described by a differential equation which has time-varying coefficients. This complicates determination of the general loop response; however, an exact solution is obtainable for the first-order case. This solution can be utilized to determine the loop time constant, the steady-state error, and the system tracking error. Additionally, the analysis provides insight which is helpful in understanding the operation of baseband AGC. In an analysis of tracking error, the only concern is how well the receiver loop tracks the transmitter loop gain variations. If these gain variations are specified, only the receiver

loop need be considered in the analysis. Therefore, the transmitter loop will be assumed to be first-order in the following analysis.

Since the receiver loop responds only to variations in the pilot amplitude, the pilot frequency can be translated to dc for purposes of analysis. This results in the reduction of the receiver loop in Figure 5-1 to the simplified model shown in Figure 5-3. The lowpass filter represents the cascade combination of the loop lowpass filter and the lowpass equivalent of the pilot bandpass filter. Usually, the pilot bandpass filter will have a much larger bandwidth than the loop lowpass filter and can be neglected in an analysis not concerned with noise and interference. Also, the position of the comparison device has been changed for simplicity. The loop input, $e_i(t)$, is the assumed pilot envelope at the transmitter loop output.

General Solution. In order to compute the output, $e_o(t)$, of the system in Figure 5-3, an expression for the gain, K(t), is necessary. Then $e_o(t)$ can be computed from

$$e_o(t) = K(t)e_i(t) \ . \tag{5.5}$$

The gain is assumed to be a linear function of the error signal, $\varepsilon(t)$, so that

$$K(t) = 1 + \varepsilon(t) \ . \tag{5.6}$$

Since the analysis is for a first-order loop filter, let the loop filter impulse response be

$$y(t) = \beta e^{-\beta t} \ . \tag{5.7}$$

Since the input to the filter is $E_p - e_o(t)$ and the filter output is $\varepsilon(t)$, the differential equation describing $\varepsilon(t)$ is

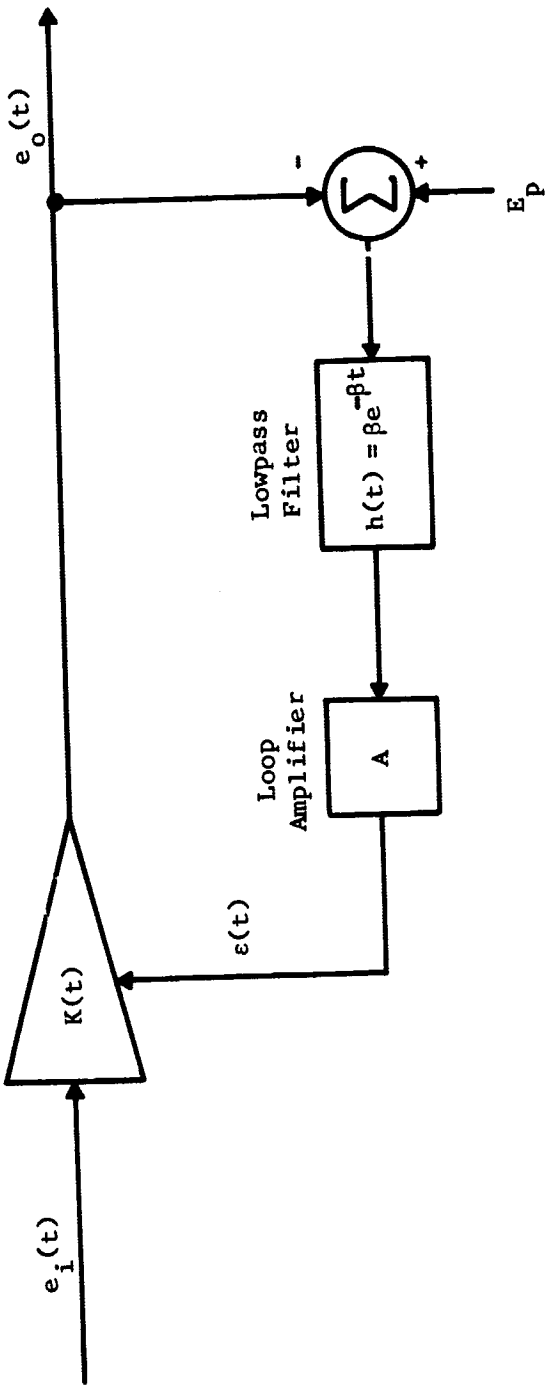

Figure 5-3 Model of Receiver AGC Loop

$$\frac{d\varepsilon(t)}{dt} + \beta\varepsilon(t) = A\beta\left[E_p - e_o(t)\right] \quad . \tag{5.8}$$

Substituting (5.5) and (5.6) into (5.8), this equation can be written in the standard form

$$\frac{dK(t)}{dt} + \beta\left[1 + Ae_i(t)\right]K(t) = \beta\left[1 + AE_p\right] \quad . \tag{5.9}$$

Using the integrating factor

$$\exp\left[\int_o^t \beta\left[1 + Ae_i(x)\right]dx\right]$$

allows (5.9) to be solved yielding

$$\begin{aligned} K(t)\exp\left[\int_o^t \beta\left[1 + Ae_i(x)\right]dx\right] \\ = \int_o^t \beta\left[1 + Ae_p\right]\exp\left[\int_o^\tau \beta\left[1 + Ae_i(x)\right]dx\right]d\tau + C \quad , \end{aligned} \tag{5.10}$$

where C is the constant of integration which is unity if the initial condition g(0) = 0 is assumed. Accordingly, (5.10) can be simplified to yield the general first-order solution[23]

$$\begin{aligned} K(t) = \exp\left[-\int_o^t \beta\left[1 + Ae_i(x)\right]dx\right] \\ + \beta\left[1 + AE_p\right]\int_o^t \exp\left[-\int_\tau^t \beta\left[1 + Ae_i(x)\right]dx\right]d\tau \quad . \end{aligned} \tag{5.11}$$

This expression can be used to determine the loop time constant, the steady-state error, and the tracking error.

Time Constants. The time constant of an AGC loop is defined in the conventional manner from the step-function response. To determine

the time constant of the receiver loop, let

$$e_i(t) = E_p + \Delta \ . \tag{5.12}$$

Substituting (5.12) in (5.11) yields

$$K(t) = \exp\left[-\int_o^t \beta\left[1 + AE_p + A\Delta\right]dx\right] + \beta\left[1 + AE_p\right]\int_o^t \exp\left[-\int_\tau^t \beta\left[1 + AE_p + A\Delta\right]dx\right]d\tau \ , \tag{5.13}$$

which, after performing the integrations, becomes

$$K(t) = \frac{1}{1 + A(E_p + \Delta)}\left[(1 + AE_p) + A\Delta\left[\exp -\left[\beta + \beta A(E_p + \Delta)\right]t\right]\right] \ . \tag{5.14}$$

From this equation, the time constant of the receiver loop is, by definition,

$$T_r = \frac{1}{\beta + \beta A(E_p + \Delta)} \ . \tag{5.15}$$

The preceding expression illustrates that the time constant of the receiver loop is dependent upon both the magnitude and polarity of the step. It should be kept in mind that a positive Δ corresponds to a step decrease in load factor, since Δ represents the change in pilot amplitude. The dependency of T_r on the loop input signal makes it extremely difficult to specify the loop time constant or the effective loop bandwidth for a general input signal.

It follows from the similarity of the transmitter and receiver loops that if a step function is applied to the input of a first-order transmitter loop, the pilot amplitude at the loop output will be of the form

$$e_i(t) = E_p + \Delta(1 - e^{-\alpha t}) \ . \tag{5.16}$$

By definition, the time constant of the transmitter loop, T_t, is

$$T_t = 1/\alpha \ . \tag{5.17}$$

Steady-State Errors. If the steady-state value of $e_i(t)$ is different from E_p, then $\varepsilon(t)$ cannot be zero and a steady-state error will result. Assuming that $e_i(t) = E_p + \Delta$, the steady-state value of K(t), i.e., K(∞), can be computed from (5.9). By definition of steady-state, d/dt K(t) at t = ∞ is zero. Thus,

$$K(\infty) = \frac{1 + AE_p}{1 + A(E_p + \Delta)} \ . \tag{5.18}$$

The steady-state error, ε_{ss}, is given by

$$\varepsilon_{ss} = e_o(\infty) - E_p = K(\infty)(E_p + \Delta) - E_p = \frac{\Delta}{1 + A(E_p + \Delta)} \tag{5.19}$$

In a practical system this value can be made negligible by making A sufficiently large. Of course, the steady-state error in no way depends upon the loop lowpass filter if H(0) is unity. Thus, unlike the general solution and the expression derived for the time constants, (5.19) is valid for any choice of loop filter.

Tracking Error for Step Changes in Load Factor. From Figure 5-2 the tracking error, ε_T, of an AGC system is given by

$$\varepsilon_T = K(t)e_i(t) - E_p \ . \tag{5.20}$$

For a first-order system ε_T can be obtained from (5.11), the general solution for K(t). If $e_i(t)$ results from a step change in load factor at the input of a first-order transmitter loop, it will have the form given by (5.16). Substituting (5.16) into (5.11) yields

$$K(t) = \exp\left[-\int_0^t \beta\left[1 + A\left[E_p + \Delta - \Delta e^{-\alpha x}\right]\right]dx\right]$$
$$+ \beta\left[1 + AE_p\right]\int_0^t \exp\left[-\int_\tau^t \beta\left[1 + A\left[E_p + \Delta - \Delta e^{-\alpha x}\right]\right]dx\right]d\tau \,, \tag{5.21}$$

which can be written as

$$K(t) = \exp\left[-\beta t - A\beta(E_p + \Delta)t - \frac{A\beta\Delta}{\alpha}(e^{-\alpha t} - 1)\right]$$
$$+ \beta\left[1 + AE_p\right]\exp\left[-\beta t - A\beta(E_p + \Delta)t - \frac{A\beta\Delta}{\alpha}e^{-\alpha t}\right] \tag{5.22}$$
$$\times \int_0^t \exp\left[\beta\tau + \beta A(E_p + \Delta)\tau + \frac{A\beta\Delta}{\alpha}e^{-\alpha\tau}\right]d\tau \,.$$

Using (5.15) and letting $T_r = r$ to simplify notation allows (5.22) to be written as

$$K(t) = \exp\left[-\frac{t}{r} - \frac{A\beta\Delta}{\alpha}(e^{-\alpha t} - 1)\right]$$
$$+ \beta\left[1 + AE_p\right]\exp\left[-\frac{t}{r} - \frac{A\beta\Delta}{\alpha}e^{-\alpha t}\right] \tag{5.23}$$
$$\times \int_0^t \exp\left[\frac{\tau}{r} + \frac{A\beta\Delta}{\alpha}e^{-\alpha\tau}\right]d\tau \,.$$

This equation can be expressed as

$$K(t) = \left[\exp\left[-\frac{t}{r} - be^{-\alpha t}\right]\right]\left[e^b + \beta\left[1 + AE_p\right]g(b;t)\right] \,, \tag{5.24}$$

where $b = A\beta\Delta/\alpha$ and

$$g(b;t) = \int_0^t \exp\left[\frac{\tau}{r} + be^{-\alpha\tau}\right]d\tau \,. \tag{5.25}$$

A simpler form for $g(b;t)$ can be obtained by making the change of variable

$$y = be^{-\alpha\tau} \,. \tag{5.26}$$

By observing that

$$\lambda = \frac{T_t}{T_r} = \frac{1}{\alpha r} \tag{5.27}$$

(5.25) can be placed in the form

$$g(b;t) = \frac{1}{\alpha} b^{\lambda} \int_{be^{-\alpha t}}^{b} y^{-(1+\lambda)} e^{y} dy \ . \tag{5.28}$$

Replacing e^{y} by its series expansion yields

$$g(b;t) = \frac{1}{\alpha} b^{\lambda} \int_{be^{-\alpha t}}^{b} \sum_{k=0}^{\infty} \frac{y^{(k-1-\lambda)}}{k!} dy \ . \tag{5.29}$$

The term in which $k = \lambda$ must be integrated separately since it yields a $\ln(y)$ term. Thus, (5.28) becomes

$$g(b;t) = \frac{1}{\alpha} b^{\lambda} \left[\sum_{\substack{k=0 \\ k \neq \lambda}}^{\infty} \frac{y^{k-\lambda}}{k!(k-\lambda)} + \frac{1}{\lambda!} \ln y \right]_{be^{-\alpha t}}^{b} , \tag{5.30}$$

which can be written

$$g(b;t) = \frac{1}{\alpha} b^{\lambda} \left[\frac{\alpha t}{\lambda!} + y^{-\lambda} \sum_{\substack{k=0 \\ k \neq \lambda}}^{\infty} \frac{y^{k}}{k!(k-\lambda)} \Bigg|_{be^{-\alpha t}}^{b} \right] . \tag{5.31}$$

Substituting (5.31) into (5.24) yields the final result for K(t)

$$K(t) = \exp\left[-\frac{t}{T_r} - be^{-\alpha t}\right] \left\{ e^{b} + \frac{1}{\alpha} b^{\lambda} \beta \left[1 + AE_p\right] \left[\frac{\alpha t}{\lambda!} + y^{-\lambda} \sum_{\substack{k=0 \\ k \neq \lambda}}^{\infty} \frac{y^{k}}{k!(k-\lambda)} \Bigg|_{be^{-\alpha t}}^{b} \right] \right\} . \tag{5.32}$$

From this expression K(t) can be determined for any choice of system parameters. Tracking error is then determined using (5.20).

Tracking Error for Low-Frequency Modulation. Tracking error can also result from low-frequency modulation which produces dominant low-frequency components in the transmitter error signal, $\varepsilon'(t)$. There are several ways in which this can occur, the simplest being when a single channel is modulated by a low-frequency sinusoid. If all other channels in the baseband are unmodulated, the input to the transmitter is

$$s(t) = \cos \omega_r t \cos \omega_m t + \cos \omega_p t \tag{5.33}$$

where ω_n, ω_m and ω_p are the channel carrier, modulating, and pilot frequencies, respectively. The output of the squaring network is

$$s^2(t) = \frac{3}{4} + \frac{1}{4} \cos 2\omega_m t + \Theta(t) \tag{5.34}$$

where $\Theta(t)$ contains only higher frequency terms. The dc term is the desired term since it is proportional to the mean-square value of the transmitter input. If the frequency $2\omega_m$ is sufficiently low to be passed by the lowpass filter in the transmitter loop, the gain of the transmitter loop will be perturbed and tracking errors can result. However, if the frequency is sufficiently low, the receiver can track the variation and no error results, and if the frequency is much higher than the cutoff frequency of the transmitter-loop lowpass filter, there will be no transmitter loop response.

Since the gain of the transmitter loop will be $\cos 2\omega_m t$, the tracking error can be obtained by substituting this for $e_i(t)$ in (5.11) and solving for K(t). Tracking error can then be determined from (5.20). However, since the input is now a function of time, the

analysis is far more complex than for step changes in load factor. Thus, simulation is used to determine tracking error curves.

D. SIMULATION RESULTS

In the previous section the tracking error due to step-type changes in load factor was determined for a first-order loop. Since the analysis for higher order loops is much more difficult, simulation was used to obtain results for a second-order loop. Also, for convenience a first-order loop was simulated. Additionally, a simulation was used to yield tracking error due to low-frequency modulation for first-order and second-order loops. In the simulation the transmitter loop was replaced by a lowpass filter to give the proper pilot response with a step-function input. The receiver loop was simulated as represented in Figure 5-3.

Figure 5-4 shows the tracking error for a step in load factor at the transmitter loop input for a first-order system. The curves were described mathematically in the previous section. Figure 5-5 gives the results for a second-order system. These families of curves provide the designer with information concerning the effect of the time constant ratio, λ, on the magnitude and duration of the peaks in tracking error resulting from step inputs. A comparison of the first- and second-order results indicate that the second-order loop has a lower peak tracking error than the first-order loop. However, the second-order loop has the disadvantage of requiring compensation to prevent excessive ringing and long settling times. The compensator utilized was a first-order lead network placed in cascade with the lowpass filter and was designed to yield minimum settling time.

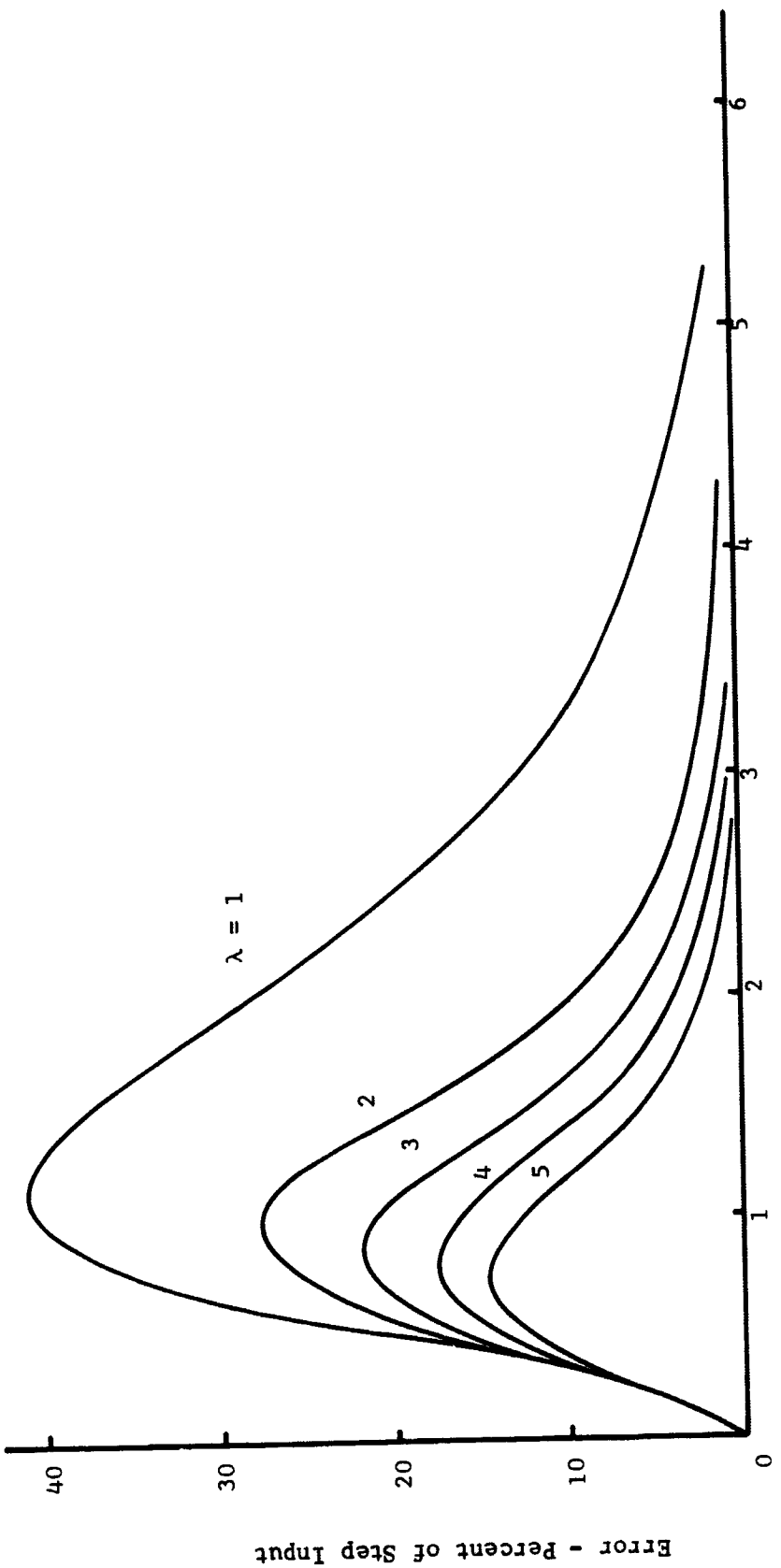

Figure 5-4 Tracking Error for First-Order Loop

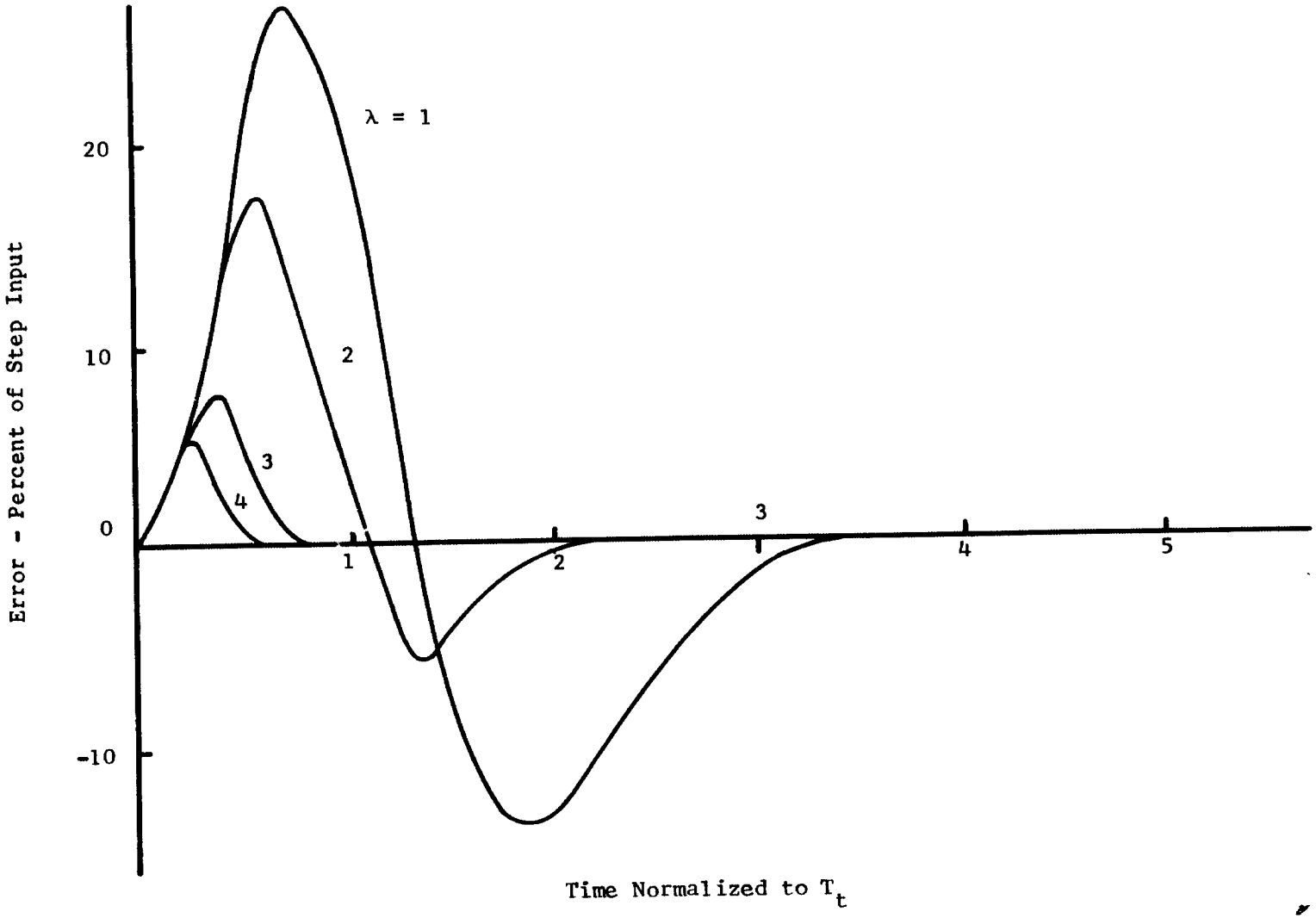

Figure 5-5 Tracking Error for Second-Order Loop

The tracking error resulting from low-frequency modulation is illustrated in Figure 5-6 for a first-order system. The abscissa represents the frequency $2\omega_m$ normalized to the transmitter-loop cutoff frequency, which is the reciprocal of the transmitter-loop time constant for the first-order case. The frequency $2\omega_m$ is used because, as shown in (5.34), this is the frequency at which the transmitter-loop gain, $\mu(t)$, is perturbed. The same curves for a second-order system are illustrated in Figure 5-7. In the second-order loop the peak tracking error is lower in amplitude and occurs at approximately twice the transmitter-loop cutoff frequency. For both systems, the effect of low-frequency modulation can be significant.

E. SUMMARY

The use of AGC yields an increase in the individual channel signal-to-noise ratio when data is non-stationary, but the AGC system itself introduces errors which can decrease system accuracy. These are primarily tracking errors which result from rapid changes in baseband load factor or from low-frequency modulation. The magnitude of the tracking error is a decreasing function of the ratio of transmitter-to-receiver time constants. Additionally, steady-state errors result in the tracking process, but these can be made negligible by using sufficient loop gain.

Because the AGC loop is defined by a differential equation having coefficients dependent upon the input signal, which is time varying, the loop time constant is a function of the input signal. This fact makes it difficult to specify effective AGC bandwidth when differing types of rapid transients or steps of different magnitude are likely to be encountered.

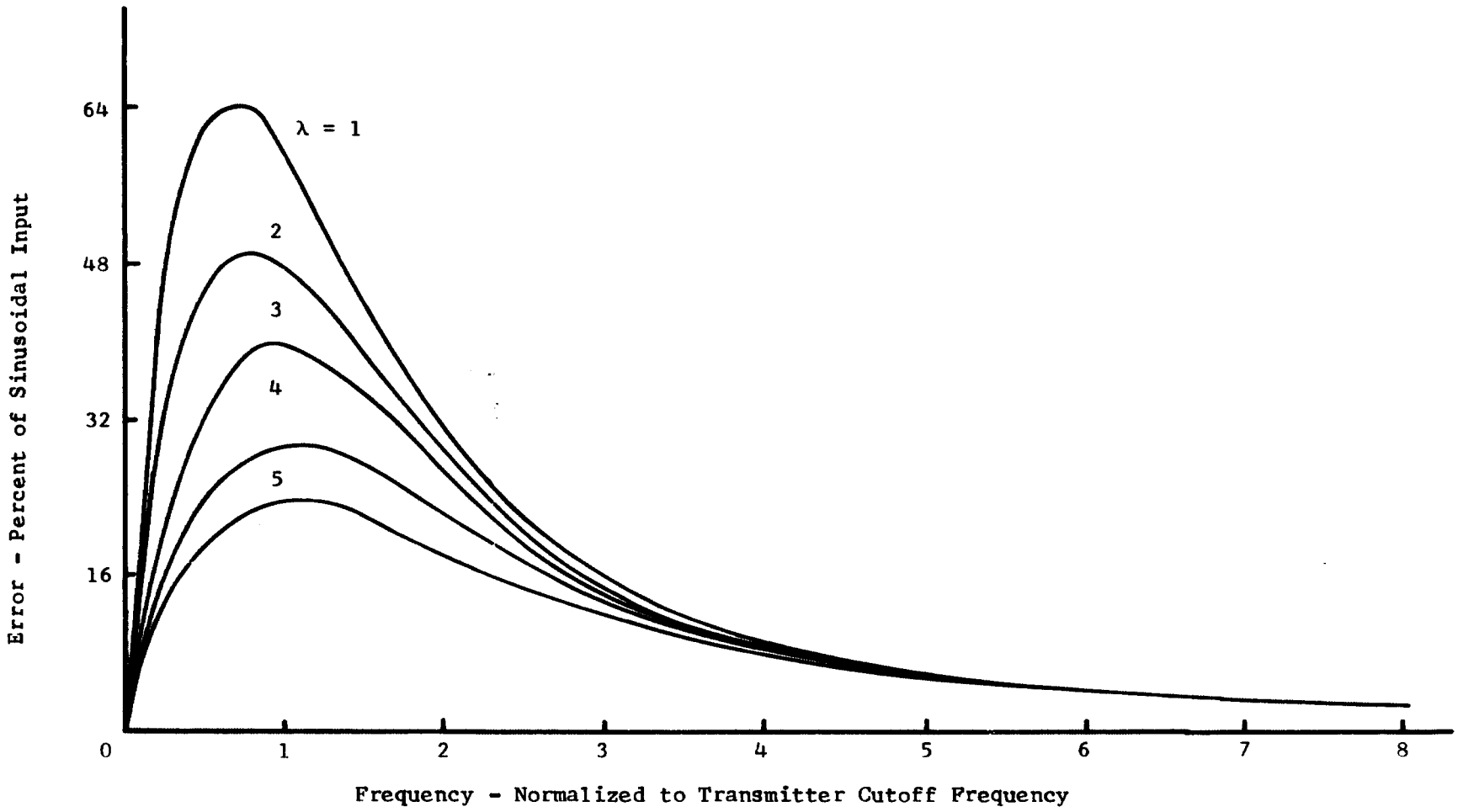

Figure 5-6 Effect of Low-Frequency Modulation for First-Order Loop

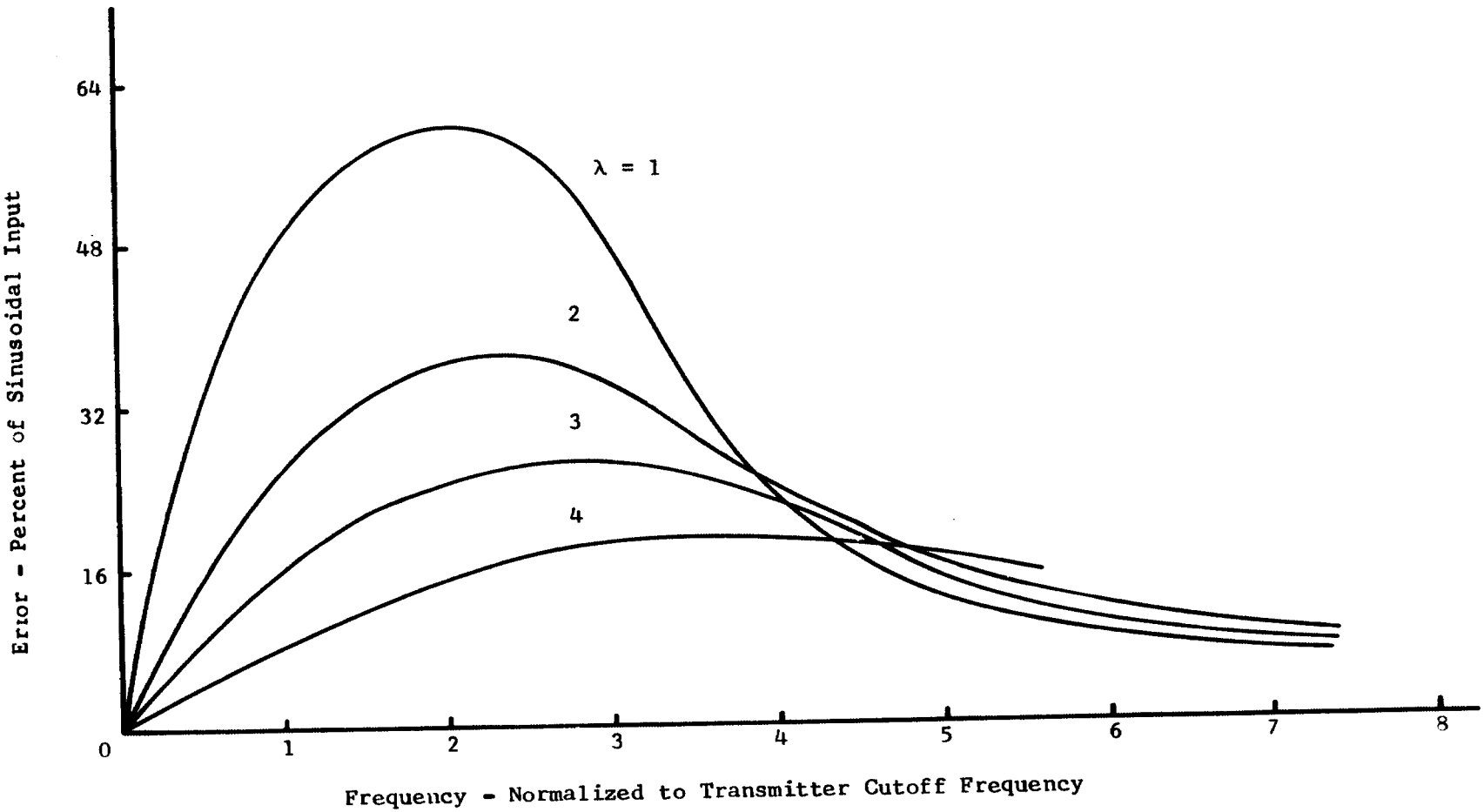

Figure 5-7 Effect of Low-Frequency Modulation for Second-Order Loop

CHAPTER VI

CONCLUSIONS

The results of the various analyses are summarized at the end of the chapters, and these results will not be repeated here. However, several general conclusions should be mentioned.

If the baseband of an AM/FM telemetry system contains only DSB channels, the carriers necessary for demodulation can be derived from either a common pilot or from the modulated channel carrier. However, if the baseband contains SSB or QDSB channels, a pilot must usually be used for synthesis. If a common pilot is used for synthesis of all demodulation carriers, then the carrier synthesis portion of the system is common to all channels.

In both techniques of carrier synthesis, errors result from baseband recorder flutter. These errors can be minimized by matching the time delays through the data path and the carrier synthesis path, but these errors can never be completely eliminated. This effect imposes a restriction on the baseband tape recorder when the system is required to operate with a given accuracy.

There are several effects of noise which are of particular interest. In the LDRM technique of carrier synthesis, noise can cause pulse dropout of the MSMV output. However, this effect has a negligible probability of occurrence for practical signal-to-noise ratios. One important consideration in the common pilot system is that if a pilot phase error occurs, an error results in all demodulated outputs. This means that sufficient power should be used in

the pilot to insure the required phase stability, which is much greater in SSB and QDSB systems than in DSB systems.

Baseband AGC is particularly attractive if the majority of the channels are changing slowly in rms value so that large tracking errors can be avoided. However, if high accuracy data is required the tracking error can outweigh the potential improvement of a higher signal-to-noise ratio resulting from the use of AGC. When this is the case, a system is desirable in which channels carrying critical signals are not subjected to the AGC process. Such a system can be easily implemented by summing together some of the channels ahead of the transmitter AGC loop and the remaining channels after the loop.

APPENDIX A

FLUTTER AND TIME-BASE ERROR IN TAPE RECORDING

In this appendix the effect of flutter is determined for both direct and FM recording, and the conditions under which the effect of flutter is a simple TBE are investigated.[24]

A. FLUTTER IN DIRECT RECORDING

In the recording process the instantaneous flutter, $g_r(t)$, is defined as

$$g_r(t) = \frac{v_r(t) - V_r}{V_r} , \tag{A.1}$$

where $v_r(t)$ is the instantaneous tape velocity and V_r is the mean tape velocity. From (A.1)

$$v_r(t) = V_r \left[1 + g_r(t)\right] . \tag{A.2}$$

Distance along the tape, $w(\tau)$, can be obtained by integrating (A.2) to give

$$w(\tau) = V_r \left[\tau + \int_o^\tau g_r(t)\, dt\right] . \tag{A.3}$$

If time-base error (TBE) is defined as

$$h_r(\tau) = \int_o^\tau g_r(t)\, dt , \tag{A.4}$$

(A.3) can be written

$$\tau = \frac{w(\tau)}{V_r} - h_r(\tau) . \tag{A.5}$$

Since the peak value of TBE is typically on the order of a millisecond or less, the second term in (A.5) is usually negligible compared to the first term. Thus τ can be approximated by w/V_r in the argument of $h_r(\tau)$, where w is understood to be a function of τ. Thus,

$$\tau = \frac{w}{V_r} - h_r \frac{w}{V_r} \quad . \tag{A.6}$$

The record circuit will be assumed to result in a tape flux, $\phi(\tau)$, proportional to the recorded signal, or

$$\phi(\tau) = K_1 e_r(\tau) \quad , \tag{A.7}$$

where K_1 is a recorder constant having units of webers per volt. Substituting (A.6) into (A.7) yields

$$\phi(w) = K_1 e_r \left[\frac{w}{V_r} - h_r \left[\frac{w}{V_r} \right] \right] \quad , \tag{A.8}$$

an expression for flux along the tape as a function of distance.

Upon playback, the voltage at the output of the read head, $e_o(t)$, is given by

$$e_o(t) = K_2 \frac{d}{dt} \phi(w) \quad , \tag{A.9}$$

where K_2 is a recorder constant having units of volts-seconds per weber. Substituting (A.8) into (A.9) yields

$$e_o(t) = K \frac{de_r(\tau)}{dt} \quad , \tag{A.10}$$

where K is the overall recorder constant, $K_1 K_2$, and τ is related to w by (A.6). Application of the chain rule yields

$$e_o(t) = K \frac{de_r(\tau)}{d\tau} \frac{d\tau}{dw} \frac{dw}{dt} \quad , \tag{A.11}$$

which, with the use of (A.6) can be evaluated as

$$e_p(t) = \frac{K}{V_r} \frac{dw}{dt} \left[1 - h'_r\left[\frac{w}{V_r}\right]\right] e'_r\left[\frac{w}{V_r} - h_r\left[\frac{w}{V_r}\right]\right] \quad . \tag{A.12}$$

In analogy to (A.5) the expression relating time and distance along the tape during playback is

$$w(t) = V_p\left[t + h_p(t)\right] \quad , \tag{A.13}$$

where $h_p(t)$ is the playback TBE and V_p is the mean tape velocity during playback. Substituting (A.13) into (A.12) and letting V_r equal V_p yields

$$\begin{aligned} e_o(t) = K\Big[1 + h'_p(t) - h'_r\left[t + h_p(t)\right] - h'_p(t)\, h'_r\left[t + h_p(t)\right]\Big] \\ \times\left[e'_r\left[t + h_p(t)\right] - h_r\left[t + h_p(t)\right]\right] \end{aligned} \quad . \tag{A.14}$$

If an overall TBE is defined as

$$h(t) = h_p(t) - h_r\left[t + h_p(t)\right] \quad , \tag{A.15}$$

it follows that the overall flutter, $g(t)$, is given by

$$g(t) = \frac{d}{dt} h(t) = h'_p(t) - h'_r\left[t + h_p(t)\right] - h'_p(t)\, h'_r\left[t + h_p(t)\right] \quad . \tag{A.16}$$

Substituting (A.15) and (A.16) into (A.14) yields

$$e_o(t) = K\left[1 + g(t)\right] e'_r\left[t + h(t)\right] \quad , \tag{A.17}$$

which indicates that flutter results in both a perturbed time base and amplitude, However, if the peak flutter is small, (A.17) can be approximated as

$$e_o(t) = K\, e'_r\left[t + h(t)\right] \quad . \tag{A.18}$$

The derivative indicates that the playback signal must be integrated to yield the output signal

$$e_p(t) = K\, e_r\left[t + h(t)\right] \quad , \tag{A.19}$$

which is the recorded signal perturbed by TBE.

B. FLUTTER IN FM RECORDING

If $e_r(t)$ is assumed to have the form

$$e_r(t) = E_c \sin\left[\omega_c t + \frac{\omega_d}{E_m}\int_o^t e_m(t)\, dt\right] \quad , \tag{A.20}$$

the playback signal can be obtained using (A.17) to yield

$$\begin{aligned} e_p(t) = K\, E_c \omega_c \left[1 + g(t)\right]\left[1 + \frac{\omega_d}{\omega_c}\frac{e_m\left[t + h(t)\right]}{E_m}\right] \\ \times \cos\left[\omega_c\left[t + h(t)\right] + \frac{\omega_d}{E_m}\int_o^{t+h(t)} e_m(t)\, dt\right] \quad . \end{aligned} \tag{A.21}$$

Demodulation of the playback signal yields the output signal, $e_b(t)$, corresponding to the input signal, $e_m(t)$. Thus, determining the instantaneous frequency of the argument of the cosine term in (A.21) yields

$$e_b(t) = \frac{K_d \omega_d}{E_m}\left[e_m\left[t + h(t)\right] + g(t)\left[E_m + e_m\left[t + h(t)\right]\right]\right] \quad . \tag{A.22}$$

where K_d is a discriminator constant having units of volts per hertz. If g(t) is small (A.22) may be approximated as

$$e_b(t) = \frac{K_d \omega_d}{E_m} e_m\left[t + h(t)\right] \quad . \tag{A.23}$$

As for direct recording the effect of flutter in FM recording is a time-base perturbation, provided the flutter is sufficiently small to allow the additive noise term in (A.22) to be ignored.

APPENDIX B

RESPONSE OF A LINEAR NETWORK TO A VARIABLE FREQUENCY INPUT

The output of a linear network to a frequency modulated input can be determined by using the spectral approach,[25] or the dynamic approach.[26] The spectral approach has the disadvantage of yielding an infinite series for the output, which usually cannot be expressed in closed form. For this reason, the dynamic approach is used in the analysis. Additionally, the quasi-steady-state approximation is made in order to achieve results which are easily interpreted. In this appendix, the quasi-steady-state approximation and the conditions which must hold for it to be valid are developed.

Consider a network where

$e_{in}(t)$ = input to the network,

$e_{out}(t)$ = output of the network,

$y(t)$ = unit impulse response, and

$Y(s)$ = the Laplace transform of $y(t)$.

Let the input to the network be written as

$$e_{in}(t) = \exp j\theta(t) = \exp\left[j \int \omega_i(t)dt\right] \tag{B.1}$$

where $\omega_i(t)$ represents the instantaneous frequency of the input. Assuming all poles to be first-order, the transfer function of the network, $Y(s)$, can be written as

$$Y(s) = \sum_k \frac{A_k}{s - s_k} , \tag{B.2}$$

where the s_k's are the poles of the function Y(s). Consistent with (B.2), the unit impulse response can be written as

$$y(t) = \begin{cases} \sum_k A_k e^{s_k t} & t \geq 0 \\ 0 & t < 0 \end{cases} \qquad \text{(B.3)}$$

The output of the network can be obtained by using the convolution integral

$$e_{out}(t) = \int_0^t y(t-\tau)\, e_i(\tau)\, d\tau \quad . \qquad \text{(B.4)}$$

Substituting (B.3) in (B.4) yields

$$e_{out}(t) = \sum_k e_k(t) \quad , \qquad \text{(B.5)}$$

where

$$e_k(t) = A_k e^{s_k t} \int_0^t e^{-s_k \tau}\, e_i(\tau)\, d\tau \quad . \qquad \text{(B.6)}$$

Using (B.1), $e_k(t)$ can be written in terms of the instantaneous input frequency as

$$e_k = A_k e^{s_k t} \int_0^t \exp\left[-s_k \tau + j\int \omega_i(\tau)\right] d\tau \quad . \qquad \text{(B.7)}$$

In order to perform the integration indicated in (B.7), it is convenient to introduce a function $p(\tau)$, defined as

$$p(\tau) = -s_k \tau + j\int \omega_i(\tau)\, d\tau \quad . \qquad \text{(B.8)}$$

Equation (B.7) then becomes

$$e_k(t) = A\, e^{s_k t} \int_o^t e^{p(\tau)}\, d\tau \quad , \tag{B.9}$$

which can be integrated by parts by considering

$$\int_o^t e^{p(\tau)}\, d\tau = \int_o^t \frac{e^{p(\tau)}\, \frac{dp(\tau)}{d\tau}}{\frac{dp(\tau)}{d\tau}}\, d\tau \tag{B.10}$$

and by defining

$$v = e^{p(\tau)} \quad ,$$

$$dv = e^{p(\tau)}\, \frac{dp(\tau)}{d\tau}\, d\tau \quad ,$$

$$u = \frac{1}{\frac{dp(\tau)}{d\tau}} \quad , \text{ and} \tag{B.11}$$

$$du = \frac{\frac{-d^2 p(\tau)}{d\tau^2}}{\left[\frac{dp(\tau)}{d\tau}\right]^2}\, d\tau$$

Thus,

$$\int_o^t e^{p(\tau)}\, d\tau = \frac{e^{p(\tau)}}{\frac{dp(\tau)}{d\tau}} \Bigg|_o^t + \int_o^t \frac{d^2 p(\tau)}{d\tau^2}\, \frac{e^{p(\tau)}}{\left[\frac{dp(\tau)}{d\tau}\right]^2}\, d\tau \quad . \tag{B.12}$$

Since

$$\frac{dp(\tau)}{d\tau} = -s_k + j\omega_i(\tau) \tag{B.13}$$

and

$$\frac{d^2 p(\tau)}{d\tau^2} = j\, \frac{d\omega_i(\tau)}{d\tau} \quad , \tag{B.14}$$

The first term of (B.12) becomes

$$\left.\frac{e^{p(\tau)}}{\frac{dp(\tau)}{d\tau}}\right|_o^t = \frac{\exp\left[-s_k t + j\int_o^t \omega_i(\tau)\,d\tau\right]}{-s_k + j\omega_i(t)} - \frac{1}{-s_k + j\omega_i(o)} \quad , \tag{B.15}$$

and the second term of (B.12) becomes

$$\int_o^t \frac{d^2p(\tau)}{d\tau^2}\frac{e^{p(\tau)}}{\left[\frac{dp(\tau)}{d\tau}\right]^2}d\tau = \int_o^t j\,\frac{d\omega_i(\tau)}{d\tau}\,\frac{\exp\left[-s_k + j\int_o^\tau \omega_i(\tau)\,d\tau\right]}{\left[-s_k + j\omega_i(\tau)\right]^2}d\tau \quad . \tag{B.16}$$

Therefore,

$$e_k = A_k\,\frac{\exp\left[j\int_o^t \omega_i(\tau)\,d\tau\right]}{-s_k + j\omega_i(t)} - A_k\,e^{s_k t}\,\frac{1}{-s_k + j\omega_i(o)}$$

$$+ A_k e^{s_k t}\, j\int_o^t \frac{d\omega_i(\tau)}{d\tau}\,\frac{\exp\left[-s_k + j\int_o^\tau \omega_i(\tau)\,d\tau\right]}{\left[-s_k + j\omega_i(\tau)\right]^2}d\tau \quad , \tag{B.17}$$

The steady-state response to a sinusoidal input can now be found. The second term in (B.17) is the transient term which tends to be zero as t gets large, provided that the real part of s_k is negative for all k. For a stable network, this is true since all poles are located in the left-half plane. The third term is negligible if

$$\left|\frac{\frac{d\omega_i(\tau)}{d\tau}}{\left[-s_k + j\omega_i(\tau)\right]^2}\right| << 1 \tag{B.18}$$

for all k and τ. If this is true, we are left with the quasi-steady-state solution

$$e_k(t) = A_k \frac{\exp\, j \int_o^t \omega_i(\tau)\, d\tau}{-s_k + j\omega_i(t)} \qquad (B.19)$$

Since $e_{out}(t)$ is the sum of all $e_k(t)$ terms

$$e_{out}(t) = \sum_k \exp\left[j \int_o^t \omega_i(\tau)\, d\tau \right] \frac{A_k}{-s_k + j\omega_i(t)} \qquad (B.20)$$

Referring to (B.2), (B.20) can be written as

$$e_{out}(t) = \exp\left[j \int_o^t \omega_i(\tau)\, d\tau \right] Y(\omega_i) \ , \qquad (B.21)$$

where it is understood that ω_i is a function of t.

If $Y(\omega_i)$ is represented as

$$Y(\omega_i) = \left| Y(\omega_i) \right| e^{j\phi(\omega_i)} \ , \qquad (B.22)$$

then

$$e_{out}(t) = Y(\omega_i) \exp\left[j \int_o^t \omega_i(\tau)\, d\tau + \phi(\omega_i) \right] \ . \qquad (B.23)$$

The term

$$\int_o^t \omega_i(\tau)\, d\tau$$

is the instantaneous input phase, which can be represented as

$$\int_o^t \omega_i(\tau)\, d\tau = \omega_n t + \theta(t) \ , \qquad (B.24)$$

where ω_n is the nominal carrier frequency and $\theta(t)$ is the phase perturbation on that carrier. Using this substitution, (B.23) becomes

$$e_{out}(t) = \left| Y(\omega_i) \right| e^{j\left[\omega_n t + \theta(t) + \phi(\omega_i) \right]} \ . \qquad (B.25)$$

If the network is such that

$$\left|Y(\omega_i)\right| = 1 \tag{B.26}$$

for all ω_i, then

$$e_{out}(t) = e^{j\left[\omega_n t + \theta(t) + \phi(\omega_i)\right]} \tag{B.27}$$

for

$$e_{in}(t) = e^{j\left[\omega_n t + \theta(t)\right]} . \tag{B.28}$$

The assumption that this is true forms the basis for the analysis carried out in Chapters II and IV.

APPENDIX C

QUASI-STEADY-STATE ANALYSIS OF A NONLINEAR PHASE NETWORK

The analysis in Chapters II and IV is based on the assumption that the filters had unit amplitude and linear phase in the passband. This appendix illustrates the difficulty encountered when this assumption is not made.

Consider a simple bandpass filter of the form

$$H(\omega) = \frac{j\omega B}{\omega_n^2 + j\omega B - \omega^2} \quad , \tag{C.1}$$

where B is the bandwidth and ω_n is the center frequency of the filter. The input to the filter is assumed to be the general angle modulated signal

$$e_{in}(t) = \cos\left[\omega_n t + \mu(t)\right] \quad . \tag{C.2}$$

Using the quasi-steady-state approximation developed in Appendix B yields

$$e_{out}(t) = \mathrm{Re}\left[H(\omega_i)e^{j\left[\omega_n t + \mu(t)\right]}\right] \tag{C.3}$$

for the filter output.

The term $H(\omega_i)$ is determined from (C.1), and the result is

$$H(\omega_i) = \frac{jB\left[\omega_n + \dot{\mu}(t)\right]}{j\left[\omega_n + \dot{\mu}(t)\right] - 2\omega_n\dot{\mu}(t) - \dot{\mu}^2(t)} \quad , \tag{C.4}$$

which can be written

$$H(\omega_i) = \frac{1}{1 + j\frac{\dot{\mu}(t)}{B}\left[\frac{2\omega_n + \dot{\mu}(t)}{\omega_n + \dot{\mu}(t)}\right]} . \qquad (C.5)$$

In most practical systems, the deviation is small compared to the center frequency, so that

$$\frac{2\omega_n + \dot{\mu}(t)}{\omega_n + \dot{\mu}(t)} \approx \frac{2\omega_n}{\omega_n} = 2 . \qquad (C.6)$$

This yields

$$H(\omega_i) = \frac{1}{1 + j2\frac{\dot{\mu}(t)}{B}} \qquad (C.7)$$

or

$$H(\omega_i) = \frac{B}{\sqrt{B^2 + 4\dot{\mu}^2(t)}} e^{-j \tan^{-1} \frac{2}{B}\dot{\mu}(t)} . \qquad (C.8)$$

Thus, the filter output is

$$e_{out}(t) = \frac{B}{\sqrt{B^2 + 4\dot{\mu}^2(t)}} \cos\left[\omega_n t + \mu(t) - \tan^{-1}\frac{2}{B}\dot{\mu}(t)\right] . \qquad (C.9)$$

Both the amplitude and the phase are perturbed by $\mu(t)$.

In order to understand the complications of the above expression, it will be used to analyze the system studied in Chapter II. The following definitions are made

$\theta(t)$ = phase perturbation of the pilot,

B_p = pilot filter bandwidth,

B_n = channel filter bandwidth, and

ω_m = modulating frequency.

The assumed pilot is given by

$$e_{np}(t) = \cos\left[\omega_p t + \theta(t)\right] \tag{C.10}$$

so that the output of the pilot filter is

$$e_{pf}(t) = \frac{B_p}{\sqrt{B_p^2 + 4\dot{\theta}^2(t)}} \cos\left[\omega_p t + \theta(t) - \tan^{-1}\frac{2}{B_p}\dot{\theta}(t)\right] . \tag{C.11}$$

The frequency divider is assumed to operate only on zero crossings; therefore, the amplitude perturbation is of no interest. The synthesized demodulation carrier, $e_{sc}(t)$, is

$$e_{sc}(t) = \cos\left[\omega_n t + \frac{\omega_n}{\omega_p}\theta(t) - \frac{\omega_n}{\omega_p}\tan^{-1}\frac{2}{B_p}\dot{\theta}(t)\right] . \tag{C.12}$$

The Channel n signal, $e_{ns}(t)$, which is to be demodulated, is assumed to be the SSB signal

$$e_{ns}(t) = \cos\left[(\omega_n + \omega_m)t + \frac{\omega_n + \omega_m}{\omega_p}\theta(t)\right] . \tag{C.13}$$

The instantaneous frequency deviation of this signal, $\dot{\mu}(t)$, is

$$\dot{\mu}(t) = \omega_m + \frac{\omega_n + \omega_m}{\omega_p}\dot{\theta}(t) , \tag{C.14}$$

so that the output of the channel filter, $e_{cf}(t)$, is

$$e_{cf}(t) = \frac{B_n}{\sqrt{B_n^2 + 4\left[\omega_m + \frac{\omega_n + \omega_m}{\omega_p}\dot{\theta}(t)\right]^2}} \cos\left[\omega_n t + \frac{\omega_n + \omega_m}{\omega_p}\theta(t) - \tan^{-1}\frac{2}{B_n}\left[\omega_m + \frac{\omega_n + \omega_m}{\omega_p}\dot{\theta}(t)\right]\right] . \tag{C.15}$$

This is demodulated using (C.12) so that the demodulated output $e_d(t)$, becomes

$$e_d(t) = \frac{B_n}{\sqrt{B_n^2 + 4\left[\omega_m + \frac{\omega_n + \omega_m}{\omega_p}\dot{\theta}(t)\right]^2}} \cos\left[\omega_m t + \frac{\omega_m}{\omega_p}\theta(t) + \tan^{-1}\frac{2}{B_n}\left[\omega_m + \frac{\omega_n + \omega_m}{\omega_p}\dot{\theta}(t)\right] - \frac{\omega_n}{\omega_p}\tan^{-1}\frac{2}{B_p}\dot{\theta}(t)\right] . \tag{C.16}$$

Let

$$\xi = \tan^{-1}\frac{2}{B_n}\left[\omega_m + \frac{\omega_n + \omega_m}{\omega_p}\dot{\theta}(t)\right] - \frac{\omega_n}{\omega_p}\tan^{-1}\frac{2}{B_p}\dot{\theta}(t) . \tag{C.17}$$

Since

$$\tan^{-1} x = x + \sum_{n=2}^{\infty} (-1)^{n+1}\frac{x^{2n-1}}{(2n-1)}, \tag{C.18}$$

(C.17) can be written

$$\xi = \frac{2}{B_n}\left[\omega_m + \frac{\omega_n + \omega_m}{\omega_p}\dot{\theta}(t)\right] - \frac{2}{B_p}\frac{\omega_n}{\omega_p}\dot{\theta}(t) + \sum_{n=2}^{\infty}\frac{(-1)^{2n-1}}{(2n-1)}\left[\frac{2}{B_n}\left[\omega_m + \frac{\omega_n + \omega_m}{\omega_p}\dot{\theta}(t)\right]\right]^{2n-1} - \frac{\omega_n}{\omega_p}\sum_{n=2}^{\infty}\left[\frac{2}{B_p}\dot{\theta}(t)\right]^{2n-1} , \tag{C.19}$$

which is

$$\xi = \frac{2}{B_n}\omega_m + \frac{2}{B_n}\frac{\omega_m}{\omega_p}\dot{\theta}(t) + \left[\frac{2}{B_n} - \frac{2}{B_p}\right]\frac{\omega_n}{\omega_p}\dot{\theta}(t) + \eta , \tag{C.20}$$

where η represents the higher order terms

$$\sum_{n=2}^{\infty}\frac{(-1)^{2n-1}}{(2n-1)}\left[\left[\frac{2}{B_n}\left[\omega_m + \frac{\omega_n + \omega_m}{\omega_p}\dot{\theta}(t)\right]\right]^{2n-1} - \frac{\omega_n}{\omega_p}\left[\frac{2}{B_p}\dot{\theta}(t)\right]^{2n-1}\right] .$$

If these terms are neglected, the demodulated output becomes

$$e_d(t) = \frac{B_n}{\sqrt{B_n^2 + 4\left[\omega_m + \frac{\omega_n + \omega_m}{\omega_p}\dot{\theta}(t)\right]^2}}\cos\left[\omega_m t + \frac{\omega_m}{\omega_p}\theta(t) + \frac{2}{B_n}\omega_m + \frac{2}{B_n}\frac{\omega_m}{\omega_p}\dot{\theta}(t) + \left[\frac{2}{B_n} - \frac{2}{B_p}\right]\frac{\omega_n}{\omega_p}\dot{\theta}(t)\right] . \tag{C.21}$$

If the filters are "matched" and the amplitude perturbation is neglected,

(C.21) becomes

$$e_d(t) = \cos\left[\omega_m t + \frac{\omega_m}{\omega_p}\theta(t) + S_n\omega_m + S_n\frac{\omega_m}{\omega_p}\dot{\theta}(t)\right] \qquad (C.22)$$

for

$$S_n = \frac{2}{B_n} \quad . \qquad (C.23)$$

This is the result obtained in Chapter II.

If the Channel n signal is DSB_c a term can be added to (C.13) to account for the other sideband. The channel filter output for this case will be (C.15) with a lower sideband term added. This additional term will be (C.15) with ω_m replaced by $-\omega_m$. Thus, the amplitude of the upper and lower sideband components will not be equal and coherent addition will be impossible. This further complicates an exact analysis.

Several observations can be made which strengthen the assumptions made in obtaining the result given in (C.22). In general the carrier synthesis loop will consist of digital dividers or phase-lock loops preceded by limiters, neither of which are amplitude sensitive. Thus, (C.12) is generally valid. Filters usually have sufficient bandwidth to pass the sidebands of a modulated signal with negligible distortion. If this is not the case, the system is of poor design. Finally, the nonlinear phase characteristics of practical filters are negligible in the passband. Thus, the only region where (C.22) is likely not to accurately describe the demodulated output is when the channel signal has a high amplitude component on the channel filter skirt and $\dot{\theta}(t)$ is large.

APPENDIX D

EFFECT OF DEMODULATION PHASE ERRORS

In surpressed carrier systems errors result in the demodulated waveform if a phase error exists in the synthesized carrier used for demodulation. The manner in which this phase error affects the demodulated output is of considerable practical importance. In this appendix, the effect of demodulation phase error is determined for DSB, SSB, and QDSB modulation.

A. PHASE ERRORS IN A DSB SYSTEM

A general DSB signal, prior to demodulation, can be expressed as

$$e_{DSB}(t) = m(t) \cos \omega_n t \ , \qquad (D.1)$$

where ω_n is the carrier frequency and m(t) is the information bearing signal. The demodulation carrier, $e_{sc}(t)$, can be expressed as

$$e_{sc}(t) = 2 \cos\left[\omega_n t + \phi(t)\right] \ , \qquad (D.2)$$

where $\phi(t)$ represents the phase error. Multiplying (D.1) and (D.2) and filtering out the components centered about $2\omega_n$ yields

$$e_d(t) = m(t) \cos \phi(t) \qquad (D.3)$$

for the demodulated output.

In order to investigate the error introduced by a nonzero $\phi(t)$, an error function, E(t) is defined as the difference between $e_d(t)$, the actual demodulated output, and m(t), the ideal demodulated output. For the DSB case the error function, $E_{DSB}(t)$, is

$$E_{DSB}(t) = \left[1 - \cos\ \phi(t)\right] m(t) \ . \tag{D.4}$$

In practical cases, $\phi(t)$ will be small since this is a requirement for good system performance. Thus without great loss of generality, $\phi(t)$ can be assumed sufficiently small to make $\phi^n(t)$ negligible for $n \geq 3$. This assumption allows cos $\phi(t)$ to be replaced by the first two terms of its series expansion so that

$$E_{DSB}(t) \approx \frac{1}{2}\ \phi^2(t)m(t) \ . \tag{D.5}$$

The mean-square error, $\overline{E_{DSB}^2(t)}$, can be written as

$$\overline{E_{DSB}^2(t)} = \frac{1}{4}\ \overline{\phi^4(t)m^2(t)} \ . \tag{D.6}$$

In general $\phi(t)$ and $m(t)$ will be statistically independent so that

$$\overline{E_{DSB}^2(t)} = \frac{1}{4}\ \overline{\phi^4(t)}\ \ \overline{m^2(t)} \ . \tag{D.7}$$

Both the modulating signal, $m(t)$, and the phase error, $\phi(t)$, are assumed to be zero mean Gaussian random variables with variances σ_m^2 and σ_ϕ^2, respectively. Thus,

$$\overline{m^2(t)} = \sigma_m^2 \ . \tag{D.8}$$

In order to simplify the integration, the value of $\overline{\phi^4(t)}$ will be determined by defining

$$\xi(t) = \phi^2(t) \tag{D.9}$$

and determining the mean square value of ξ. Since the density function for $\phi(t)$ is

$$p(\phi) = \frac{1}{\sigma_\phi\sqrt{2\pi}} \exp\left[-\phi^2/2\sigma_\phi^2\right], \tag{D.10}$$

the density function for ξ is[27]

$$p(\xi) = \frac{1}{\sigma_\phi \sqrt{2\pi\xi}} \exp\left[-\xi/\sigma_\phi^2\right], \tag{D.11}$$

which yields

$$\overline{\xi^2(t)} = \frac{1}{\sigma_\phi \sqrt{2\pi}} \int_0^\infty \xi^{3/2} \exp\left[-\xi/\sigma_\phi^2\right] d\xi \tag{D.12}$$

From (D.9) this becomes

$$\overline{\phi^4(t)} = \frac{1}{\sigma_\phi \sqrt{2\pi}} \int_0^\infty \phi^3 \exp\left[-\phi^2/2\sigma_\phi^2\right] 2\phi \, d\phi \quad , \tag{D.13}$$

which can be integrated to yield

$$\overline{\phi^4(t)} = 3\sigma_\phi^4 \, . \tag{D.14}$$

Substituting (D.8) and (D.14) into (D.7) yields

$$\overline{E_{DSB}^2(t)} = \frac{3}{4} \sigma_\phi^4 \sigma_m^2 \tag{D.15}$$

for the system mean-square error, or

$$E_{N(DSB)} \approx \frac{3}{4} \sigma_\phi^4 \, , \tag{D.16}$$

where $E_{N(DSB)}$ is the system mean-square error normalized with respect to the mean-square value of m(t). The function

$$\sqrt{E_{N(DSB)}} \approx \sqrt{\frac{3}{4}} \sigma_\phi^2 \tag{D.17}$$

is the normalized rms error and is the usual quantity of interest.

B. PHASE ERRORS IN A QDSB SYSTEM

A general QDSB signal, prior to demodulation, can be expressed as

$$e_Q(t) = m_1(t) \cos \omega_n t + m_2(t) \sin \omega_n t \, , \tag{D.18}$$

where $m_1(t)$ and $m_2(t)$ represent the two information bearing signals on the two quadrature carriers. Multiplying (D.18) and (D.2) will demodulate $m_1(t)$, and in like manner, a demodulation carrier of

$$2 \sin\left[\omega_n t + \varepsilon(t)\right]$$

will demodulate $m_2(t)$. Because of the symmetry involved, it is necessary only to consider one of these processes. If the mean-square values of $m_1(t)$ and $m_2(t)$ are equal, the error expression will be the same for both cases.

Multiplying (D.14) and (D.2) yields

$$e_d(t) = m_1(t) \cos \phi(t) + m_2(t) \sin \phi(t) \tag{D.19}$$

after the $2\omega_n$ terms are filtered. Using the approximation that $\phi^n(t)$ is negligible for $n \geq 3$ yields

$$e_d(t) \approx m_1(t)\left[1 - \frac{1}{2}\overline{\phi^2(t)}\right] + m_2(t)\phi(t) \tag{D.20}$$

for the demodulated output. Thus, the error function for QDSB, $E_Q(t)$, is

$$E_Q(t) = \frac{1}{2}\phi^2(t)m_1(t) - \phi(t)m_2(t) \tag{D.21}$$

and the mean-square error is

$$\overline{E_Q^2(t)} = \frac{1}{4}\overline{\phi^4(t)m_1^2(t)} - \overline{\phi^3(t)m_1(t)m_2(t)} + \overline{\phi^2(t)m_2^2(t)} \; . \tag{D.22}$$

The functions $\phi(t)$, $m_1(t)$, and $m_2(t)$ are all assumed statistically independent random variables with zero means. From (D.22) and (D.14) we have

$$\overline{E_Q^2(t)} = \frac{3}{4}\,\sigma_\phi^4\sigma_{m_1}^2 + \sigma_\phi^2\sigma_{m_2}^2 \,. \tag{D.23}$$

If the signals $m_1(t)$ and $m_2(t)$ have equal variances (D.23) can be written

$$\overline{E_Q^2(t)} = \left(\frac{3}{4}\,\sigma_\phi^4 + \sigma_\phi^2\right)\sigma_m^2 \tag{D.24}$$

where

$$\sigma_m^2 = \sigma_{m_1}^2 = \sigma_{m_2}^2 \,. \tag{D.25}$$

This yields a normalized rms error of

$$\sqrt{E_{N(Q)}} = \sigma_\phi\sqrt{\frac{3}{4}\,\sigma_\phi^2 + 1} \,. \tag{D.26}$$

C. PHASE ERRORS IN A SSB SYSTEM

If in (D.19) $m_1(t)$ is set equal to $m(t)$ and $m_2(t)$ is set equal to $m(t)$, the Hilbert transform of $m(t)$, the result is the SSB signal[28]

$$e_{SSB}(t) = m(t)\cos\omega_n t + m(t)\sin\omega_n t \,. \tag{D.27}$$

Comparison of (D.27) with (D.22) shows that

$$\overline{E_{SSB}^2(t)} = \frac{1}{4}\,\overline{\phi^4(t)}\;\;\overline{m^2(t)} - \overline{\phi^3(t)}\;\;\overline{m(t)m(t)} + \overline{\phi^2(t)}\;\;\overline{m^2(t)} \tag{D.28}$$

since $\phi(t)$ and $m(t)$ are assumed statistically independent. It is easily shown that[29]

$$\overline{\dot{m}^2(t)} = \overline{m^2(t)} \tag{D.29}$$

so that (D.28) can be written

$$\overline{E_{SSB}^2(t)} = \frac{3}{4}\,\sigma_\phi^4\sigma_m^2 + \sigma_\phi^2\sigma_m^2 \,. \tag{D.30}$$

Comparison of (D.30) with (D.24) shows that the mean-square error for SSB is exactly the same as the mean-square error in a QDSB system if all modulating signals have the same mean-square value.

In Figure D-1 the normalized rms error is illustrated for the three cases of interest. The curve clearly illustrates that DSB is much less sensitive to a phase error in the demodulation carrier than either SSB or QDSB.

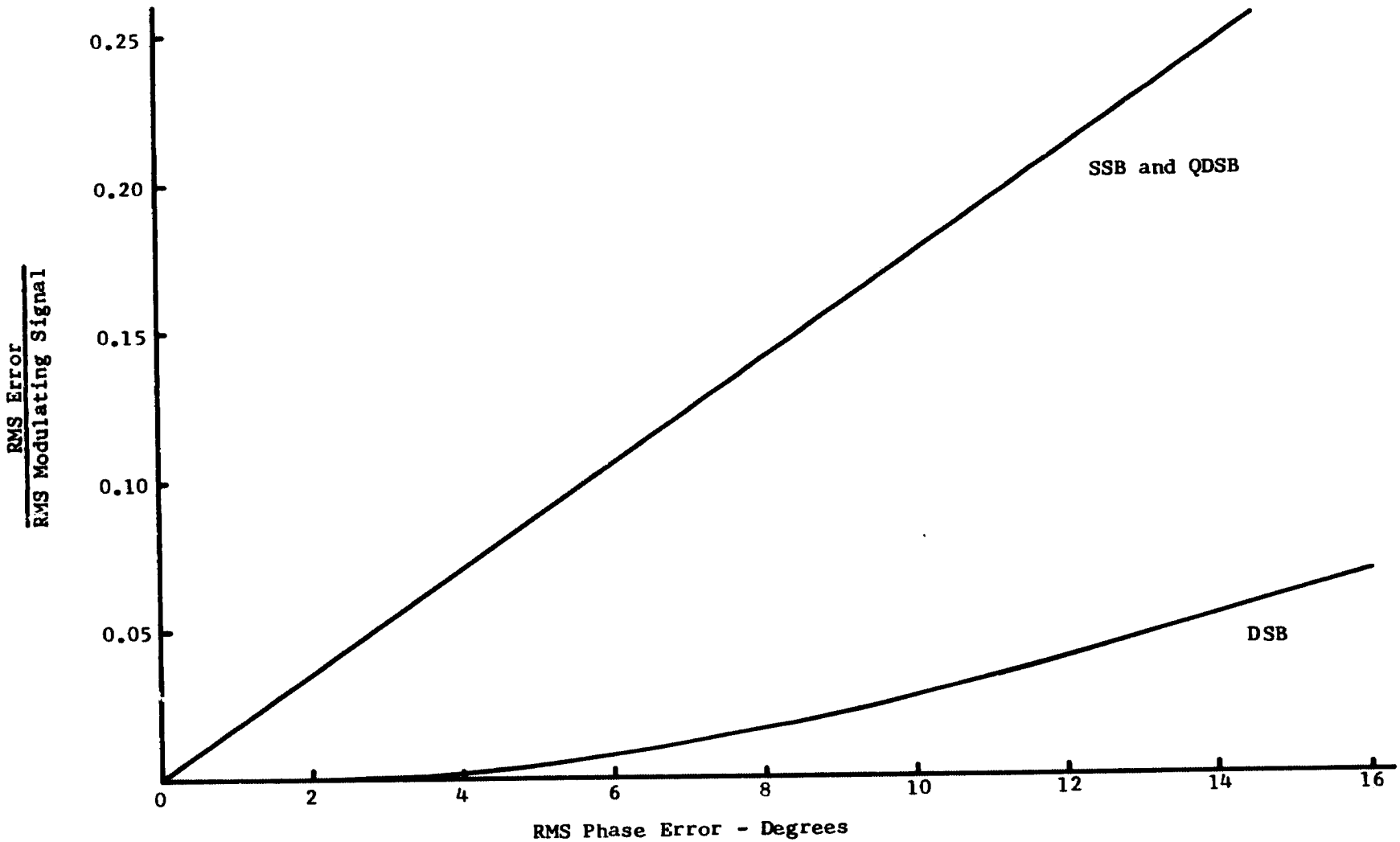

Figure D-1 Effect of Demodulation Phase Errors

APPENDIX E

PHASE-LOCK LOOP BEHAVIOR IN THE PRESENCE OF FLUTTER

In order for the demodulation phase error to be minimized, the synthesized demodulation carrier must follow the baseband TBE, as shown in Chapter II. The carrier synthesis loop will usually contain a PLL, and the bandwidth of the PLL must be adjusted such that the phase error, due to imperfect tracking of the loop, is less than some chosen value. In a practical system the allowable phase error is much less than 90 degrees, 5 degrees being a typical value, so that the linear model of the PLL is valid for analysis.[30]

In order to compute the necessary bandwidth of the PLL for a given error, the TBE spectrum must be known as well as the phase-error transfer function of the PLL. Assuming a second-order PLL with a damping ratio of 0.707 yields a phase transfer function, $\frac{\theta_e(f)}{\theta_i(f)}$, which can be approximated by the one given in Figure E-1(a).[31] The flutter spectrum of most modern recorders, with servo speed control, is reasonably flat. This means that the TBE spectrum can often be approximated by K/f^2, which yields K^2/f^4 for the TBE power spectrum as shown in Figure E-1(b).

Since the phase error is the TBE scaled by frequency, the phase error spectrum has the same shape as the TBE spectrum. Thus, the time-base-error spectrum at the PLL output is

$$\Phi_{he}(f) = \left| \frac{\theta_e(f)}{\theta_i(f)} \right|^2 \Phi_h(f) , \qquad \text{(E.1)}$$

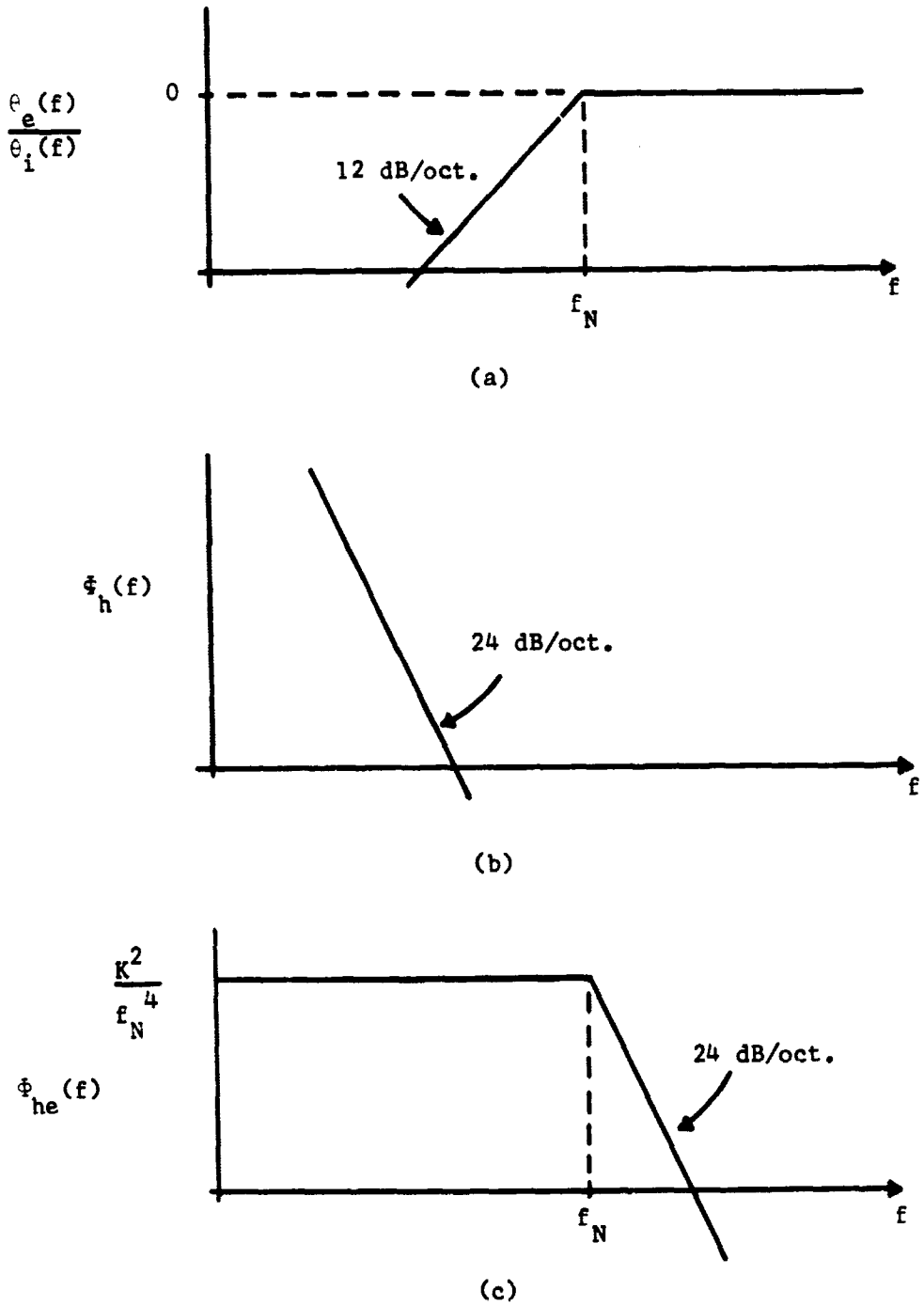

Figure E-1 Derivation of $\Phi_{he}(f)$

which can be approximated by the spectrum shown in Figure E-1(c). The mean-square TBE is found by integrating $\Phi_{he}(f)$ from 0 to ∞. This yields, for sufficiently small K,

$$\sigma_{he}^2 = \frac{K^2}{f_N^4}(f_N) + K^2 \int_{f_N}^{\infty} \frac{df}{f^4}, \qquad \text{(E.2)}$$

which reduces to

$$\sigma_{he}^2 = \frac{4}{3}\frac{K^2}{f_N^3} \qquad \text{(E.3)}$$

Data taken on modern recorders indicates a typical value of K^{32} is $10^{-7}/4$. This yields

$$\sigma_{he}^2 = \frac{10^{-7}}{3}\frac{1}{f_N^3} \qquad \text{(E.4)}$$

and the value of f_N, the natural frequency of the PLL is chosen to make this σ_{he}^2 sufficiently small.

For example, if a 50 kHz pilot is to have an rms phase error of 5 degrees or less, the allowable rms time error is

$$\sigma_{he} = 0.278\ \mu\text{ s}.$$

Using this value in (E.4) yields

$$f_N = 75\ \text{Hz}\ .$$

Thus, the required PLL bandwidth is approximately 75 Hz.

Since tape recorders differ greatly in TBE characteristics, (E.4) should not be taken as a general result. The expected TBE spectrum should be carefully considered before a PLL bandwidth is chosen.

APPENDIX F

CARRIER SYNTHESIS BY FREQUENCY DIVISION

In Chapter II it was stated that if all channel carriers are harmonically related, they can be synthesized from a master oscillator by dividing the proper master oscillator frequency by an appropriate number. There are many ways by which this can be accomplished. The purpose of this appendix is to illustrate one of these methods in order to make the system model clearer, and to give a technique for performing the division.

A. CARRIER SYNTHESIS

For purposes of illustration, assume that the baseband is a 16 channel format with the pilot at Channel-16. The frequency of the Channel-1 carrier is ω_1, and

$$\omega_n = n\omega_1 \ , \tag{F.1}$$

where ω_n is the Channel-n carrier frequency. The pilot frequency, ω_p, is given by (F.1) with n equal to 16.

A synthesis scheme is shown in Figure F-1 which allows the Channel 16,15,12,10,8,6,5,4, and 3 carriers to be synthesized directly from a master oscillator running at a frequency of 480 ω_1. The remaining channel carriers can be synthesized by the multiplication technique illustrated where the multipliers are followed by bandpass filters having appropriate center frequencies. The frequency division process is illustrated in Figure F-2 where

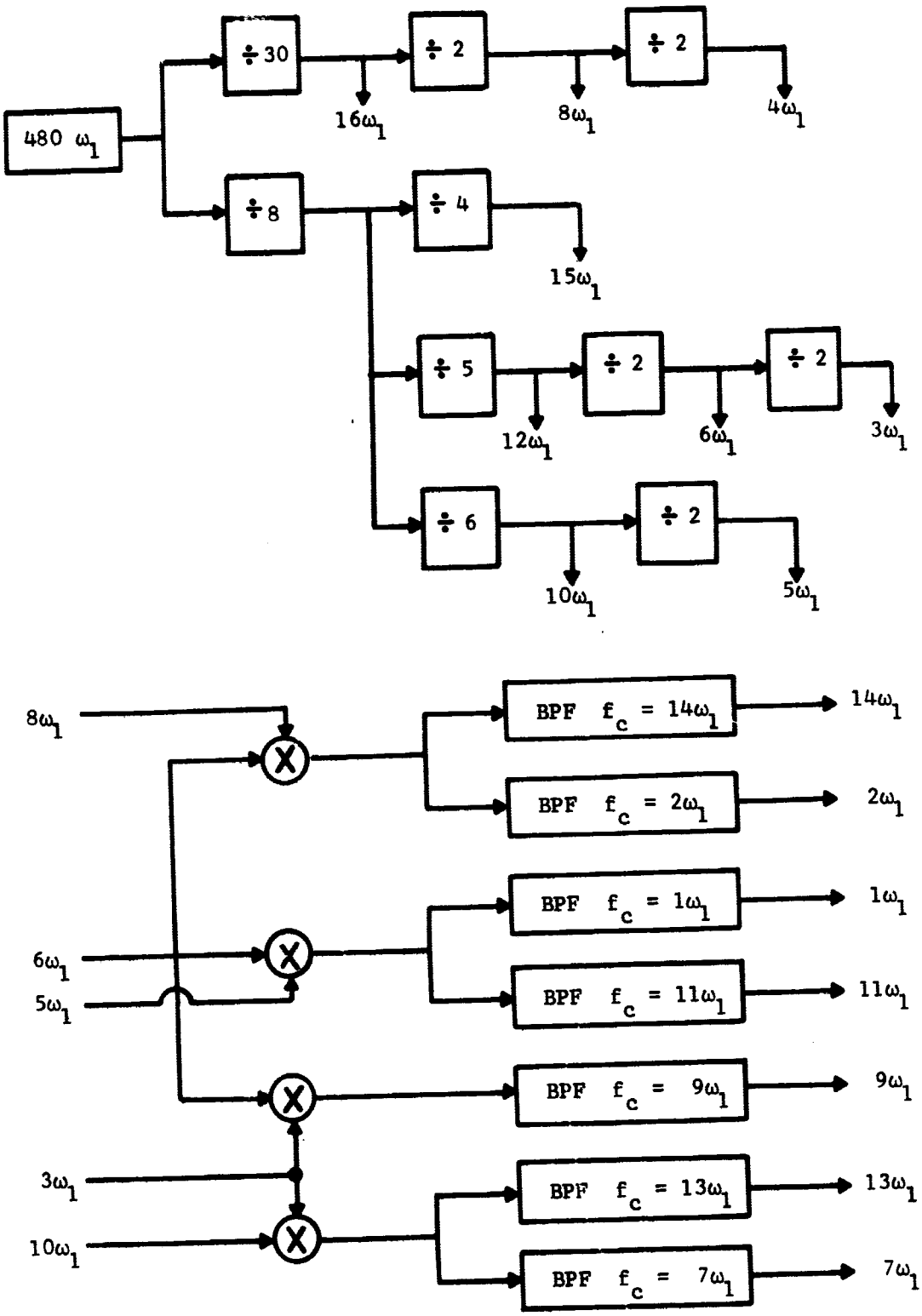

Figure F-1 Carrier Synthesis

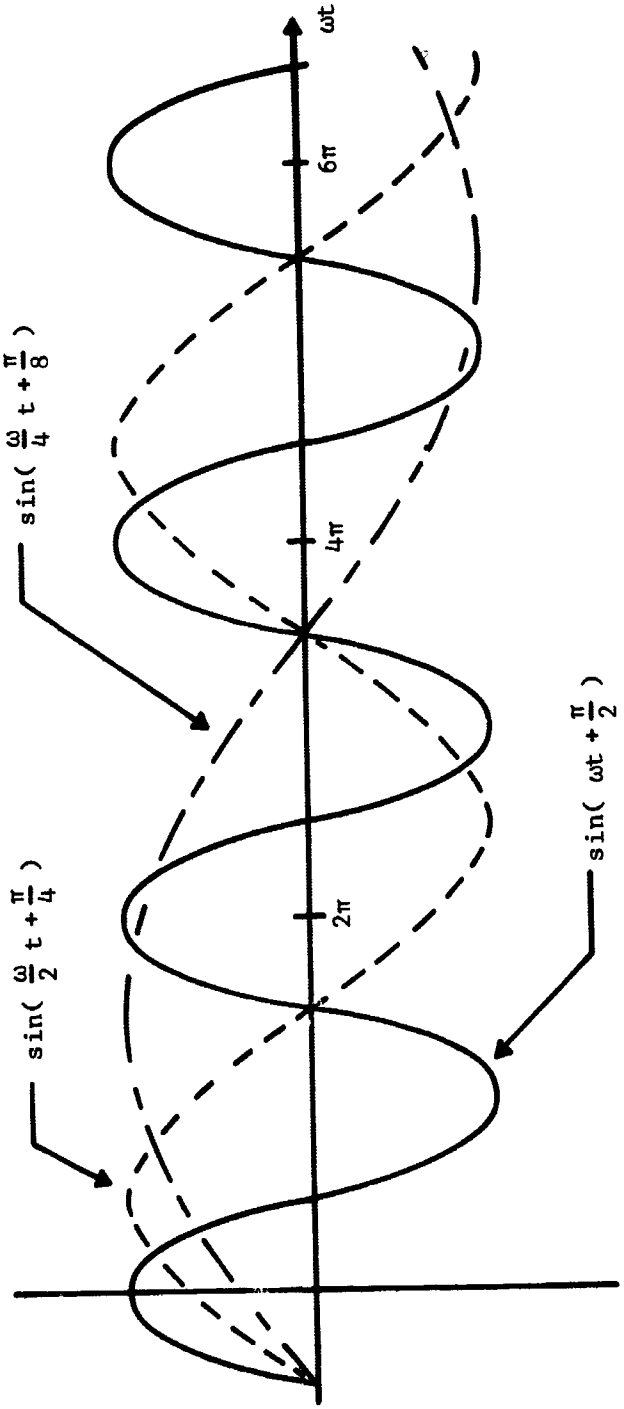

Figure F-2 Illustration of Frequency Division

$$\sin\left(\omega t + \frac{\pi}{2}\right)$$

is divided by two and by four.

B. FREQUENCY DIVISION USING TWO PHASE-LOCK LOOPS

One of the many techniques of performing frequency division is illustrated in Figure F-3. The two phase-lock loops illustrated are conventional loops with one exception, the VCO in the first loop is running at the fundamental frequency, ω_1. The output of this VCO is a pulse train with duty cycle chosen to provide components with adequate power at each channel carrier frequency. These components are then tracked by the second PLL.

The operation can be explained in the following manner. Assume that the pilot frequency is $K\omega_1$. The output of the lowpass filter is the product of the $K^{\underline{th}}$ harmonic of the VCO output and the pilot with all but the dc term filtered out. The loop then operates in the conventional manner such that the pilot is tracked by the PLL. The $n^{\underline{th}}$ component of the VCO output is then tracked by the second PLL.

Since good system performance requires low phase errors, the linear model of the phase-lock loop is assumed valid.[33] The linear model for the cascade PLL is simply the linear model of the two PLL's placed in cascade. This is illustrated in Figure F-4, where K_1 and K_2 are the VCO constants, A_1 and A_2 are the loop amplifier gains and $F_1(s)$ and $F_2(s)$ are the total loop filter transfer functions. The function G(s) and the summer in the second loop will be discussed later.

From Figure F-3 it follows that

$$\frac{\theta_{o1}(s)}{\theta_{i1}(s)} = \frac{K_1 A_1 F_1(s)}{s + K_1 A_1 F_1(s)} \quad , \qquad \text{(F.2)}$$

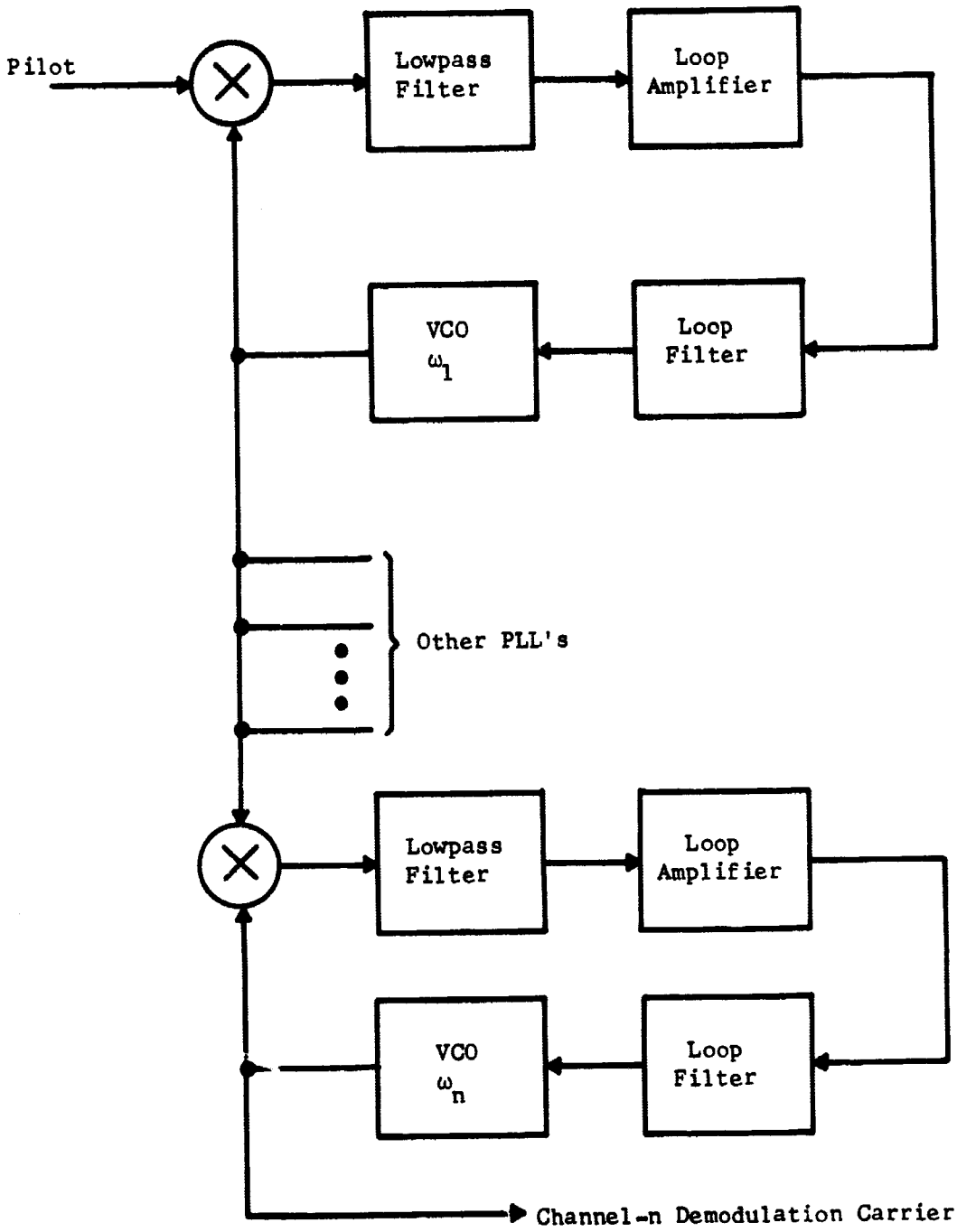

Figure F-3 Cascade Phase-Lock Loops

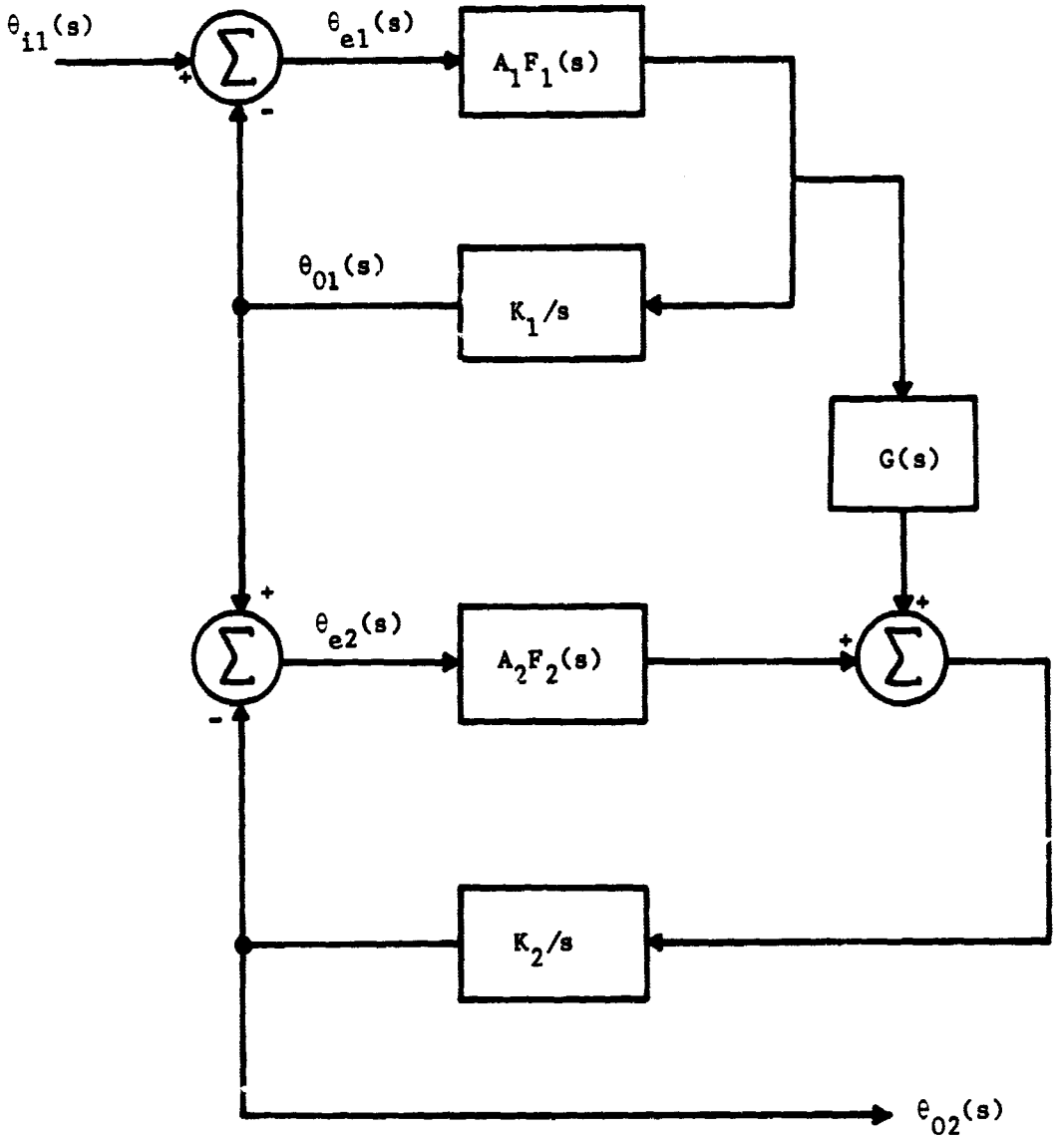

Figure F-4 Model of Cascade Phase-Lock Loops

and if G(s) is zero

$$\frac{\theta_{02}(s)}{\theta_{01}(s)} = \frac{K_2A_2F_2(s)}{s + K_2A_2F_2(s)} \quad . \tag{F.3}$$

This yields

$$\frac{\theta_{02}(s)}{\theta_{i1}(s)} = \frac{K_1K_2A_1A_2F_1(s)F_2(s)}{\left[s + K_1A_1F_1(s)\right]\left[s + K_2A_2F_2(s)\right]} \quad . \tag{F.4}$$

for the complete transfer function. This transfer function can be used to determine the loop characteristics.

A perhaps useful design technique is to make the transfer function of the cascade combination of the two loops independent of the second loop. This can be accomplished by the proper choice of G(s). If G(s) is not zero, then

$$\frac{\theta_{02}(s)}{\theta_{01}(s)} = \frac{K_2A_2F_2(s) + s\left[K_2/K_1\right]G(s)}{s + K_2A_2F_2(s)} \quad . \tag{F.5}$$

This yields

$$\frac{\theta_{02}(s)}{\theta_{01}(s)} = \frac{K_1A_1F_1(s)}{s + K_1A_1F_1(s)} \cdot \frac{K_2A_2F_2(s) + s\left[K_2/K_1\right]G(s)}{s + K_2A_2F_2(s)} \tag{F.6}$$

for the overall transfer function. Inspection of (F.6) shows that if

$$G(s) = \frac{K_1}{K_2} \tag{F.7}$$

the overall transfer function reduces to

$$\frac{\theta_{02}(s)}{\theta_{i1}(s)} = \frac{K_1A_1F_1(s)}{s + K_1A_1F_1(s)} \quad , \tag{F.8}$$

which is simply the transfer function of the first loop. This greatly simplifies the design problem.

REFERENCES

1. A. O. Roach, "The use of suppressed carrier modulation as a sub-carrier for vibration telemetry," Proceedings of the 1964 National Telemetering Conference, June, 1964, paper 5-3.

2. S. C. Chao, "Flutter and time errors in magnetic data recorders," Proceedings of the International Telemetering Conference, vol. 1, 1965, p. 582.

3. M. Schwartz, W. R. Bennett and S. Stein, Communication Systems and Techniques, New York: McGraw-Hill, 1966, pp. 229-232.

4. Chao, op. cit., p. 585.

5. Petr Beckmann, Probability in Communication Engineering, New York: Harcourt, Brace and World, 1967, p. 223.

6. S. O. Rice, "Statistical properties of a sine wave plus random noise," Bell System Technical Journal, vol. 27, No. 1, January, 1948, pp. 109-157.

7. Ibid., p. 120.

8. J. C. Hancock, An Introduction to the Principles of Communication Theory, New York: McGraw-Hill, 1961, pp. 133-136.

9. W. H. Tranter and G. D. Weathers, "An investigation of baseband phase characteristics of an FM transmission link," Sperry Rand Technical Report, September 20, 1968.

10. J. P. Costas, "Synchronous communications," Proceedings of the IRE, vol. 44, no. 12, December, 1965, pp. 1713-1718.

11. Roach, loc. cit.

12. R. C. Payne, "DSB and its utilization in telemetry systems," Proceedings of the National Telemetering Conference, April, 1965, pp. 160-163.

13. R. S. Simpson and W. H. Tranter, "Carrier synthesis from perturbed DSB/SC signals," Proceedings of the International Telemetering Conference, vol. 3, October, 1967, pp. 371-381.

14. F. M. Gardner, Phaselock Techniques, New York: John Wiley and Sons, 1966, p. 17.

15. S. O. Rice, "Mathematical analysis of random noise," Bell System Technical Journal, vol. 24, no. 1, January, 1945, p. 55.

16. Gardner, op. cit., p. 33.

17. S. O. Rice, "Statistical properties of a sine wave plus random noise," Bell System Technical Journal, vol. 27, no. 1, January, 1948, p. 120.

18. Ibid., p. 130.

19. Chao, op. cit., p. 585.

20. Gardner, op. cit., p. 22.

21. B. P. Lathi, Communication Systems, New York: John Wiley and Sons, 1968, pp. 336-339.

22. W. O. Frost, "Single sideband FM telemetry," Aerospace Telemetry, Englewood Cliffs, N. J.: Prentice-Hall, 1966, pp. 118-119.

23. H. Schachter and L. Bergstein, "Noise analysis of an automatic gain control system," IEEE Transactions on Automatic Control, vol. AC-9, July, 1964, p. 250.

24. R. S. Simpson and W. H. Tranter, "Effect of recorder time-base error on an AM-baseband system," IEEE Transactions on Communication Technology, vol. COM-16, no. 2, April, 1968, pp. 316-320.

25. Elie J. Baghdady, "Theory of low distortion reproduction of FM signals in linear systems," IEEE Transactions on Circuit Theory, vol. CT-5, no. 3, September, 1958, pp. 202-214.

26. J. R. Carson and T. C. Fry, "Variable-frequency electric circuit theory," Bell System Technical Journal, vol. 16, October, 1937, pp. 513-540.

27. A Papoulis, Probability, Random Variables, and Stochastic Processes, New York: McGraw-Hill, 1965, p. 130.

28. Lathi, op. cit., p. 181.

29. J. C. Hancock and P. A. Wintz, Signal Detection Theory, New York: McGraw-Hill, 1966, p. 229.

30. Andrew J. Viterbi, Principles of Coherent Communication, New York: McGraw-Hill, 1966, p. 18.

31. Gardner, op. cit., p. 11.

32. M. H. Nichols and F. J. Schmitt, "Cause and effect of time base errors in coherent demodulation of a suppressed carrier AM multiplex," Proceedings of the International Telemetering Conference, vol. 4, 1968, p. 400.

33. Viterbi, loc. cit.

BIBLIOGRAPHY

BOOKS

Beckmann, Petr, Probability in Communication Engineering, New York: Harcourt, Brace and World, 1967.

Bennett, W. R., and Davy, J. R., Data Transmission, New York: McGraw-Hill, 1965.

Davenport, Wilber B., Jr., and Root, William L., An Introduction to the Theory of Random Signals and Noise, New York: Mc-Graw-Hill, 1965.

D'Azzo, J. J., and Houpis, C. H., Feedback Control System Analysis and Synthesis, New York: McGraw-Hill, 1965.

Davies, Gomer L., Magnetic Tape Instrumentation, New York: McGraw-Hill, 1961.

Gardner, F. M., Phaselock Techniques, New York: John Wiley and Sons, 1966.

Hancock, J. C., An Introduction to the Principles of Communication Theory, New York: McGraw-Hill, 1961.

Harman, Willis W., Principles of the Statistical Theory of Communication, New York: McGraw-Hill, 1963.

Lathi, B. P., Communication Systems, New York: John Wiley and Sons, 1968.

Panter, Philip F., Modulation, Noise and Spectral Analysis, New York: McGraw-Hill, 1965.

Papoulis, A., Probability, Random Variables, and Stochastic Processes, New York: McGraw-Hill, 1965.

Rowe, Harrison E., Signals and Noise in Communication Systems, Princeton, New Jersey: D. Van Nostrand, 1965.

Swartz, M., Bennett, W. R. and Stein, S., Communication Systems and Techniques, New York: McGraw-Hill, 1966.

Viterbi, A. J., Principles of Coherent Communication, New York: McGraw-Hill, 1966.

ARTICLES, REPORTS AND PAPERS

Baghdady, Elie J., "Theory of low-distortion reproduction of FM signals in linear systems," IRE Transactions on Circuit Theory, vol. CT-5, pp. 202-214, September, 1958.

Banta, E. D., "Analysis of an automatic gain control (AGC)," IEEE Transactions on Automatic Control, vol. AC-9, pp. 181-182.

Carson, J. R., and Fry, T. C., "Variable-frequency electric circuit theory," Bell System Technical Journal, vol. 16, pp. 513-540, October, 1937.

Chao, S. C., "Flutter and time errors in magnetic data recorders," Proceedings of the International Telemetering Conference, vol. 1, pp. 578-594, May, 1965.

Costas, J. P., "Synchronous communications," Proceedings of the IRE, vol. 44, no. 12, pp. 1713-1718, December, 1956.

Frost, W. O., "Single sideband FM telemetry," Aerospace Telemetry, Englewood Cliffs, N. J.: Prentice-Hall, pp. 118-119, 1966.

Gill, W. J., and Leong, W. K. S., "Response of an AGC amplifier to two narrow-band input signals," IEEE Transactions on Communication Technology, vol. COM-14, pp. 407-417, August, 1966.

Morley, G. A., "Phase delay variations in an FM receiver," Canadian Armament Research and Development Establishment Technical Memorandum 344/60, July, 1960.

Nichols, M. H., "Some analysis of the WSMR test results on DSB," Proceedings of the International Telemetering Conference, vol. 3, pp. 361-370, October, 1967.

Nichols, M. H., and Rauch, L. L., "Telemetry," USAF Report No. ESD-TR-66-464, July, 1966.

Nichols, M. H., and Schmitt, F. J., "Cause and effect of time base errors in coherent demodulation of a suppressed carrier AM multiplex," Proceedings of the International Telemetering Conference, vol. 4, pp. 399-406, October, 1968.

Oliver, B. M., "Automatic volume control as a feedback problem," Proceedings of the IRE, vol. 36, pp. 466-473, April, 1948.

Payne, R. C., "DSB and its utilization in telemetry systems," Proceedings of the National Telemetering Conference, pp. 160-163, April, 1965.

Ratz, Alfred G., "The effect of tape transport flutter on spectrum and correlation analysis," IEEE Transactions on Space Electronics and Telemetry, vol. SET-10, pp. 129-134, December, 1964.

Rice, S. O., "Mathematical analysis of random noise," Bell System Technical Journal, vol. 23, pp. 282-232, July, 1944.

Rice, S. O., "Mathematical analysis of random noise," Bell System Technical Journal, vol. 24, pp. 46-156, January, 1945.

Rice, S. O., "Statistical properties of sine wave plus random noise," Bell System Technical Journal, vol. 27, pp. 109-157, January, 1948.

Roach, A. O., "The use of double sideband suppressed carrier modulation as a subcarrier for vibration telemetry," Proceedings of the National Telemetering Conference, paper 5-3, June, 1964.

Schachter, H., and Bergstein, L., "Noise analysis of an automatic gain control system," IEEE Transactions on Automatic Control, vol. AC-9, pp. 249-255, July, 1964.

Schmitt, F. J., "Double sideband suppressed carrier telemetry system," Proceedings of the International Telemetering Conference, vol. 3, pp. 347-360, October, 1967.

Simpson, R. S., and Tranter, W. H., "Effect of recorder flutter on coherent demodulation in an AM-baseband system," Proceedings of the National Telemetering Conference, pp. 46-49, May, 1967.

Simpson, R. S., and Tranter, W. H., "Carrier synthesis from perturbed DSB/SC signals," Proceedings of the International Telemetering Conference, vol. 3, pp. 371-381, October, 1967.

Simpson, R. S., and Tranter, W. H., "Effect of recorder time-base error on an AM-baseband telemetry system," IEEE Transactions on Communication Technology, vol. COM-16, no. 2, pp. 316-320, April, 1968.

Simpson, R. S., and Tranter, W. H., "Baseband AGC in AM/FM systems," Record of the 1969 National Telemetering Conference, pp. 241-246, April, 1969.

Tranter, W. H., and Weathers, G. D., "An investigation of baseband phase characteristics of an FM transmission link," Sperry Rand Technical Report, September 20, 1969.

Van der Pol, B., "The fundamental principles of frequency modulation," Journal of the Institution of Electrical Engineers, vol. 93, Part III, pp. 153-158, May, 1946.

Victor, W. K., and Brockman, M. H., "The application of linear servo theory to the design of AGC loops," Proceedings of the IRE, vol. 48, pp. 234-238, February, 1960.

COMMUNICATION SYSTEMS GROUP

RECENT REPORTS

An Exponential Digital Filter for Real Time Use, R. S. Simpson, C. A. Blackwell and W. H. Tranter, July, 1965.

An Evaluation of Possible Modifications of the Existing IRIG FM/FM Telemetry Standards, R. S. Simpson, C. A. Blackwell and J. B. Cain, May, 1966.

Analysis of Premodulation Gain in a SS/FM Telemetry System, R. S. Simpson and C. A. Blackwell, June, 1966.

Tape Recorder Flutter Analysis and Bit-Rate Smoothing of Digital Data, R. S. Simpson and R. C. Davis, June, 1966.

A Study of Redundancy in Saturn Flight Data, R. S. Simpson and J. R. Haskew, August, 1966.

AM-Baseband Telemetry Systems, Vol. 1: Factors Affecting a Common Pilot System, R. S. Simpson and W. H. Tranter, February, 1968.

Waveform Distortion in an FM/FM Telemetry System, R. S. Simpson, R. C. Houts and F. D. Parsons, June, 1968.

A Digital Technique to Compensate for Time-Base Error in Magnetic Tape Recording, R. S. Simpson, R. C. Houts and D. W. Burlage, August, 1968.

A Study of Major Coding Techniques for Digital Communication, R. S. Simpson and J. B. Cain, January, 1969.

AM-Baseband Telemetry Systems, Vol. 2: Carrier Synthesis from AM Modulated Carriers, R. S. Simpson and W. H. Tranter, June, 1969.

AM-Baseband Telemetry Systems, Vol. 3: Considerations in the Use of AGC, R. S. Simpson and W. H. Tranter, July, 1969.

AM-Baseband Telemetry Systems, Vol. 4: Problems Relating to AM-Baseband Systems, R. S. Simpson and W. H. Tranter, August, 1969.

AM-Baseband Telemetry Systems, Vol. 5: Summary, R. S. Simpson and W. H. Tranter, August, 1969.